IMPACT OF URBANIZATION ON HYDROGEODYNAMIC SYSTEMS: A CASE STUDY: BORNOVA REGION (İZMİR, TURKEY)

A Thesis Submitted to
the Graduate School of
İzmir Institute of Technology
in Partial Fulfillment of the Requirements for Degree of

MASTER OF SCIENCE

In Civil Engineering

by

Bahadır ÖZTÜRK

December 2021
İZMİR

ACKNOWLEDGEMENTS

First of all, I would like to thank my advisor Prof. Dr. Alper Baba, for the guidance and support during my M.Sc. study. This thesis wouldn't be completed without his kind, supportive, and patient guidance and teachings. I also want to thank him for encouraging and financially supporting me to attend and share my studies in international conferences and symposiums. Besides my advisor, I would like to thank my co-advisor, Dr. Volkan İşbuğa, for his help, contributions, and ideas for this thesis.

I would like to thank Prof. Dr. Gökmen Tayfur for sharing his valuable guidance and expertise when it's needed.

I would like to thank my co-workers Ms. Esra Bilgiç and Dr. Taygun Uzelli, for their help in the fieldwork necessary for this thesis.

I would like to thank my precious friends Mr. Kadir Aktaş, Ms. Nisa Bahadıroğlu, Mr. Volkan Gökçe Eren, Ms. Merve Özkahya, and Ms. Yasemin Varmış for sharing their experiences and friendships. Knowing that they are always by my side gave me more than strength and confidence.

I would like to thank my brother Mr. Can Öztürk. His presence always gives me confidence and comfort.

Finally, I want to thank my most precious treasures, parents; my mother, Ms. Hayriye Öztürk, and my father, Mr. Coşkun Öztürk. Without their love, caring, sharing, and patience, I could never make it. I want to thank them for giving me every chance they can to make me a better person.

ABSTRACT

IMPACT OF URBANIZATION ON HYDROGEODYNAMIC SYSTEMS: A CASE STUDY: BORNOVA REGION (İZMİR, TURKEY)

Urbanization is one of the most critical processes affecting land and water use. Understanding urbanization and its impact on ground systems gained prominence with global climate change and population increase. This study focuses on the new city center Bornova Plain, İzmir; Turkey, used as agricultural land until the 1950s. Later, the region was opened for settlement, and excessive urbanization decreased the hydraulic conductivity of the surface area of the plain with the constructed buildings, road pavements, and other surface coverings. Effects of the land use- land cover changes on the hydrodynamic system of Bornova Plain's aquifers were investigated in three parts.

Firstly, GIS-based hydrological models with two different periods (2004 and 2020) scenarios were developed with ArcSWAT for this thesis. Using SWAT models, elements of the water budget equation were determined. With SWAT Models, Recharge/Precipitation, Streamflow/Precipitation, and Baseflow/Total flow ratios were found to decrease 52%, 26.09%, and 11.86%, respectively, and Surface Runoff/Total Flow, and ET/Precipitation ratios were found to increase 20.59%, and 15.09% with urbanization increment comparing 2004 and 2020.

Secondly, soil's bearing capacity changes with groundwater level changes within a year were investigated using five observation wells. Conceptual models were created for each well. Maximum of 14.82% of bearing capacity change was observed in the wells.

Thirdly, PLAXIS 3D models were created to understand the effect of the groundwater level changes on pile settlements for sandy and clayey soils in the region. Conceptual models created and maximum of 12.74% settlement difference was observed for different groundwater levels.

ÖZET

KENTLEŞMENİN HİDROJEODİNAMİK SİSTEMLER ÜZERİNDEKİ ETKİSİ: BİR VAKA ÇALIŞMASI: BORNOVA BÖLGESİ (İZMİR, TÜRKİYE)

Kentleşme, arazi ve su kullanımını etkileyen en kritik süreçlerden biridir. Kentleşmeyi ve bunun yeraltı sistemleri üzerindeki etkisini anlamak, küresel iklim değişikliği ve nüfus artışı ile ön plana çıkmıştır. Bu çalışma 1950'li yıllara kadar tarım arazisi olarak kullanılan, İzmir-Türkiye'nin yeni kent merkezi Bornova Ovası'na odaklanmaktadır. 1950'lerden sonra bölge yerleşime açılmış ve aşırı kentleşme hızla gerçekleşmiş, inşa edilen binalar, yol kaplamaları ve diğer yüzey kaplamaları ile ova yüzey alanının hidrolik iletkenliği azalmıştır. Bornova Ovası akiferlerinin hidrodinamik sistemi üzerinde arazi kullanım-arazi örtüsü değişikliklerinin etkileri üç bölümde incelenmiştir.

Bu tez için ilk olarak ArcSWAT ile iki farklı dönem (2004 ve 2020) senaryolu CBS tabanlı hidrolojik modeller geliştirilmiştir. SWAT modelleri kullanılarak su bütçesi denkleminin unsurları belirlenmiştir. SWAT Modelleriyle, Beslenme/Yağış, Akarsu Akışı/ Toplam Akış, Baz Akışı/ Toplam Akış oranlarının kentleşme artışıyla birlikte sırasıyla %52, %26.09 ve %11.86 oranında azaldığı bulunmuştur. Yüzeysuyu Akışı/ Toplam Akış ve Evapotranspirasyon/Yağış oranlarının kentleşme artışıyla birlikte sırasıyla %20.59 ve %15.09 oranında arttığı bulunmuştur.

İkinci olarak, beş gözlem kuyusu kullanılarak bir yıl içinde yeraltı suyu seviyesi değişimi ile zeminin taşıma gücü değişimleri incelenmiştir. Her kuyu için kavramsal modeller oluşturulmuştur. Kuyularda en fazla %14,82 taşıma gücü değişimi gözlenmiştir.

Üçüncü olarak, bölgedeki kumlu ve killi zeminler için yeraltı suyu seviyesi değişimlerinin kazık oturmaları üzerindeki etkisini anlamak için PLAXIS 3D modelleri oluşturulmuştur. Kavramsal modeller oluşturulmuş ve farklı yeraltı suyu seviyeleri için maksimum %12,74 oturma farkı gözlemlenmiştir.

TABLE OF CONTENTS

LIST OF FIGURES

Figure **Page**

Figure **Page**

Figure **Page**

LIST OF TABLES

Table **Page**

CHAPTER 1

INTRODUCTION

Water, specifically freshwater, is referred to be life by the most since all the living creatures desperately depend on it. Throughout history, many civilizations have been established near water resources. People transitioned from nomadic life to a settled life, and they used water for agriculture. Water started to be transported to locations where no water was available with canals, pipes, and aqueducts. Water resources development, technology, and science have grown ever since (Yevjevich 1992).

In order to understand the water, its existence and movement on the Earth, and its atmosphere, the hydrological cycle (Figure 1.1) is used in hydrological sciences. The hydrological cycle is subdivided into parts of water's movement as precipitation, condensation, transpiration, evaporation, evapotranspiration, surface runoff, infiltration, groundwater flow, melting, etc. The process of water evaporating from surface water resources like the lakes, rivers, oceans, seas, etc., and the land is called Evaporation (transforming from liquid phase to gas phase). The process of water turning to the gas phase from the plants is called transpiration. The process of condensing water vapor and coming back to the Earth's surface is called Precipitation. Not all the precipitated water is infiltrated by the soil. Water that does not infiltrate at all is called surface runoff, and water that goes through the soil layer is called infiltration. Infiltrated water that reaches the groundwater level is called groundwater recharge, and water that does not reach the groundwater table is called soil moisture (Todd and Mays 1959).

Urbanization, industry, and population increase all have a cumulative influence on natural landscapes and the hydrological response of basins. While artificial forces impact many aspects of the natural surroundings in terms of routes and hydrologic abstractions, the hydrological cycle's fundamental structure stays intact in urbanized regions. However, urbanization's influence on the ecology and the necessity to provide water supplies to the urban population significantly alter the hydrologic cycle. Hence, it has been noticed that the hydrological cycle becomes even more complicated in urban

regions as a consequence of several anthropogenic influences; thus, the ensuing "urban" hydrological cycle is referred to as the urban water cycle (Figure 1.2) (Marsalek, Jiménez-Cisneros, Karamouz, Malmquist, Goldenfum, and Chocat 2006).

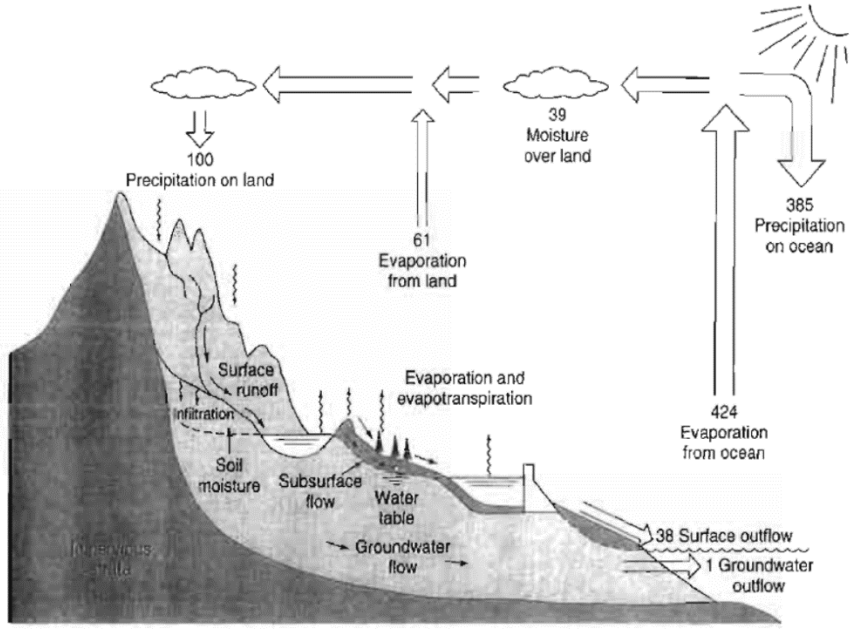

Figure 1.1. Hydrological Cycle

(Source: Todd and Mays 1959)

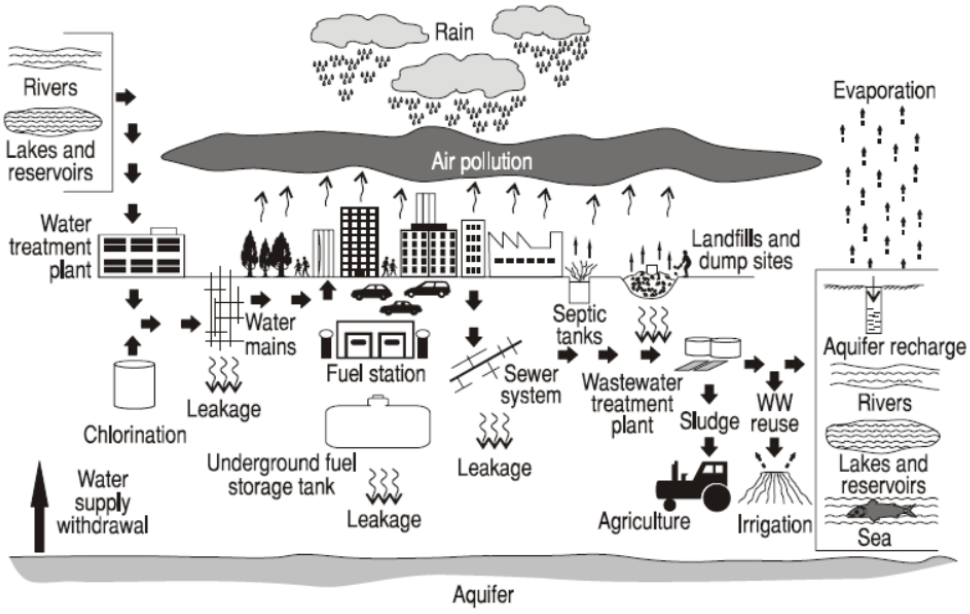

Figure 1.2. Urban Water Cycle

(Source: Marsalek, Jiménez-Cisneros, Karamouz, Malmquist, Goldenfum, and Chocat 2006)

1.1. Problem Description

The study area was mainly used as agricultural land until the 1950s. After the 1950s, the region was opened to settlement and exposed to excessive urbanization following years. As the settlement in the region increased, so did the population, more than ten times, from 70 thousand to approximately 750 thousand people in less than 70 years. This excessive urbanization has led to the permeable surfaces of the region being covered with impermeable layers such as pavement, buildings, roads, etc. Hydrological and hydrodynamical effects of these surface coverings need to be investigated. Groundwater recharge and surface water runoff are known to be directly influenced by these coverings.

The majority of the region's water demand is supplied from groundwater resources. As the urbanization and population in the region increase, water demand and extraction also increase. With disrupted groundwater recharge caused by impermeable surface coverings and excessive groundwater extraction, groundwater level also changes artificially.

Groundwater level changes within a year are expected to be more significant in more urbanized regions. In geotechnical designs, the groundwater level is used to calculate both soil’s bearing capacity and settlement of the soil and foundation. The groundwater level is supplied to geotechnical engineers with boring log data. Most of the constructions in Turkey happen in summers to prevent the rain from affecting construction sites, and boring log data is also taken from construction sites in summers. In urbanized areas, groundwater levels are expected to be lower in summers compared with other seasons since the water demand increases. So most geotechnical designs are conducted at a lower groundwater level compared with the rest of the year.

1.2. Motivation and Aim of the Thesis

Groundwater is one of the most valuable natural resources and also of the most endangered natural resources by human activities and climate change. Groundwater resources affect and are affected by urbanization severely. In order to understand how the

groundwater is affected in excessively urbanized areas efficiently, all the components of the hydrological cycle must be understood and studied.

This thesis aims to numerically investigate the impact of urbanization on groundwater resources, the soil's bearing capacity, and the settlement of pile foundations in the study area. Regarding this, firstly, SWAT Models were created to understand all the hydrological parameters of the study area.

The objectives of the thesis are as follows:

- To derive SWAT models for different periods to calculate groundwater recharge and surface water runoff ratios with respect to urbanization
- To observe groundwater level fluctuations with urbanization within a year
- To analyze the soil's bearing capacity decrease within a year with respect to groundwater level changes
- To derive Plaxis 3D models to understand the effect of groundwater level changes on the settlement of foundations of the buildings in the study area

1.3. Outline of the Thesis

In this thesis, there are 7 Chapters: Introduction, Literature Survey, Hydrological Modeling of the Study Area, Bearing Capacity Analysis, Pile Settlement, Results & Discussion, and Conclusion.

In Chapter 2, the literature review of groundwater recharge, bearing capacity analysis, and settlement analysis are presented.

In Chapter 3, information about the study area, SWAT Modeling and modeling inputs, model calibration, and validation using SWAT-CUP are presented. Detailed information about how the model inputs were conducted and used are also presented in this chapter.

In Chapter 4, inputs and the technique used for the bearing capacity analysis are presented. This chapter also presents drilling wells in the study area to observe groundwater level changes within a year.

In Chapter 5, PLAXIS 3D software and settlement of single piles are presented. Model parameters and soil parameters are also presented in this chapter.

In Chapter 6, model results of Chapters 3, 4, and 5 are presented. SWAT Models of two time periods and change of recharge rate are discussed. Sensitivity analysis, calibration, and validation results are discussed as well. q/q_{max} graphs are presented in this chapter for each observation well, and yearly bearing capacity decrease is discussed in this chapter. PLAXIS 3D model results are also shown in this chapter, and changes in settlement percentages for different groundwater levels are also discussed in this chapter.

In Chapter 7, the results and future works, and recommendations are discussed in this chapter.

CHAPTER 2

LITERATURE SURVEY

2.1. Groundwater Recharge

2.1.1. Groundwater Recharge Estimation

Groundwater recharge estimation is critical for aquifer sustainability, water resource management, and determining the basin's future water potential. Determining recharge is challenging in regions with a deep groundwater table and restricted water availability on the soil surface owing to external circumstances such as nutrient availability, evaporation, precipitation, temperature, and climatic influences (De Silva 2015). Groundwater recharge is critical in groundwater hydrology studies. Groundwater recharge will become increasingly important in the future as the world's fast-rising population consumes more water and demands more water storage in the event of a water crisis (Devine 1995).

Many researchers have used many different groundwater recharge estimation methods in the literature. These methods can be categorized as chemical, physical, numerical, etc.

2.1.1.1. Chemical Methods

Tracers and Chloride Mass Balance methods are amongst the most commonly used chemical groundwater recharge techniques.

Chemical tracers can be categorized into historical, artificial, and environmental. Artificial chemical tracers are implemented onto or under the soil layer. Techniques such

as historic tracers in the unsaturated zone need a low recharge rate to carry the tracer across the unsaturated zone (Scanlon, Healy, and Cook 2002).

The groundwater recharge can be approximated using the Chloride Mass Balance method, utilizing chloride ions to substitute major anions. Chloride is often utilized to estimate smaller recharge rates (Wood and Sanford 1995).

2.1.1.2. Physical Methods

Physical methods can be subcategorized base-flow, seepage meter, channel-water budget, etc.

In the base-flow method, recession curves are used to analyze the recession parameters of river/stream hydrographs. Recharge can be calculated using the mean of recharge values obtained via base-flow recession analysis when groundwater data is insufficient (Uma and Egboka 1988).

2.1.1.3. Numerical Methods

Groundwater recharge can be estimated using softwares MODFLOW, SEAWAT, SEEP/W, WetSoa, WetSpass, SWAT, etc. Numerical methods are generally cheaper and less time-consuming than physical and chemical methods. SWAT software was chosen to estimate groundwater recharge rate changes for this study. SWAT is a widely used software to estimate water budget equation terms.

SWAT models are widely used in arid and semi-arid regions. In general, the hydrological processes that occur in arid and semi-arid climatic zones are akin to those that occur in every other climatic region on Earth. According to Lloyd (1986), the sole distinction is that the interrelationships between various water cycle components are stressed more under arid circumstances. For example, rainfall, a critical hydrological process, is very variable geographically and seasonally in arid and semi-arid regions, resulting in highly variable recharge rates. In semi-arid locations, rainfall episodes are often brief and manifest as intense rainstorms. These factors affect the infiltration process

by limiting direct recharge and boosting indirect recharge through accumulated runoff pools, intermittent streams, and preferred paths (Lerner, Issar, and Simmer 1990; HAPS 2006).

In arid and semi-arid regions, evapotranspiration dominates the water budget, in contrast to humid regions, where precipitation dominates. As a result, many simple assumptions built into various recharge techniques may be invalid in dry and semi-arid regions. For example, the water balance approach is extensively employed in all climatic areas due to its simplicity and accessibility of essential data. However, such a strategy is not necessarily practical in dry regions since recharging accounts for a lower fraction of the water budget in such areas. The recharge component accumulates mistakes in all other equation variables (Lerner, Issar, and Simmer 1990; Gee and Hillel 1988).

2.1.2. Impact of Urbanization

Soil bearing capacity and settlement amounts are affected by groundwater level changes. Therefore, it is crucial to determine how the groundwater level will change depending on urbanization and climate change. When the studies in the literature are examined, it has been seen that many researchers study areas with intense urbanization and especially investigate groundwater recharge (Jat, Khare, and Garg 2009; Minnig, Moeck, Radny, and Schirmer 2018; Tam and Nga 2018; Wakode, Baier, Jha, and Azzam 2018).

Minnig, Moeck, Radny, and Schirmer (2018) examined the impact of urbanization on the groundwater recharge of Dübendorf, the rapidly urbanizing city of Switzerland. The 13.6 km^2 study area was divided into 17 sub-basins and four different classes according to land use, as agricultural, forest, unproductive, and urban areas, and calculated the evapotranspiration, runoff, and seepage values in these sub-basins using the groundwater budget equation. With these calculated values, groundwater recharge increased from 6% to 44% for four different years (1880, 1955, 1985, 2009) with the urban area, groundwater recharge increased from 241.5 mm to 374.2 mm, evapotranspiration increased from 676.8 mm to 494.1 mm. The surface flow was found to increase from 29 mm to 121 mm.

Tam and Nga (2018) stated that although the urbanized surface area in Hanoi, the second largest city of Vietnam with an area of 3300 km^2, increased from 181 km^2 to 476 km^2 between 1990-2015, groundwater recharge decreased very little. Still, the decreasing groundwater level was due to excessive groundwater withdrawal. This study, it is aimed to calculate how the groundwater recharge changes depending on the land-use land-cover change by using the WetSpa rainfall-runoff hydrological model. Groundwater recharge value; It has been examined in 6 sections as recharge on agricultural and natural lands caused by rain, recharge on urbanized areas due to rain, recharge from surface water, recharge from the Red River, recharge from the city's water network, and recharge from the city's wastewater systems. The study was modeled for between 1991 and 2015. Dry and rainy periods were examined separately. Depending on urbanization, an annual decrease of 1.1% in the dry period and 1.5% in the rainy period was found in groundwater recharge. It was stated that this decrease was due to the decrease in precipitation.

Jat, Khare, and Garg (2009) calculated groundwater recharge using GIS (Geographical Information Systems) and groundwater balance equation. Everything entering the system is considered “input” in the groundwater balance equation, and everything leaving the system is considered “output.” This method; provides a reliable approximation in predominantly rocky areas, areas with baseflow data, or where base flow is negligible. Data of 21 wells were obtained for use in the GIS database. The study covers the years 1991 and 2005. This study calculated groundwater volume change due to precipitation and groundwater recharge. It has been determined that there is a loss due to urbanization in groundwater recharge. In this study, the change in groundwater volume was calculated, but the level change was not calculated.

Wakode, Baier, Jha, and Azzam (2018) created personal water-use estimates by estimating population growth in Hyderabad, the fourth largest city in India, with a population of 7.75 million. Natural groundwater recharge and net urban groundwater recharge were calculated separately. Net urban groundwater recharge was 568 mm/year, and natural groundwater recharge was 53 mm/year. Actual evapotranspiration and runoff were estimated by remote sensing and GIS to calculate natural groundwater recharge with precipitation. In this study, to calculate the net urban groundwater recharge, leakage in water distribution systems, leakage in sewage systems, recharge from industrial wastewater, and feeding from domestic wastewater are considered, unlike other studies.

2.2. Soil's Bearing Capacity

A lot of research has been done to develop a method for calculating soil bearing capacity. The first of these studies was done by Rankine in 1857. In Rankine's study, he accepted that the horizontal stresses and passive stresses are equal, and he created the bearing capacity equations. Since the foundation size is ignored in the Rankine bearing capacity formula, it is not suitable for use on all soils.

2.2.1. Terzaghi's Method of Bearing Capacity

Terzaghi (1943) developed his still very widely used bearing capacity of shallow foundation equation concerning foundation size different from Rankine. Terzaghi also included surcharge load (which is the effective pressure of soil above the foundation) to his calculation. The equation can be used for both total and effective parameters. The used assumptions for Terzaghi's bearing capacity equation is as follows:

- Soil is homogenous.
- The groundwater table is well below the foundation (so the water does not affect the foundation at all).
- No settlement on the soil.
- No slipping between the soil and the foundation
- The depth of the foundation should be less or equal to the width of the foundation

Terzaghi's bearing capacity equation differs for different types of footings as follows:

$$q_u = c'N_c + qN_q + \frac{1}{2}B\gamma N_\gamma \ (strip\ foundation) \tag{2.1}$$

$$q_u = 1.3c'N_c + qN_q + 0.4B\gamma N_\gamma \ (square\ foundation) \tag{2.2}$$

$$q_u = 1.3c'N_c + qN_q + 0.3B\gamma N_\gamma \ (circular\ foundation) \tag{2.3}$$

Where

c' is the cohesion of the soil, γ is the unit weight of the soil, q is the equivalent surcharge, B is the shorter side of the footing N_c, N_q, N_γ are bearing capacity factors that are non-dimensional and are functions only of the soil friction angle ϕ'.

2.2.2. Meyerhof's Method of Bearing Capacity

Terzaghi's equation is only valid for the strip, circular and square foundations where rectangular footing is not addressed. Meyerhof (1963) suggested the following equation for bearing capacity calculations concerning shape, depth, and inclination factors.

$$q_u = c'N_cF_{cs}F_{cd}F_{ci} + q'N_qF_{qs}F_{qd}F_{qi} + \frac{1}{2}B\gamma'N_\gamma F_{\gamma s}F_{\gamma d}F_{\gamma i} \tag{2.4}$$

Where

c' is the cohesion of the soil, γ is the unit weight of the soil, q is the equivalent surcharge, B is the shorter side of the footing (or diameter of the circular foundation) N_c, N_q, N_γ are bearing capacity factors that are non-dimensional and are functions only of the soil friction angle ϕ', F_{cs}, F_{qs}, $F_{\gamma s}$ are shape factors, F_{cd}, F_{qd}, $F_{\gamma d}$ are depth factors, and F_{ci}, F_{qi}, $F_{\gamma i}$ are load inclination factors.

Bearing capacity factors for Meyerhof's equation is calculated as follows:

$$N_q = \tan^2\left(45 + \frac{\phi'}{2}\right)e^{\pi \tan \phi'} \tag{2.5}$$

$$N_c = \left(N_q - 1\right) \tan\ \phi' \tag{2.6}$$

$$N_\gamma = 2\left(N_q + 1\right) \tan\ \phi' \tag{2.7}$$

2.3. Pile Settlement

The term "piles" refers to structural components consisting of wood, concrete, or steel. They are categorized as single or group piles. They are often employed to transfer superstructure loads to or through a soil layer and to regulate settlements in (very) compressible strata.

2.3.1. Finite Element Method

In soil behavior analysis, empirical relations are generally used because the environment is complex, and the behavior depends on various factors. The analyses made with these relations developed during geotechnical engineering applications generally give approximate results, but sometimes they can give unreliable results that are far from the actual value.

Since theories based on physical foundations consist of mathematical differential equations, simple assumptions must be made to reach the implicit solution. However, this approach is a solution for most practical situations, the inhomogeneity of geological environments, discontinuities in them, arbitrary geometry, etc. Due to its complex features, it does not allow the problems to reach realistic solutions. For this reason, numerical methods have been developed that simultaneously consider many of the factors mentioned above in the analysis of geomechanical problems (İncecik 1986).

The finite element method was first utilized in geotechnical engineering in 1966 by Clough and Tsui to calculate stresses and motions in embankments, and by Reyes and Deer to analyze subsurface holes in the rock.

Figure 2.1 shows the finite element method's working principle. The first two processes are standard and include converting soil and groundwater characteristics to an idealized profile. Behavioral models for the structures, the soils, and the soil-structure interactions are chosen. Structural behavior is described mathematically as elastic, elasto - plastic, and so forth. The most challenging models to define are the soil and soil-structure interfaces models. Following that, parameters denoting the media characteristics are chosen and approximated in the presence of nonhomogeneous situations. The initial stress conditions are then chosen, a process that may be especially challenging in some soil types, like overconsolidated clays. Finally, the construction order is determined, the finite element mesh is generated, and the analysis is conducted (Xanthakos 1991).

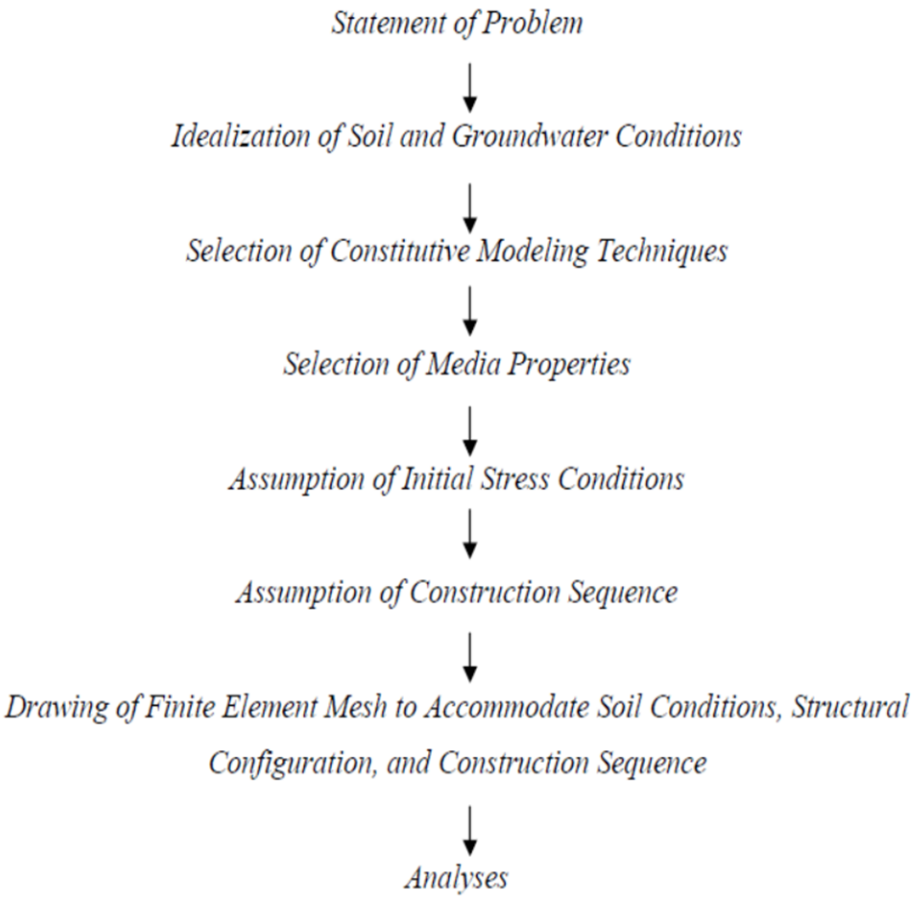

Figure 2.1. Finite Element Method Procedure

(Source: Xanthakos, 1991)

This method employs two approaches. In the first, predictions are generated and compared to observed behavior. The second is to investigate the effect of specific factors on the wall's behavior and evaluate the effect of various design choices on performance.

The finite element method has the most suitable formulation for computer software among numerical analysis methods. This is because complex boundary conditions and non-linear material behavior allow systematic programming in solving challenging and complex problems such as inhomogeneous materials. On the other hand, this method can be applied to boundary value problems in a wide range of engineering (Berilgen 1996).

Since all the pavement and soil characteristics are taken into account with the finite element model, the most significant advantage of this calculation method is that the interaction of the structure and the ground can be calculated realistically. Depending on the characteristics of the ground and building system, the load taken by each element in the composite system is determined as a natural result of the calculation flow. Thus, it is possible to follow the arching in the ground, the load and transfer, the flow of loads in the Finite element model, and direct the construction measures.

2.3.2. PLAXIS 3D

PLAXIS 3D, a finite element program, is developed for the numerical analysis of geotechnical engineering problems. The program consists of an input program that allows data entry, a calculation program in which the analysis is performed, an output program that displays the analysis results graphically, and a curve program that enables the desired graph to be created with the results obtained. This program is used in deformation and stabilization analysis, soil-structure interaction, stress-strain, loading conditions, consolidation, bearing capacity, flow network, soil dynamics needed in the design of projects, and in situations where the material is various gives almost realistic results.

The cells are divided into triangular elements during the creation of the finite element mesh in the PLAXIS 3D program. In Plaxis, these triangular elements can be selected with 6 or 15 nodes. Choosing the element with 15 nodes is more correct so that the stresses and failure surfaces can be calculated more accurately, but this takes more time.

Four different soil models can be used in PLAXIS 3D: Soft Soil Creep Model (SSC), Linear Elastic Model, Hardening Soil Model-HS, and Mohr-Coulomb (MC)

model. Young's Modulus (E), Poisson's Ratio (υ), Internal Friction Angle (φ), Dilatancy (Expansion) angle (ψ), dry and saturated unit weight of the soil (γ_{dry} and γ) horizontal and vertical permeability coefficients in Mohr-Coulomb Model (k_x and k_y) and if the soil is in contact with any element, the interface elements are defined. Strength, interface thickness, and permeability are defined for the interface element.

CHAPTER 3

HYDROLOGICAL MODELING OF THE STUDY AREA

3.1. Study Area

Bornova Basin (Figure 3.1) was selected as the study area for this study. The study area is located between 38 ◦ 25’ 10’’ and 38 ◦ 34’ 20’’ north latitudes and 27 ◦ 9’ 20’’ and 27 ◦ 24’ 20’’ east longitudes and consists of the districts Bornova, Bayraklı, and mountainous regions of Kemalpaşa and Karşıyaka. Bornova Basin was used as agricultural land until the 1950s. Later, the region was opened for settlement. The watershed’s surface area is 366 km^2 and constitutes approximately 31% of the surface area of the whole city.

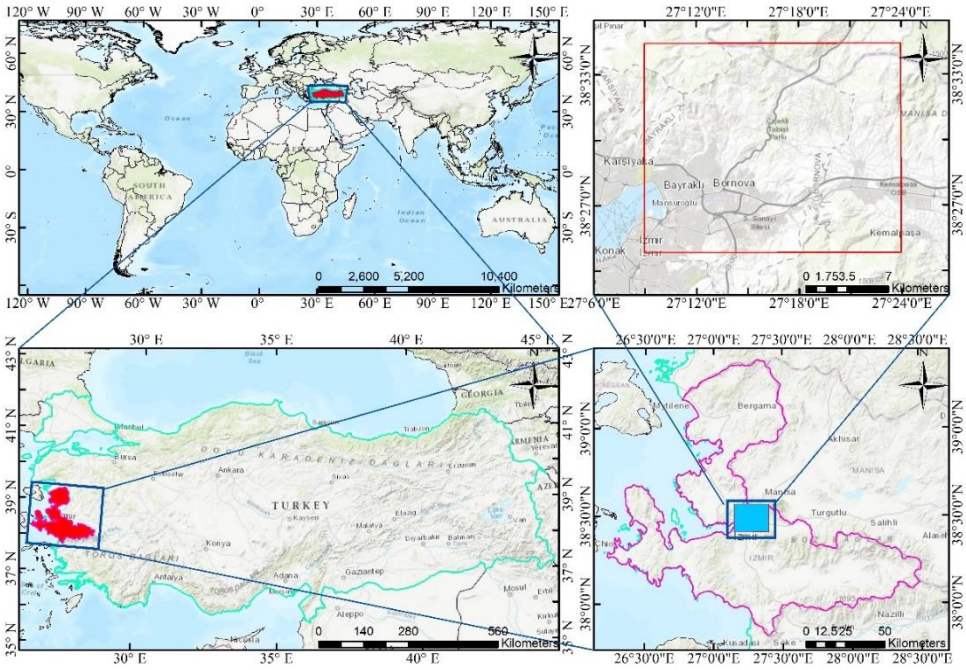

Figure 3.1. Location map of the study area

3.1.1. Population

Bornova Basin was used as agricultural land until the 1950s. After the region was opened for settlement, the region's population increased significantly. The region's population is around 750.000 and constitutes around 17% of the entire city's population (Source: TUIK, 2020). Figure 3.2. shows the population change over the years.

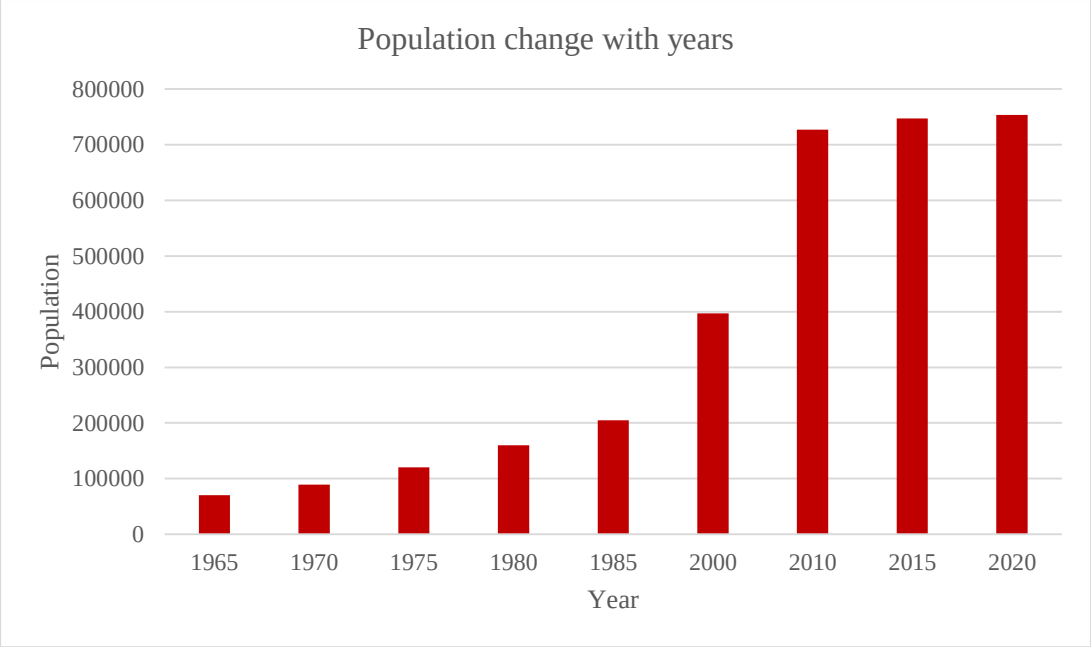

Figure 3.2. Population change over the years

3.1.2. Climate

Bornova Basin has typical Mediterranean climate characteristics seen in İzmir province. Summers in the region are hot and dry, and winters are mild and rainy. The number of days with snowfall is very few. Turkish State Meteorological Service (TSMS) has two weather stations in Bornova Basin. According to the data obtained from TSMS, between 2012 and 2019; monthly total average precipitation changes between 370 kg/m^2 and 28 kg/m^2 in rainy seasons (Figure 3.3); average temperature values change between 24 ºC and 30 ºC for hot seasons and 6 ºC and 13 ºC for cold seasons (Figure 3.4).

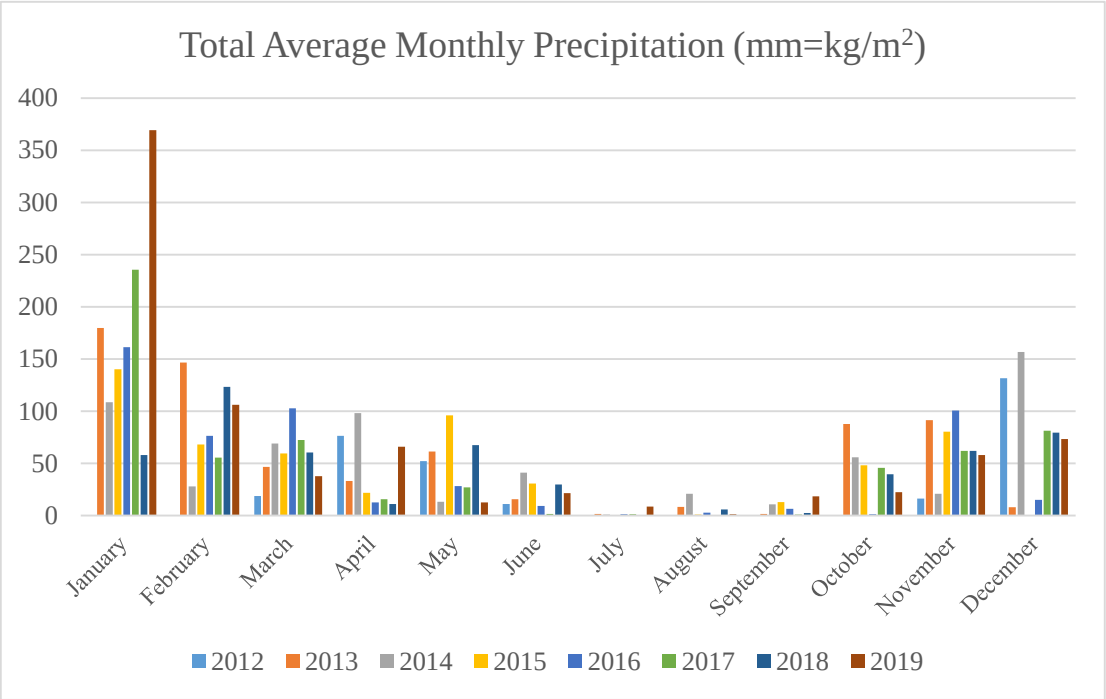

Figure 3.3. Monthly total average precipitation chart for years between 2012 and 2019

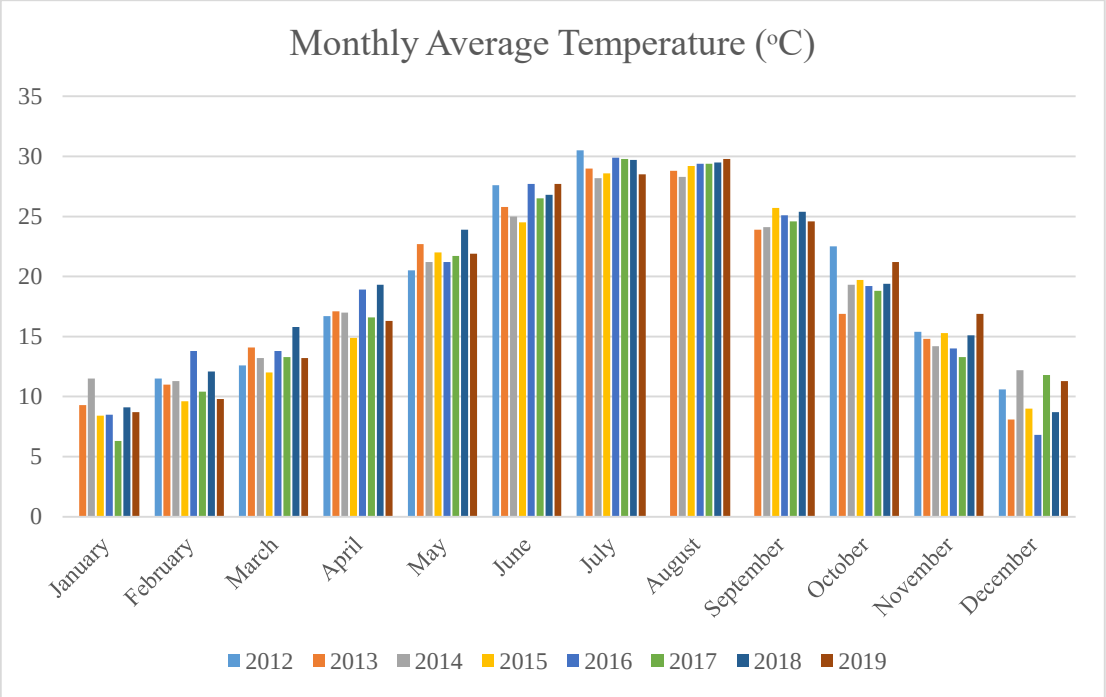

Figure 3.4. Monthly average temperature chart for years between 2012 and 2019

3.1.3. Geology

The Bornova mélange (alternatively referred to as the 'Bornova flysch zone') serves as the foundation for the Miocene to Quaternary strata that surround İzmir City (Figure 3.5). The Bornova mélange is made up of blocks of Mesozoic limestones, cherts, subsurface volcanic, and serpentinites of varied sizes buried in flysch sediment (Erdoğan 1990; Okay, Satir, Maluski, Siyako, Monie, Metzger, and Akyüz 1996). The Bornova mélange has been significantly deformed, resulting in a relatively low metamorphic grade (Erdoğan 1990; Okay and Siyako 1993; Okay and Altiner 2007; Uzel, Sozbilir, and Özkaymak 2012).

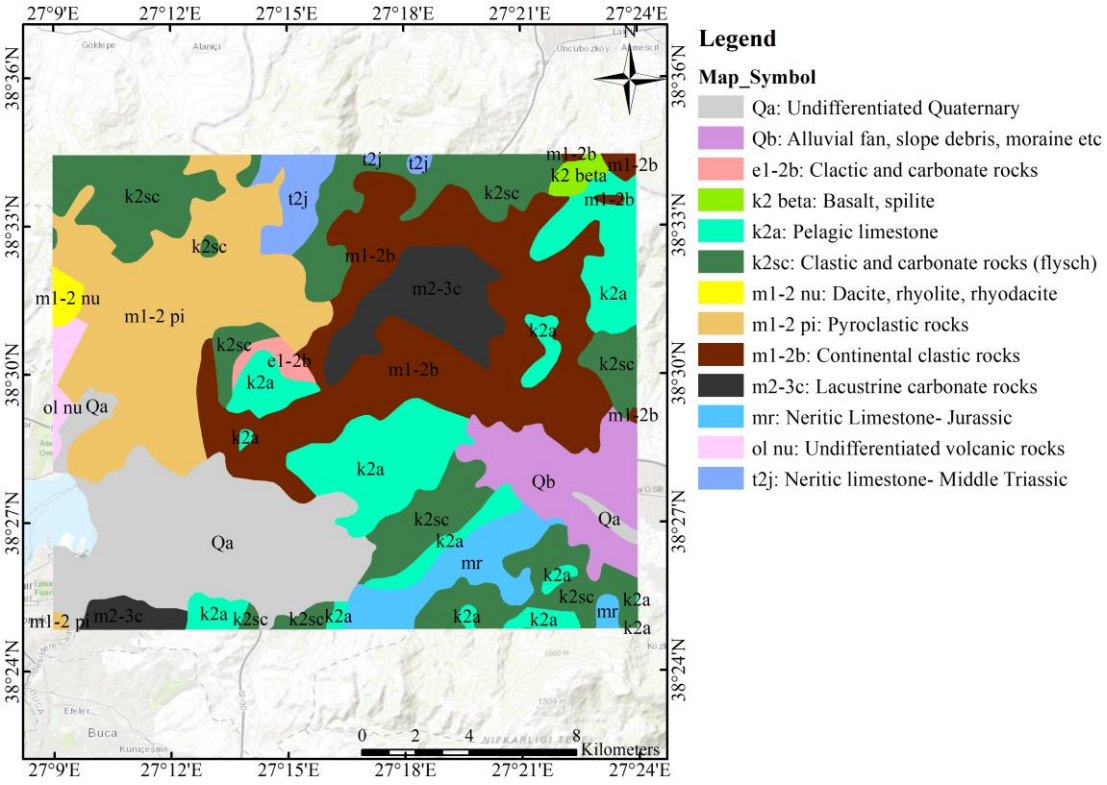

Figure 3.5. Geology map of the study area (modified from MTA, 2021)

Mesozoic limestone blocks provide the system's karstic aquifer, whereas the other Bornova mélange units are impermeable rocks. The Miocene units, which are predominantly composed of conglomerates at the base, mudstones, sandstone-shale alternations, and limestones, overlie the basement rocks in an unconformable fashion. Sandstone, limestone, and conglomerate are porous and permeable Miocene units. These rocks are also one of the system’s aquifers. Yamanlar volcanics' (calc-alkaline volcanic)

overlying units are composed of dacitic, rhyolitic, andesitic, pyroclastic rocks, and basaltic compositions. These permeable layers include groundwater resources. Yamanlar volcanic rocks have a fractured aquifer. The majority of the basin is composed of quaternary units composed of clayey, sandy, and gravely materials. The Quaternary is a significant aquifer for İzmir's groundwater resources (Baba and Yazdani 2012).

3.2. SWAT Model

3.2.1. Model Description

The Soil and Water Assessment Tool (SWAT) was developed for hydrological modeling on medium- to large-scale watershed models to predict the effects of land management practices such as land use and cover changes over long periods. SWAT is a physically-based, dimensionally semi-distributed, and optimized model that may be used to simulate a single basin or a network of connected basins. Additionally, it is capable of predicting water supply, nutrients, and sediment loading under scenarios of climate change (Neitsch, Arnold, Kiniry, and Williams 2011).

A basin is subdivided into subbasins in the SWAT model. Each subbasin is further subdivided into several uniform hydrological response units (HRUs) based on LULC variations, soil type, and slope. Simulated hydrological components, sediment production, and nutrient cycles are aggregated for each HRU and the subbasins.

SWAT simulates most hydrologic processes at the HRU level, where runoff is channeled to the reaches of subbasins and ultimately to the basin channel. Simulated SWAT model calculates hydrological components of the desired watershed; deep and shallow groundwater recharge, evapotranspiration (ET), potential evapotranspiration (PET), surface runoff, lateral flow, and return flow. SWAT prints out the calculated components on the schematic sketch (Figure 3.6).

$$SW_t = SW_0 + \sum_{i=1}^{t} \left(R_{day} - Q_{surf} - E_a - W_{seep} - Q_{gw}\right) \quad (3.1)$$

Where;

SW_t is the soil water content at time t (mm), SW_0 is the initial soil water content on the day i (mm), t is time (days), R_{day} is the amount of precipitation on the day i (mm), Q_{surf} is the amount of surface runoff on the day i (mm), $E_a$is the amount of evapotranspiration on the day i (mm), W_{seep} is the amount of water entering the vadose zone from the soil profile on the day i (mm), and Q_{gw} is the amount of return flow on the day i (mm).

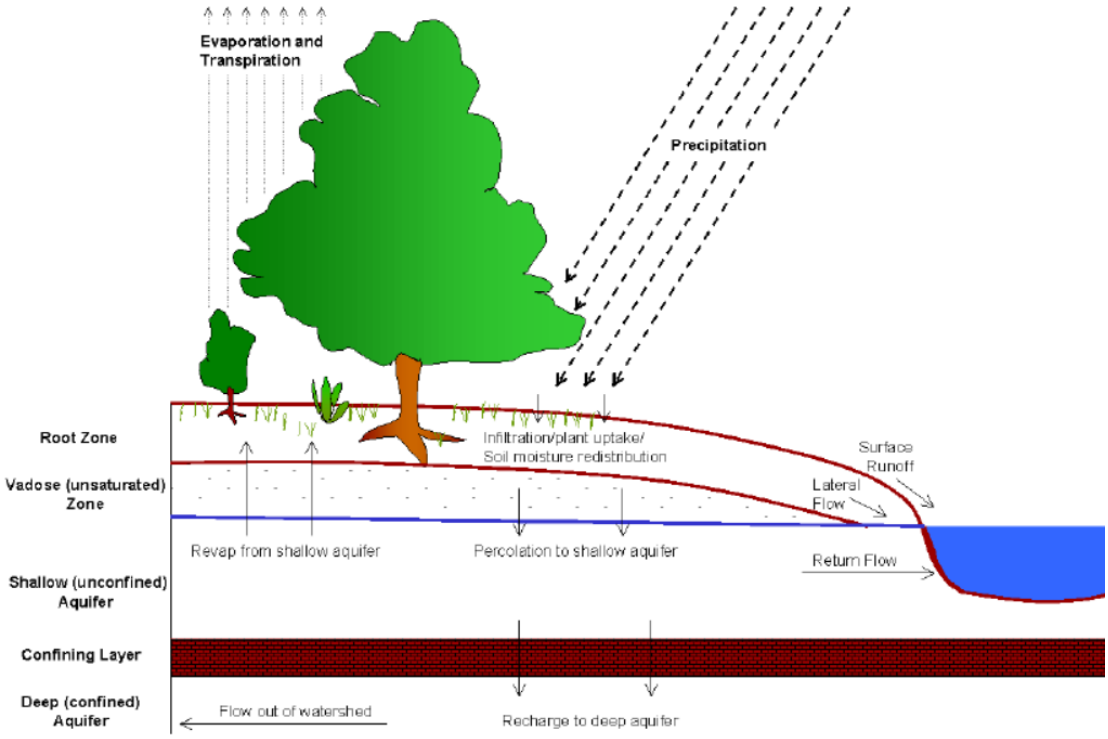

Figure 3.6. Schematic sketch of calculated components on SWAT

3.2.1.1. Rainfall

SWAT creates a random value between 0.0 and 1.0 to indicate whether a day is wet or dry using a first-order Markov-chain model with the input data. There are two different options for rainfall amount calculations in SWAT; the skewed distribution and

the exponential distribution. Nicks (1974) proposed the skewed distribution on a wet day as;

$$R_{day} = \mu_{mon} + 2 * \sigma_{mon} * \left(\frac{\left[\left(SND_{day} - \frac{g_{mon}}{6} \right) * \left(\frac{g_{mon}}{6} \right) + 1 \right]^3 - 1}{g_{mon}} \right) \quad (3.2)$$

Where;

R_{day} is the amount of rainfall on a given day (mm H_2O), $\mu_{mon}$is the mean daily rainfall (mm H_2O) for the month, σ_{mon} is the standard deviation of daily rainfall (mm H_2O) for the month, SND_{day} is the standard normal deviate calculated for the day, and g_{mon} is the skew coefficient for daily precipitation in the month.

The standard normal deviate for the day is calculated as;

$$SND_{day} = \cos(6.283 * rnd_2) * \sqrt{-2ln(rnd_1)} \quad (3.3)$$

Where;

rnd_2 and rnd_1 are random numbers between 0.0 and 1.0.

The exponential distribution is used as an alternative to the skewed distribution. The exponential distribution requires less input data and is used in areas where limited precipitation data is available. The exponential distribution is used to compute daily precipitation using the equation:

$$R_{day} = \mu_{mon} * \left(-ln(rnd_1) \right)^{rexp} \quad (3.4)$$

Where;

R_{day} is the amount of rainfall on a given day (mm H_2O), μ_{mon} is the mean daily rainfall (mm H_2O) for the month, rnd_1 is a random number between 0.0 and 1.0, and rexp is an exponent that should be set between 1.0 and 2.0.

For this study, skewed distribution was used to calculate the amount of precipitation as daily recorded precipitation data were available for simulations.

3.2.1.2. Surface Runoff

Surface runoff can be expressed as water flowing from higher elevation points to lower elevation points when the amount of precipitation is beyond the infiltration capacity of the soil. Two different surface runoff estimation methods are provided in SWAT.

The first method is the SCS curve number procedure (SCS 1972) which estimates the amount of surface runoff with changing land use and soil types. The SCS curve number is defined as (SCS 1972):

$$Q_{surf} = \frac{\left(R_{day} - I_a\right)^2}{\left(R_{day} - I_a + S\right)} \tag{3.5}$$

Where Q_{surf} is the accumulated runoff or rainfall excess (mm H_2O), R_{day} is the rainfall depth for the day (mm H_2O), I_a is the initial abstractions which include surface storage, interception, and infiltration prior to runoff (mm H_2O), and S is the retention parameter (mm H_2O). The retention parameter (S) fluctuates regionally and temporally as a result of changes in soils, land use, management, and slope. The retention parameter is expressed as;

$$S = 25.4\left(\frac{100}{CN} - 10\right) \tag{3.6}$$

Where CN is the curve number for the day. The initial abstractions, I_a is commonly approximated as 0.2S and Equation (3.5) becomes;

$$Q_{surf} = \frac{\left(R_{day} - 0.2S\right)^2}{\left(R_{day} + 0.8S\right)} \tag{3.7}$$

The runoff will take place if R_{day}>I_a. SWAT calculates runoff independently for each HRU and routes it to obtain the total runoff for each sub-basin. Then the basin's total runoff is determined by routing each sub-basin runoff.

3.2.1.3. Evapotranspiration

Evapotranspiration is expressed as water loss from soil and earth's surface to the atmosphere as a summation of evaporation from the soil, evaporation from the plants, transpiration, and sublimation. Primary water loss from a watershed or basin is caused by evapotranspiration. Potential evapotranspiration (PET) is the quantity of evapotranspiration that would occur across a surface with no water limitation. SWAT offers three methods for estimating the PET: The Hargreaves technique (Hargreaves and Allen 2003), the Priestly-Taylor method (Priestley and Taylor 1972), and the Penman-Monteith method (Monteith 1965; Allen, Sauer, Frank, and Reiff 1989). The Hargreaves method uses air temperature, and the Priestly-Taylor method uses air temperature, relative humidity, and solar radiation; the Penman-Monteith method uses air temperature, relative humidity, solar radiation, and wind speed as their input data. The Penman-Monteith method was chosen as the PET estimation method since air temperature, relative humidity, solar radiation, and wind speed data were available.

3.2.1.4. Recharge

Recharge is the process where the precipitation infiltrates through the soil layer and reaches the vadose zone. SWAT makes use of a precipitation/groundwater response model proposed by Venetis (1969) to account for the time lag in aquifer recharging after water exits the soil profile. The recharge to both aquifers on a given day is calculated:

$$w_{rchrg,i} = \left(1 - exp\left[-1/\delta_{gw}\right]\right) * w_{seep} + exp\left[-\frac{1}{\delta_{gw}}\right] * w_{rchrg,i-1} \quad (3.8)$$

Where;

$w_{rchrg,i}$ is the amount of recharge entering the aquifers on the day i (mm H_2O), δ_{gw} is the delay time or drainage time of the overlying geologic formations (days), w_{seep} is the total amount of water exiting the bottom of the soil profile on the day i (mm H_2O), and $w_{rchrg,i-1}$ is the amount of recharge entering the aquifers on the day i-1 (mm H_2O). On any given day, the total amount of water that exits the soil profile is calculated as follows:

$$w_{seep} = w_{perc,ly=n} + w_{crk,btm} \tag{3.9}$$

Where; w_{seep} is the amount of water exiting the bottom of the soil profile on a given day i (mm H_2O), $w_{perc,ly=n}$ is the amount of water percolating out of the lowest layer, n, in the soil profile on a day i (mm H_2O), $w_{crk,btm}$ is the amount of water flow past the lower boundary of the soil profile due to bypass flow on day i (mm H_2O).

The measurement of the delay time, δ_{gw} cannot be done directly. It may be calculated by modeling aquifer recharge with various values of X and comparing the simulated fluctuations in water table level to observed values.

3.2.1.5. Groundwater/Base Flow

The steady-state response of groundwater flow to recharge is (Hooghoudt 1940)

$$Q_{gw} = \frac{8000 * K_{sat}}{L_{gw}^2} * h_{wtbl} \tag{3.10}$$

Where;

Q_{gw} is the groundwater flor, or base flow, into the main channel on day i (mm H_2O), K_{sat} is the hydraulic conductivity of the aquifer (mm/day), L_{gw} is the distance from the ridge or subbasin divide for the groundwater system to the main channel (m), and h_{wtbl} is the water table height (m).

3.2.2. SWAT Model Inputs

All of the data sets and maps used in ArcGIS for the SWAT models were projected to WGS_1984_UTM_Zone_35N XY Coordinate System since ArcSWAT requires all input data to be in the same projection system to operate.

3.2.2.1. Digital Elevation Model (DEM)

The Digital Elevation Model is raster grids GIS layer representing of Earth's topographic surface altitude. The DEM is of the important SWAT Model inputs that are required for the hydrological analysis such as slope, flow direction, flow accumulation, and watershed delineation and sub-watershed delineation. High-resolution DEM data used for this study with a cell size of 12.5x12.5m has been acquired from open source ALOS PALSAR (https://asf.alaska.edu/) website and then adjusted to the study area (Figure 3.7).

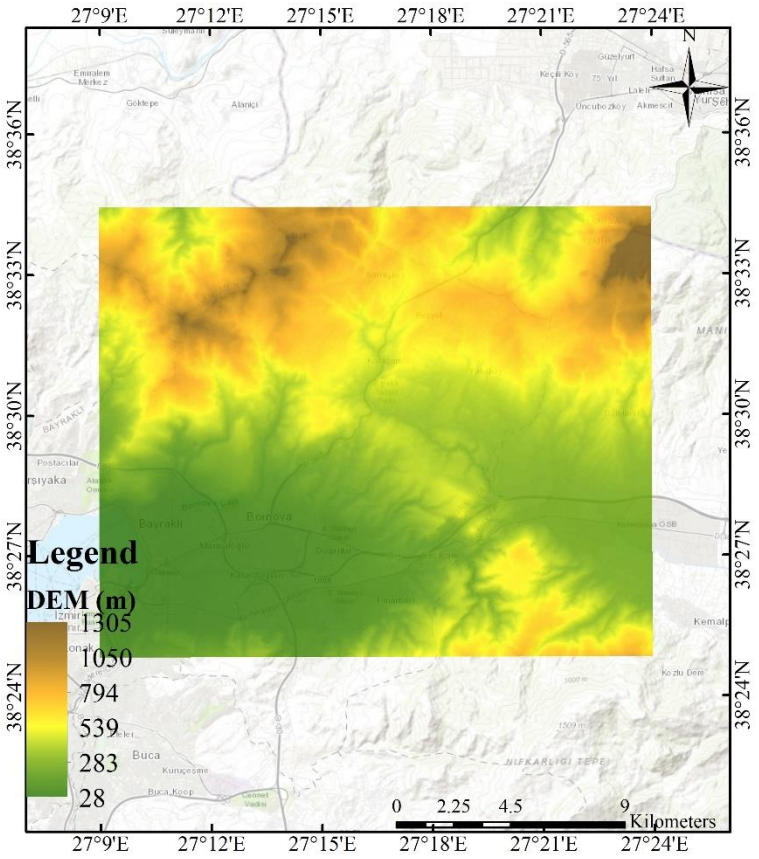

Figure 3.7. DEM of the Bornova Basin

3.2.2.2. Landuse/ Land Cover Map

Landuse/ Landcover maps are also important input of a SWAT model, which describes the study area's land usage.

Two different LULC maps were created for this study for two different time periods (2004 and 2020). Each of the LULC maps was created with the help of supervised classification for more accurate results.

High-resolution satellite images (cell size of 0.91x0.91) of the study area were acquired using Historical Imagery in Google Earth Pro computer software. Landsat imagery was tried to be chosen 0% cloud cover over the study area to minimize the LULC map errors. Obtained satellite images were then transferred to the ArcGIS and georeferenced to the WGS_1984_UTM_Zone_35N projection system.

Five different land use classes were created using Maximum Likelihood Classification for the periods 2004 and 2020.

In MLC, training samples are used to specify the LULC classes. Training samples were collected manually for each LULC class as much as possible for more accurate results. A signature file that is obligatory for MLC was created with the collected training samples. MLC creates a classified raster dataset by classifying all cells, with each class having equal probability weights attached to their signatures. MLC workflow can also be seen in Figure 3.8. Then by using raster analysis, percentages of each subcategory to the total study area for all three maps were also calculated (Table 3.1).

Table 3.1. LULC Classes Distribution as percentages over the study area

Year	**LULC Classes**				
	Forest (%)	**Pasture (%)**	**Water Body (%)**	**Urbanization (%)**	**Bare Land (%)**
2004	37.9	19.3	0.9	13.7	28.2
2020	40.1	16.9	1.2	21.5	20.3

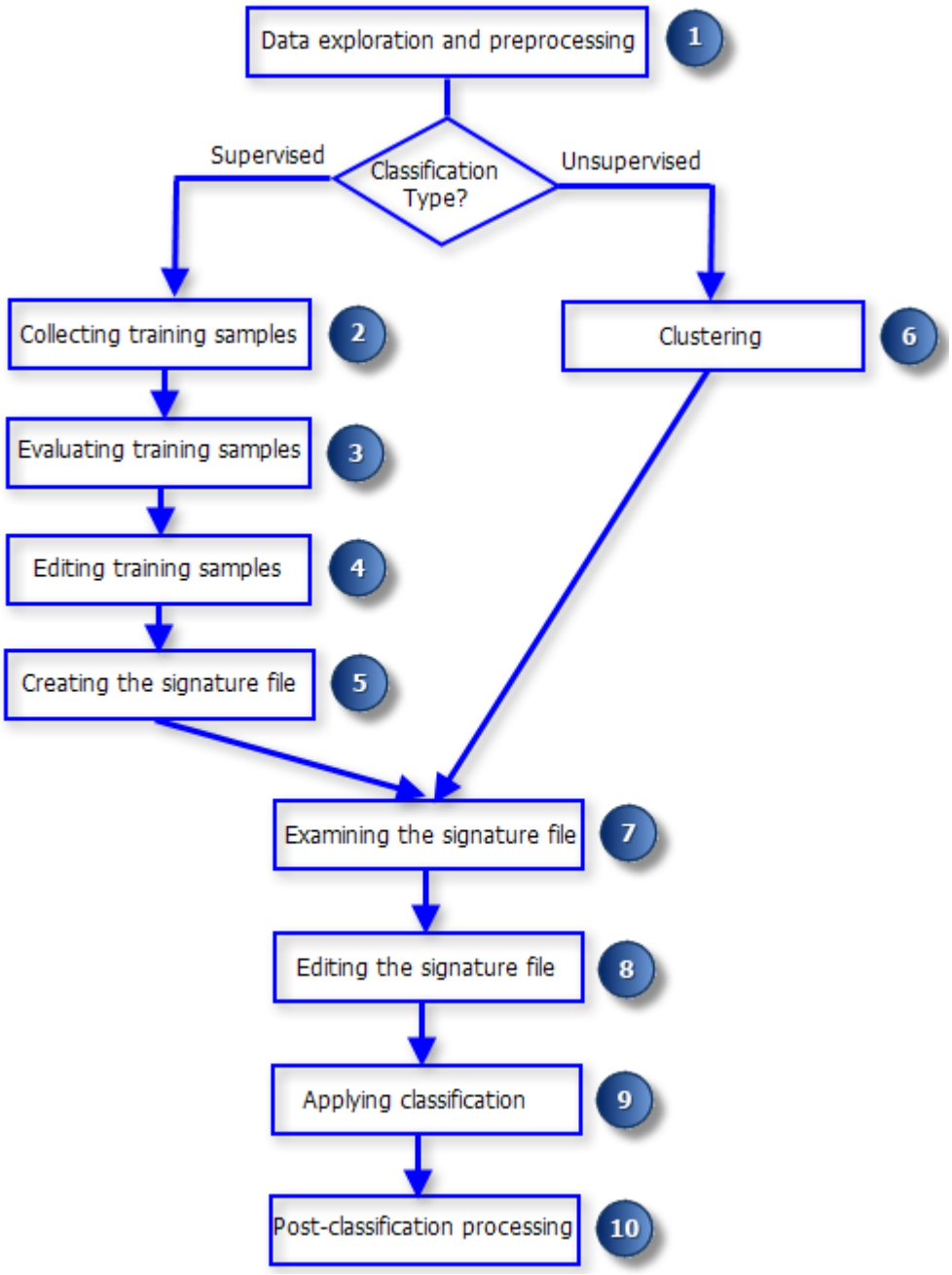

Figure 3.8. MLC workflow

(Source: arcgis.com)

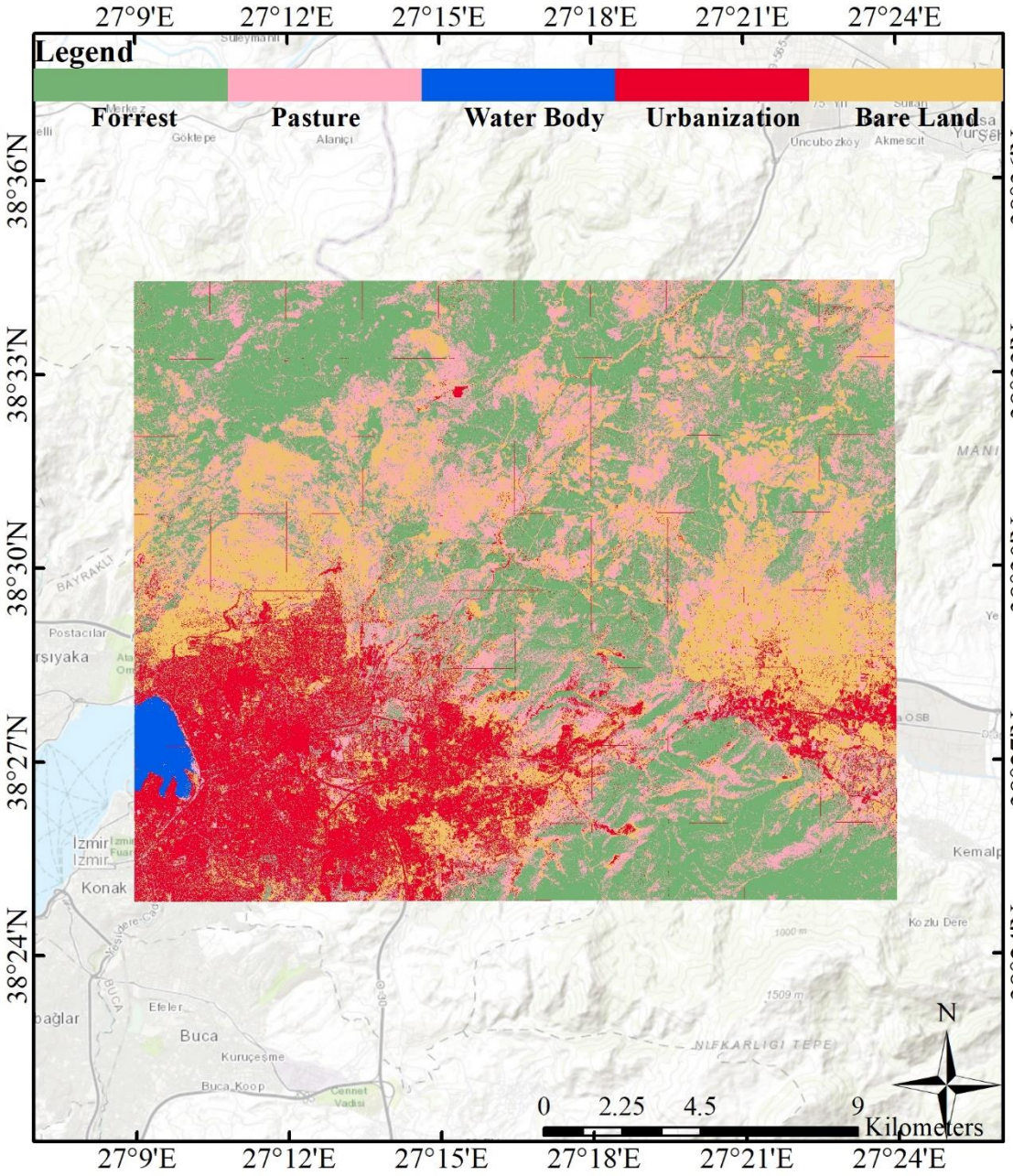

Figure 3.9. LULC map of the year 2004

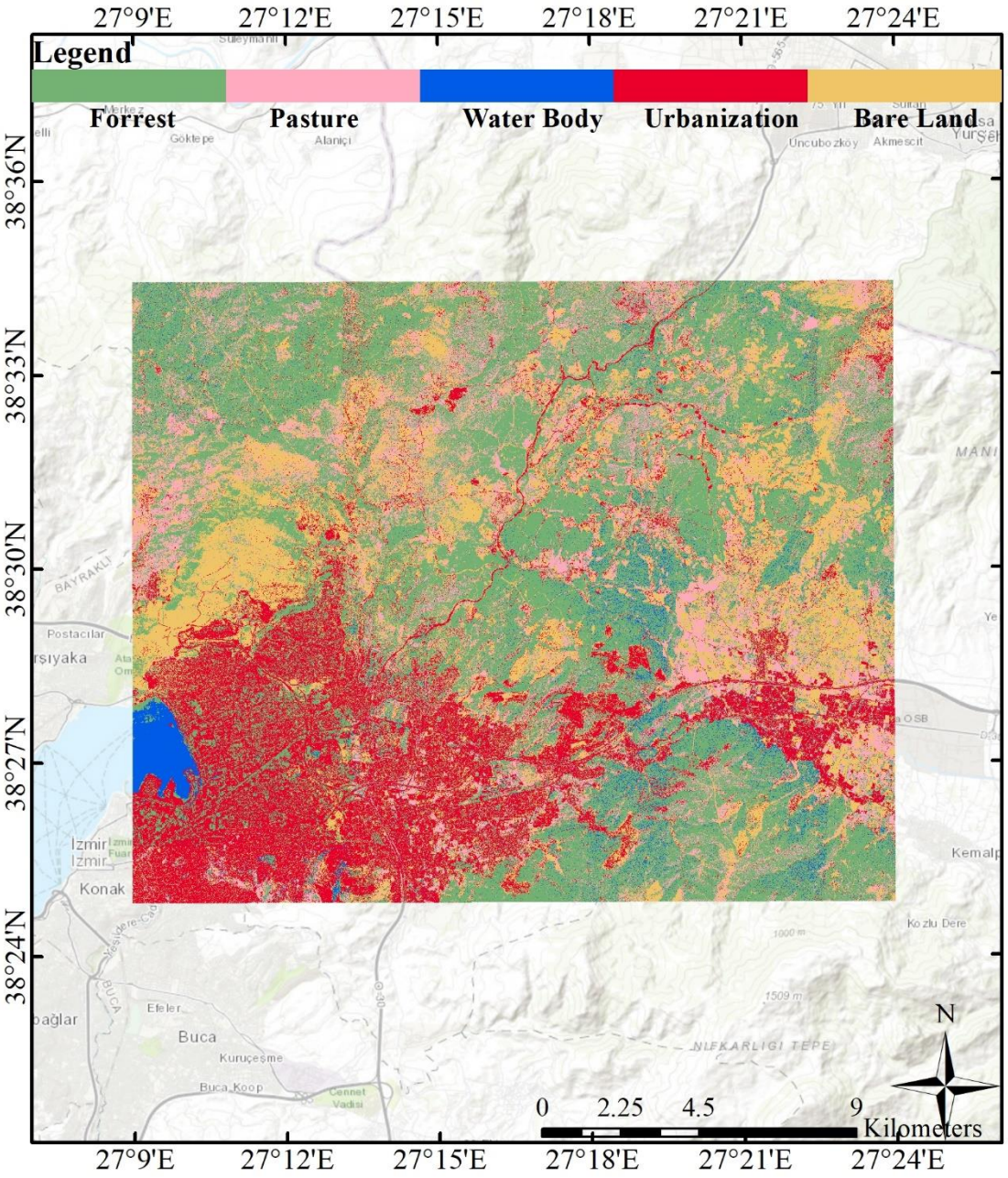

Figure 3.10. LULC map of the year 2020

3.2.2.3. Soil Map

A 1/ 5 000 000 scaled soil map in shapefile format was received from the Food and Agriculture Organization of the United Nations (FAO / UNESCO). The downloaded soil map contains information on soil types and distribution and soil features such as soil hydrologic group, soil texture, soil depth, porosity, and water capacity of soil layers; silt, clay, sand, and rock fractions, among others. FAO Soil Map then adjusted and imported to SWAT.

3.2.2.4. Meteorological Data

Daily rainfall, wind speed, solar radiation, maximum and minimum temperature data for the SWAT model are required. All the meteorological data has been obtained from the NASA POWER website (power.larc.nasa.gov.tr). One station data was obtained from NASA POWER at the latitude: 38.56 and longitude: 27.188. Available data obtained from the NASA POWER was MERRA-2 Wind Speed at 10 Meters (m/s), MERRA-2 Relative Humidity at 2 Meters (%), MERRA-2 Temperature at 2 Meters Maximum (^{o}C), MERRA-2 Temperature at 2 Meters Minimum (^{o}C), and All-Sky Surface Shortwave Downward Irradiance (MJ/m^2). The selected date range is between the years 2000 and 2020. All the downloaded meteorological data is then prepared as a .txt file to put into the SWAT model.

3.2.3. Soil and Water Assessment Tool (SWAT) Model Development

3.2.3.1. Watershed Delineation

Automatic watershed delineation was performed with the produced DEM Raster input. The previously prepared DEM Raster was uploaded to DEM Setup. Then Stream Definition was performed, which has two options for the users. The first is the DEM-based Stream Definition, and the other is Pre-defined streams and watersheds. If

previously performed, created, or obtained, stream and watershed datasets are available (which must have subbasin IDs). They can be put into the toolbar with the Pre-defined streams and watersheds option. If stream or watershed datasets are not pre-defined, then DEM-based Stream Definition must be performed. The tool uses the uploaded DEM Raster and automatically calculates flow direction and accumulation.

With flow direction and accumulation calculation, upstream drainage area values are found as 219 ha. Upstream drainage areas can be changed manually after the calculation. For the simulations, 219 ha was altered to 50 ha to obtain a more detailed drainage network. After changing the upstream drainage area to 50 ha, the tool produced streams and outlets. One hundred eighty-six linking stream added outlets were produced by the tool automatically (Figure 3.11 (a)). Automatically created outlets can be deleted manually, and new outlets can also be added to the streams manually. As shown in Figure 3.11 (b), undesired outlet points were extracted from the system, and the outlet number was decreased from 186 to 20. Afterward, all the outlets were selected, and "Delineate Watershed" was activated. After calculating subbasin parameters, the watershed delineation process was completed. Basin and 20 watersheds were created with the automatic watershed delineator in the study area. Figure 3.12 (a) shows created basin border, and Figure 3.12 (b) shows subbasin borders created over the basin.

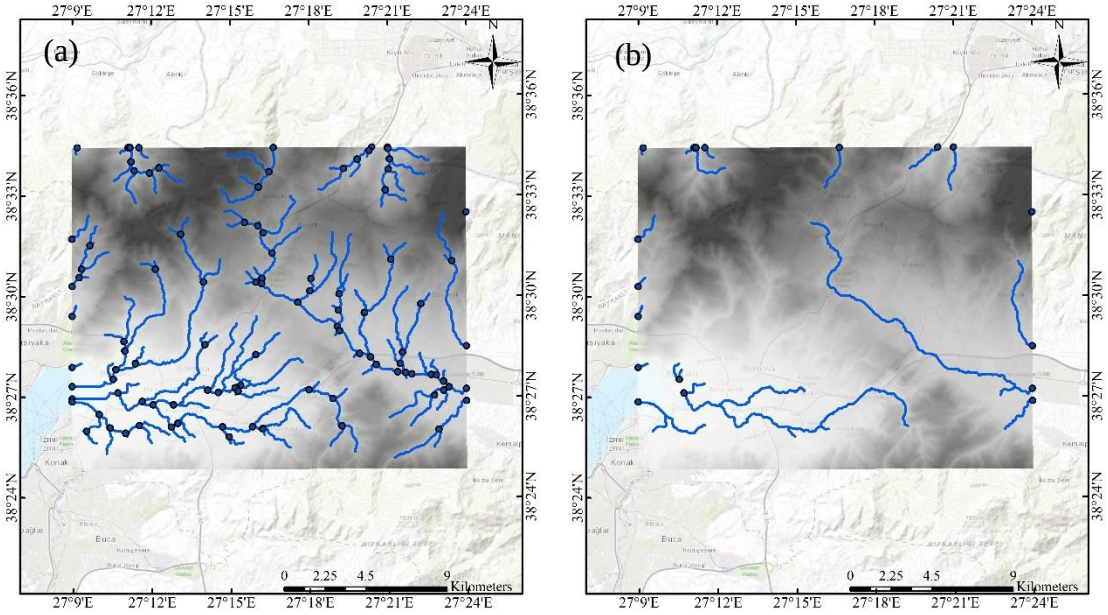

Figure 3.11. (a) Automatically created streams and outlets (b) selected streams and outlets

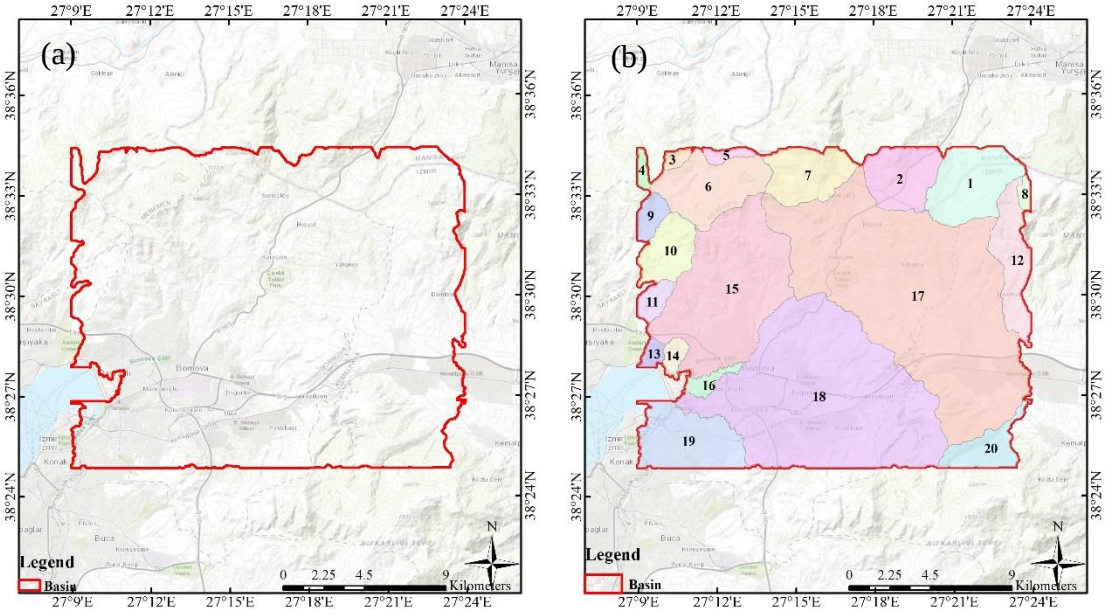

Figure 3.12. (a) Created basin border (b) subbasin borders

3.2.3.2. Hydrological Response Unit (HRU) Analysis

For SWAT to create the HRUs, Landuse/Soils/Slope definition was performed in the HRU Analysis toolbar of SWAT. Previously prepared LULC Maps were chosen as grid fields for each SWAT model.

For Landuse data definitions, lookup tables were also prepared previously. For 2004 and 2020, LULC classification is divided into five subcategories: Forest, Pasture, Water Body, Urbanization, and Bare Land (details on Chapter 3.2.2.2 Landuse/ Land Cover Map). SWAT codes of the LULC subcategories depicted in Table 3.2 are prepared as a .txt file for SWAT to automatically check and fill into the SWAT Landuse Classification Table.

Table 3.2. SWAT Codes of the LULC Categories

LULC Category	SWAT CODE
Forest	FRST
Pasture	PAST

(Continue on next page)

(Table 3.2 cont.)

Water Body	WATR
Urbanization	URHD
Bare Land	SWRN

For Soil data definition, prepared soil map was also chosen as grid field, and prepared .txt file containing soil codes was selected as UserSoil as shown in Table 3.3.

Table 3.3. SWAT Soil Classification Table

Value	**Area (%)**	**Name**
3114	74.54	I-Lc-E-2b-3114
3139	25.46	Jc49-1-3a-3139

For the Slope definition, five different slope classes were created as can be seen in Table 3.4.

Table 3.4. SWAT Slope Classification Table

Class	**> Lower Limit**	**<= Upper Limit**
1	0	5
2	5	10
3	10	15
4	15	25
5	25	9999

All three tables were reclassified and then overlaid together for the HRU Definition process. For the HRU Definition process, the Multiple HRUs options were chosen. Land use percentage over subbasin area (%) was chosen as 1%, soil class percentage over land use area (%) was chosen as 10%, slope class percentage over soil area (%) was chosen as 20% for this study for all the simulations. After, HRUs were created. SWAT created 188 HRUs for the year 2004, 187 HRUs for 2020 simulations.

3.2.3.3. Write Input Tables

Weather stations under the tool Write Input Tables were selected as the first step. WGEN_CFSR_World was chosen as the Monthly Weather Database. Afterward, previously prepared .txt files (details on Chapter 3.2.2.4 Meteorological Data) were uploaded to sections, Rainfall Data, Temperature Data, Wind Speed Data, Solar Radiation Data, and Relative Humidity data sections. As the second step, Write SWAT Input Tables under the tool Write Input Table was chosen, and all the tables were selected to be created. As the third step, Database Update under the tool Write Input Tables was selected, and all the tables were updated.

3.2.4. SWAT Model Simulation

SWAT Simulation toolbar under the SWAT tool was selected. Then the model was run. For each simulation, starting and ending dates were input. For the Rainfall Distribution, Skewed Normal was selected. Three years of the warm-up period was input for each simulation. After, SWAT Run was set up and run. Desired output files were imported to the database under the Read SWAT Output toolbar. Each simulation was saved for later use and calibration.

3.2.5. Sensitivity Analysis of the Model Parameters

Sensitivity analysis is performed to determine the sensitivity of the model parameters. Specified high-sensitive model parameters can then be selected to calibrate the model. The sensitiveness of the input parameters is decided according to their t-Stat and P-values. The model parameters are most sensitive as the greater the absolute value of t-Stat and the smaller the P-value. An automatic sensitivity analysis tool presented in SWAT-CUP was used. Twenty-two hydrological parameters were tested, and eighteen were chosen to calibrate the models according to their sensitivities. Table 3.5 shows the used twenty-two hydrological model parameters selected for the sensitivity analysis and

the range for those parameters. The maximum and minimum values for parameters were chosen by combining literature studies and the program's default minimum and maximum values.

Table 3.5. Twenty-two hydrological parameters used for sensitivity analysis and their chosen minimum and maximum values

Parameter Code	Description	Min Value	Max Value
R__CN2.mgt	SCS runoff curve number f	-0.2	0.2
V__EPCO.hru	Plant uptake compensation factor	0	1
V__ESCO.hru	Soil evaporation compensation factor	0.8	1.0
R__SOL_Z(..).sol	Depth from soil surface to bottom of layer	-0.25	0.25
R__SOL_AWC(..).sol	Available water capacity of the soil layer	-0.25	0.25
V__CANMX.hru	Maximum canopy storage	0	10
R__SOL_BD(..).sol	Moist bulk density	-0.25	0.25
V__CH_N1.sub	Manning's "n" value for the tributary channels	0	0.15
R__SOL_K(..).sol	Saturated hydraulic conductivity	-0.25	0.25
V__GW_REVAP.gw	Groundwater "revap" coefficient	0.0	0.2
V__ALPHA_BF.gw	Baseflow alpha factor (days)	0.0	1.0
V__CH_N2.rte	Manning's "n" value for the main channel	0.0	0.3
R__SOL_ALB(..).sol	Moist soil albedo	-0.25	0.25
R__CH_K1.sub	Effective hydraulic conductivity in tributary channel alluvium	0.2	200
V__GW_DELAY.gw	Groundwater delay (days)	30.0	450.0
A__REVAPMN.gw	Threshold depth of water in the shallow aquifer for "revap" to occur (mm)	0	500
V__CH_K2.rte	Effective hydraulic conductivity in main channel alluvium	0.0	130.0
R__SLSUBBSN.hru	Average slope length	-0.25	0.25
V__RCHRG_DP.gw	Deep aquifer percolation fraction	0	1
V__SURLAG.bsn	Surface runoff lag time	0.05	24
V__ALPHA_BNK.rte	Baseflow alpha factor for bank storage	0.0	1
V__GWQMN.gw	Treshold depth of water in the shallow aquifer required for return flow to occur (mm)	0.0	2.0

3.2.6. Calibration and Validation of SWAT Models

SWAT Calibration and Uncertainty Program (SWAT-CUP) was used to calibrate and validate the simulated SWAT Models. SWAT-CUP includes different procedures (SUFI-2, GLUE, ParaSol, MCMC, and PSO) as calibration methods that link inputs and outputs of SWAT (Abbaspour 2015).

Sensitive input parameters are modified within an acceptable range with model calibration to match the simulated model output with the measured data. For this study, discharge data were obtained from DSİ (State Hydraulic Works).

Monthly discharge data measured from stream gauge located on Arap Stream from 1990 to 2014 were used for calibration and validation. The obtained discharge data were separated into two groups. The data between 1990 and 2005 were used for calibration, and the data between 2006-2014 were used for validation.

SWAT offers two options to calibrate the models either manually or automatically. For this study, automatic calibration was used, and the SUFI-2 algorithm was chosen. Previously prepared SWAT model simulations' TxtInOut location was input to SWAT-CUP New Project Wizard. After the project setup, all the necessary input files are created in SWAT-CUP.

Figure 3.13 represents the creation mechanism of SUFI-2 input files. Twenty-two parameters (Table 3.5) and their methods, minimum and maximum values were input to Par_inf.txt under the Calibration Inputs toolbar.

The number of the simulation was chosen as 500. Observed and obtained discharge data then was input to observed_rch.txt file under the Observation toolbar. The number of observed variables was selected as one since the only available observed data was discharge.

Subbasin 17 was also chosen since the stream gauge is located in the seventeenth subbasin. Three years (1987-1990) was selected as the warm-up period.

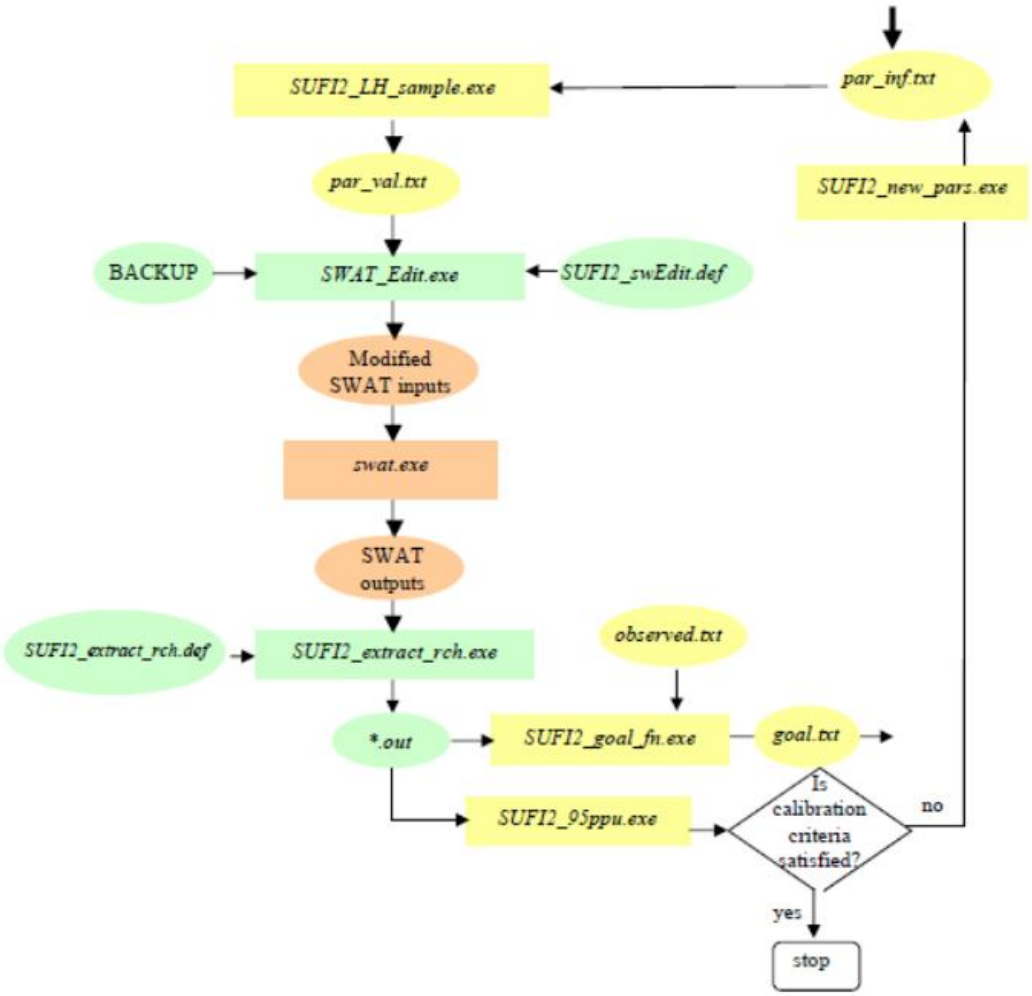

Figure 3.13. Step by step creating of SWAT-SUFI2 input files

(Source: Abbaspour 2015)

3.2.7. Model Performance Evaluation

SWAT-CUP includes ten different objective functions to evaluate the SWAT models' performances and compare simulated SWAT data to observed data. Among these ten objective functions, two of them were chosen for this study: coefficient of determination (R^2) and Nash-Sutcliffe (NS). SWAT-CUP tests are conducted on both of them to determine which one produces the best result. Numerous iterations were performed for each individual. The model concludes that the NS can be utilized as the objective function in situations that produce a superior result.

CHAPTER 4

BEARING CAPACITY ANALYSIS

4.1. Bearing Capacity Analysis

Groundwater is one of the main parameters that affect the soil bearing capacity. This chapter investigates the effect of groundwater level change caused by urbanization on soils bearing capacity. Groundwater levels decrease in the summers in the study area since the precipitation doesn't recharge the groundwater enough. Bornova and Bayraklı regions depend on groundwater as the primary freshwater source for domestic and industrial usage. With the increasing population and urbanization in the study area, the pumping of groundwater increases in the summer as the water need increases in summers and the groundwater level decreases. It's expected to have a more significant difference between groundwater level fluctuations in urban areas than the rural areas since the natural hydrological cycle is disturbed by groundwater extraction.

In Turkey, most of the constructions are conducted in summers since the rain effect doesn't impact the construction site too much. In most cases, boreholes are drilled in summers. Soil samples are taken in the summer for the laboratory tests and classification of the soil and all the necessary parameters for geotechnical designs. Also, the groundwater level that is used for the geotechnical modeling is measured with the drilling process.

Fluctuations of the groundwater level affect almost all the design parameters. Terzaghi in 1943 (Bowles 1997) suggested the following method to calculate the ultimate bearing capacity of the soil for strip foundations.

$$q_u = c'N_c + qN_q + \frac{1}{2}B\gamma N_\gamma \tag{4.1}$$

Where

c' is the cohesion of the soil, γ is the unit weight of the soil, q is the equivalent surcharge, B is the shorter side of the footing N_c, N_q, N_γ are bearing capacity factors that are non-dimensional and are functions only of the soil friction angle ϕ'.

The following equation calculates equivalent surcharge (q);

$$q = \gamma D_f \tag{4.2}$$

Where,

D_f is the depth of the foundation.

N_c, N_q, N_γ are calculated by;

$$N_c = \cot \phi' \left[\frac{e^{2\left(\frac{3\pi}{4} - \frac{\phi'}{2}\right)\tan \phi'}}{2cos^2\left(\frac{\pi}{4} + \frac{\phi'}{2}\right)} \right] \tag{4.3}$$

$$N_q = \frac{e^{2\left(\frac{3\pi}{4} - \frac{\phi'}{2}\right)\tan \phi'}}{2cos^2\left(45 + \frac{\phi'}{2}\right)} \tag{4.4}$$

$$N_\gamma = \frac{1}{2}\left(\frac{K_{p\gamma}}{cos^2\phi'} - 1\right)\tan \phi' \tag{4.5}$$

Where,

$K_{p\gamma}$ is the passive pressure coefficient.

All the soil parameters given above for Terzaghi's bearing capacity equation are affected by the water directly. For this study, the effect of the water on parameters c' and ϕ' is neglected. The impact of capillarity is also neglected.

Three different cases were suggested to modify the bearing capacity equation concerning groundwater level (Das 2007). Case I and Case II were proposed for the conditions where the water table is close or above the foundation, and Case III is proposed for the condition where the water table is far below the foundation (Figure 4.1).

Case I is where the water table is above the foundation's bottom end ($0 \leq D_1 \leq D_f$). For Case I, q is replaced as;

$$q = D_1\gamma + D_2(\gamma_{sat} - \gamma_{wat}) \tag{4.6}$$

Where;

γ_{sat} is the saturated unit weight of soil and γ_{wat} is the unit weight of water.

Last term's γ of the Equation (4.1) is changed by;

$$\gamma' = \gamma_{sat} - \gamma_{wat} \tag{4.7}$$

Combining Equation (4.6) and Equation (4.7), Equation (4.1) becomes for the Case I;

$$q_u = c'N_c + [D_1\gamma + D_2(\gamma_{sat} - \gamma_{wat})]N_q + \frac{1}{2}B(\gamma_{sat} - \gamma_{wat})N_\gamma \tag{4.8}$$

Case II is where the water table is below the foundation's bottom end, yet the water affects the foundation ($0 \leq d \leq B$) q is used as in Equation (4.2) for this case.

Last term's γ of the Equation (4.1) is changed by;

$$\bar{\gamma} = \gamma' + \frac{d}{B}(\gamma - \gamma') \tag{4.9}$$

Combining Equation (4.9) into Equation (4.1), Equation (4.1) becomes;

$$q_u = c'N_c + \gamma D_f N_q + \frac{1}{2}B(\gamma' + \frac{d}{B}(\gamma - \gamma'))N_\gamma \tag{4.10}$$

Case III is where the water table is located as $d \geq B$, and the water table doesn't affect the foundation.

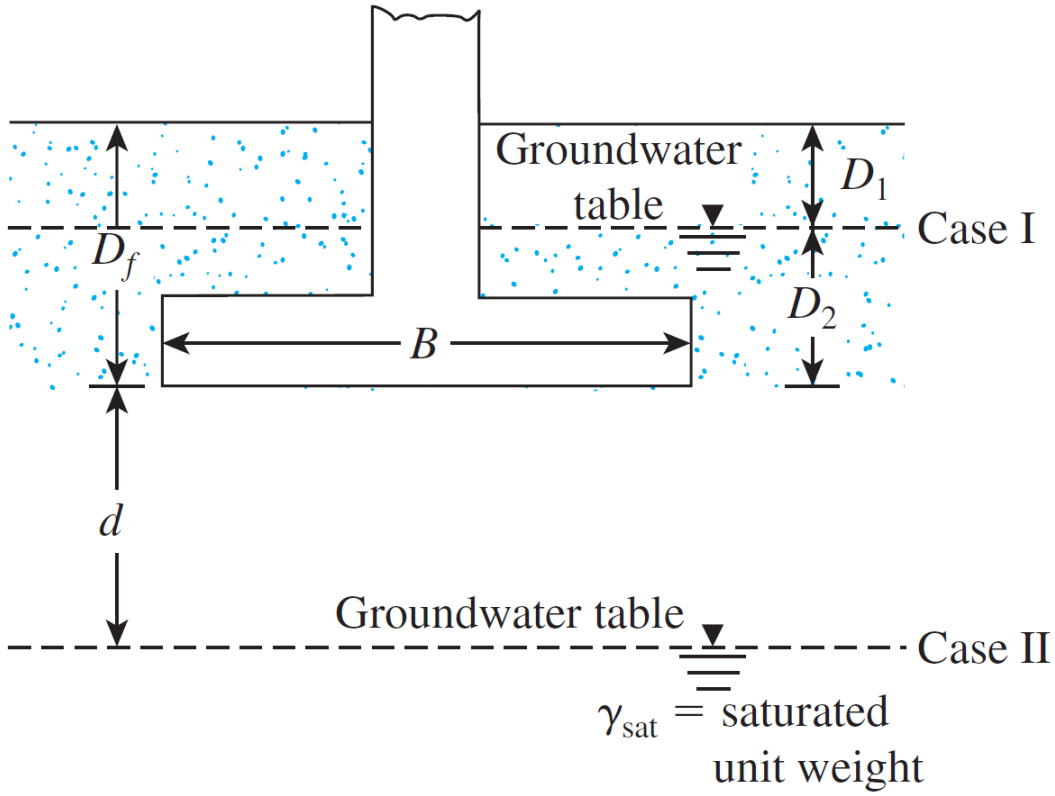

Figure 4.1. Modification of bearing capacity equations for water table (Source: Das 2007)

All the soil and foundation parameters were parameterized relative to actual field values for this study. Groundwater levels were recorded in the study area. Terzaghi's method was used to evaluate the bearing capacity of the soil.

4.1.1. Groundwater Level Measurements

Ten logging holes (Figure 4.2) were drilled in Bayraklı Region on 24 October 2020 to measure groundwater levels regularly. VanEssen branded automatic groundwater data loggers (divers) were installed in five of them (SK-1, SK-3, SK-6, SK-7, SK-9). Divers can take measurements with intended time intervals. All the divers were set to take hourly measures. Divers measure and record the groundwater's equivalent hydrostatic pressure and temperature above the pressure and temperature sensors. The accuracy of the divers is $\pm$0.5 cm H_2O in hydrostatic pressure, and $\pm$0.1 ^oC in temperature. In order to calculate the groundwater level from the hydrostatic pressure, Baro-Diver was also

installed in one well to measure barometric pressure. All the divers were attached to the wells with chrome-steel wires since chrome-steel wires are both elastic and stainless. The used wire cable lengths were recorded for later use to calculate the groundwater level to ground level. The other five wells that do not contain any divers were used for manual measurements, and monthly measurements were taken using water level meters. Diver data between 24-October-2020 and 24-October-2021 were used for this study.

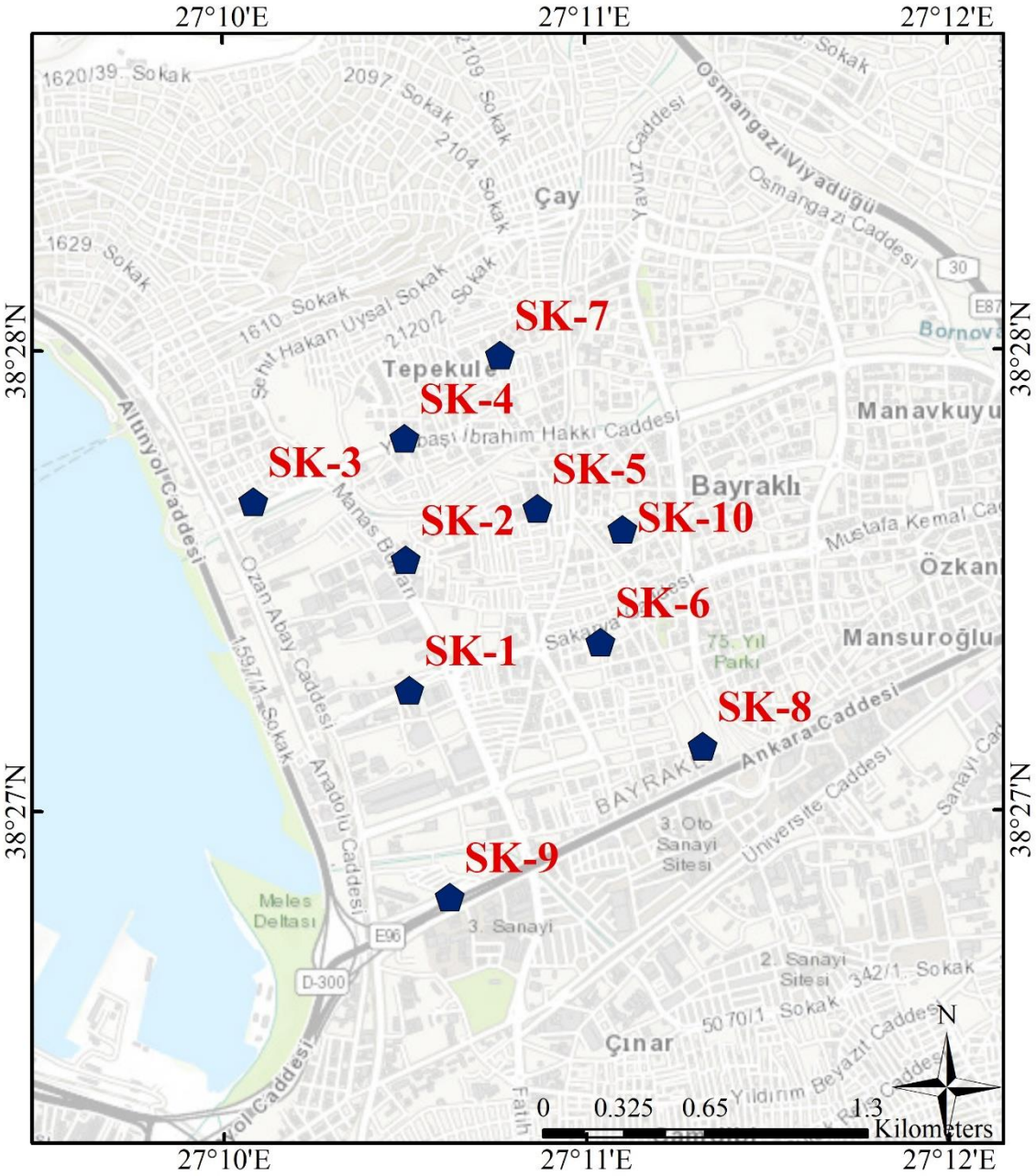

Figure 4.2. Locations of the drilled observation boreholes in the region

Divers record the measured data within their internal memory. Divers can be connected to computers with a USB device specifically designed for this purpose. After

connecting the divers to the computer, all the data within the divers' internal memory can be exported using VanEssens Instrument's Diver-Office software. All the exported data to Diver-Office can then be exported to Microsoft Excel as .csv or .xlsx files.

Imported data sheets include temperature, pressure, and time data. Pressure is the total pressure of hydrostatic water and barometric pressures. In order to calculate the water column (WC) in cmH_20;

$$WC = P - P_{baro} \tag{4.11}$$

Where;

WC is hydrostatic pressure in cmH_20, P is total pressure recorded by the sensor cmH_20, and P_{baro} is the barometric pressure obtained from the barometric diver placed in the SK-9 observation well.

The cable length of the divers was intentionally used a lot larger than the initially measured groundwater level in case of extreme groundwater decline. The groundwater level concerning the ground level can be calculated by using the following equation.

$$GWL = CL - WC \tag{4.12}$$

Where,

GWL is the groundwater level in cmH_20, and CL is the cable length of the diver.

4.1.2. Foundation Parameterization

Terzaghi suggested different formulations for bearing capacity calculations for different types of footings. For this study, strip type of footing was chosen to parameterize. Equations (4.1), (4.8), and (4.10) in Chapter 4.1 were developed for the

strip type of footings. Four different values were chosen for the (B/D_f) as 1, 0.33, 0.2, and 0.1.

4.1.3. Soil Parameterization

Soil parameters for the bearing capacity calculations were parameterized according to the study area's boring logs and experimental data. Relative averages of these data were chosen as the case data. The study area is mainly comprised of sandy and clayey soils. The cohesion of the soil was chosen as 10 kN/m^2, and the friction angle was chosen as 34 °. TThe saturated unit weight of the soil was chosen 20 kN/m^3, and the dry unit weight of the soil was chosen 16 kN/m^3. N_c, N_q, and N_γ coefficients were calculated using Equations (4.3),(4.4), and (4.5), respectively. N_c, N_q, and N_γ values were determined as 37.16, 22.46, and 19.13, respectively.

CHAPTER 5

PILE SETTLEMENT

5.1. Numerical Modeling

Bayraklı region is called the new city center of İzmir where most of the city's skyscrapers are located in the region. Tall buildings have much greater structural loads to convey to their foundation than moderately tall or low-story buildings. Piles are widely used to overcome excessive building loads. This chapter investigates pile deformation changes with varying groundwater levels caused by urbanization. In order to investigate these changes, PLAXIS 3D software was used. Two different groundwater levels were used to investigate the settlement changes with different water levels. 1.8 m and 3.5 m of groundwater levels were used for this study. Three D_p/L_p parameterizations were also used for two types of soil, and a total of 12 models were created as a result.

5.1.1. Plaxis 3D

PLAXIS 3D is a finite element program for analyzing deformation and stability in three dimensions in geotechnical engineering. It is packed with characteristics that enable it to cope with various complicated geotechnical structures and building processes using computational algorithms. PLAXIS 3D enables the definition of complicated geometries of soil and buildings in two distinct modes. These modes have been designed particularly for soil and structural modeling. Soil models can be intersected and meshed automatically. Structural elements and soil volumes can be activated and deactivated in the staged construction phase to create realistic building and excavation operations. PLAXIS 3D is a user-friendly three-dimensional geotechnical application with customizable and interoperable geometry and realistic building stage simulations (PLAXIS 2021).

5.1.1.1. Project and Model Properties

Before starting the PLAXIS 3D Analysis, project and model properties must be defined. For units, lengths were defined as m; forces were defined as kN; time was defined as day; stress was defined as kN/m^2; weight was defined as kN/m^3. Earth gravity was selected as 9.81 m/s^2 as 1.0 G (-Z direction), and γ_{water} was selected as 10 kN/m^3. Contours were created as X_{min}=0m, X_{max}=50m, Y_{min}=0m, and Y_{max}=50m for D_p/L_p=1/10, and they were created as X_{min}=0m, X_{max}=200m, Y_{min}=0m, and Y_{max}=200m for D_p/L_p=1/25 and 1/50.

5.1.1.2. Soil Parameters

Few numbers borehole data were available for the selected study area. For this study, all the soil parameters were selected relative to those boring log data. Two different soil types as Clay and Sand were used for the deformation analysis. Both soil types were included in PLAXIS 3D as Soil and interfaces materials.

For both clay and sand soils, Mohr-Coulomb material models were selected. Drainage type was selected Undrained (B) for clay and Drained for sand.

- Unsaturated unit weights (γ_{dry}) of clay and sand were selected as 16 kN/m^3, and 18 kN/m^3, respectively. Saturated unit weights (γ_{sat}) of clay and sand were selected as 20 kN/m^3, and 21 kN/m^3, respectively.

- Modulus of elasticity (E) was chosen as 24000 kN/m^2, and Poisson's ratio (υ) was chosen as 0.2 for both soils.

- Undrained shear strength ($S_{u,ref}$) was chosen as 10 kN/m^2 for clay, and cohesion (c'_{ref}) was selected as 1 kN/m^2 for sand.

- The friction angle (ϕ) was chosen 34° for sand.

These given parameters were not changed for any iterations. Table 5.1 summarizes the soil values selected for each soil.

Table 5.1. Selected values for soil parameters

Soil Type	**Material Model**	**Drainage Type**	γ_{dry}	γ_{sat}	**E**	υ	$S_{u,ref}$	c'_{ref}	ϕ
			kN/m^3	kN/m^3	kN/m^2	-	kN/m^2	kN/m^2	°
Clay	Mohr-Coulomb	Undrained (B)	16	20	24000	0.2	10	-	-
Sand	Mohr-Coulomb	Drained	18	21	24000	0.2	-	1	34

5.1.1.3. Pile Parameters

Piles were input into PLAXIS 3D as Embedded piles. Modulus of Elasticity of the piles was selected as 30000 kN/m^{2,} and the unit weight of the piles was selected as 24 kN/m^3. Pile type was selected as Predefined and it was selected as Massive circular pile. Skin resistance was selected as Linear and $T_{top,max}$ was chosen as 200 kN/m, and $T_{bot,max}$ was chosen as 500 kN/m. Base resistance (F_{max}) was chosen as 10000 kN. For the piles analyzed in PLAXIS 3D, three different types of D_p/L_p were used as 1/10, 1/25, and 1/50. 3000 kN of point load was applied on the piles for each parameterization on -z-direction only (F_z=-3000 kN). Figure 5.1 shows the representation of the embedded pile placement and load applied. Piles were placed at points x=25 m and y=25 m (midpoint of the project area) for D_p/L_p=1/10, and piles were placed at points x=100 m and y= 100 m (midpoint of the project area) for D_p/L_p=1/25 and D_p/L_p=1/50.

5.1.1.4. Mesh Properties

PLAXIS 3D includes two options in its mesh options toolbar. The first option is element distribution which includes five classes of mesh fineness: very coarse, coarse, medium, fine, and very fine. PLAXIS 3D arranges relative element size, element

dimensions, polyline angle tolerance, and surface angle tolerance automatically by choosing any of these five classes. Very fine mesh size was selected for all the parameterization in this study. The second option is the expert settings. In the expert settings option, relative element size, element dimensions, polyline angle tolerance, and surface angle tolerance are put manually.

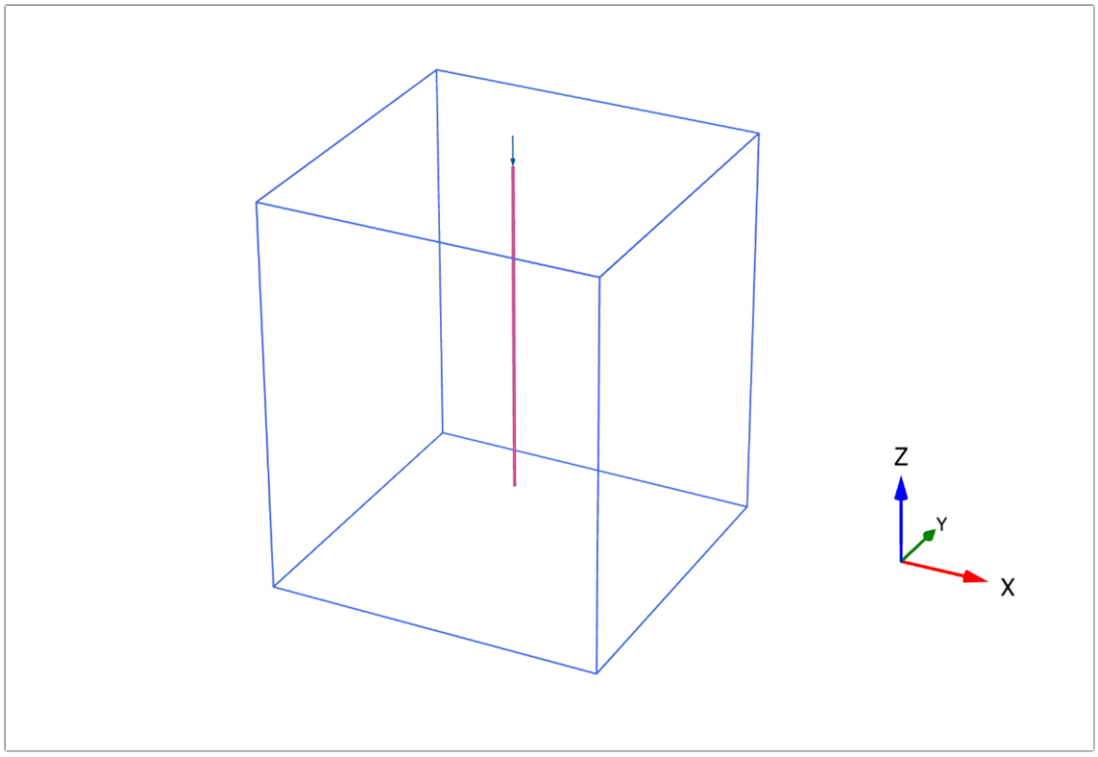

Figure 5.1. Pile and loading placements within the boundaries

5.1.1.5. Staged Construction

Numerical simulations were conducted using a staged (phase) approach for this chapter, which included the following stages:

Initial phase (InitialPhase): The initial phase was constructed using K_0 procedure calculation type to describe initial soil conditions resulting from the soil's own weight.

Piling (Phase_1): Piling phase was constructed starting from phase Initial phase. For the Piling phase, embedded piles were included in the calculations. Calculation type was chosen as plastic.

Loading (Phase_2): Loading phase was constructed starting from the Piling phase. For the Loading phase, loadings were included in the calculations. Calculation type was chosen as Plastic. For both Piling and Loading phases solver type were chosen as Picos (multicore iterative).

CHAPTER 6

RESULTS & DISCUSSION

6.1. Recharge Analysis

6.1.1. Sensitivity Analysis

All the calibration and validation data were used (1990-2014 periods) for the sensitivity analysis. Five hundred simulations were carried out with the choosing min and max values given in Table 3.5. SWAT-CUP calculated sensitivity analysis automatically with the supplied data. Nash-Sutcliffe's (NS) objective function was used to determine the sensitivity. Table 6.1 shows the used twenty-two hydrological model parameters for the sensitivity analysis and their automatically calculated t-Stats and P-values. Most sensitive 18 parameters were used for the calibration and validation for this study. SWAT-CUP also creates a graphical representation of t-Stat and P-values (Figure 6.1).

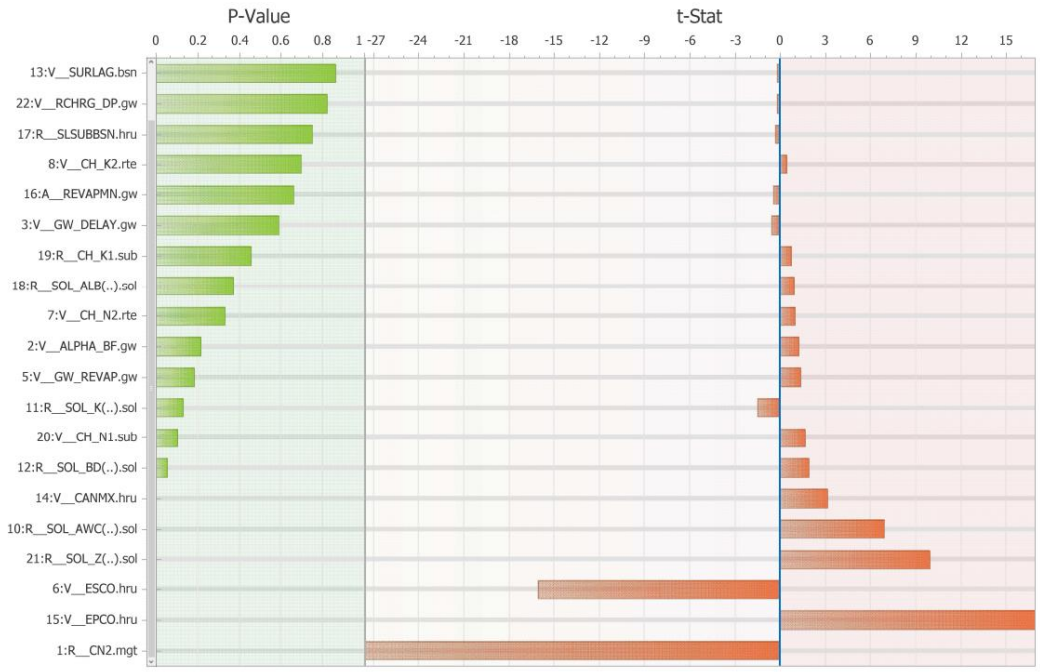

Figure 6.1. Graphical representation of t-Stat and P-value for all parameters created by SWAT-CUP

Dotty plots created by SWAT-CUP are shown in Figure 6.2, Figure 6.3, Figure 6.4, and Figure 6.5. Dotty Plots aim to represent the distribution of samples with the objective function.

Table 6.1. Eighteen hydrological parameters, their t-Stats, P-values and Sensitivity Rankings

Parameter Code	**Description**	**t-Stat**	**P-value**	**Sensitivity Rank**
R__CN2.mgt	SCS runoff curve number f	-27.546	0.000	1
V__EPCO.hru	Plant uptake compensation factor	16.896	0.000	2
V__ESCO.hru	Soil evaporation compensation factor	-16.084	0.000	3
R__SOL_Z(..).sol	Depth from soil surface to bottom of layer	9.941	0.000	4
R__SOL_AWC(..).sol	Available water capacity of the soil layer	6.879	0.000	5
V__CANMX.hru	Maximum canopy storage	3.115	0.002	6
R__SOL_BD(..).sol	Moist bulk density	1.926	0.055	7
V__CH_N1.sub	Manning's "n" value for the tributary channels	1.636	0.102	8
R__SOL_K(..).sol	Saturated hydraulic conductivity	-1.514	0.131	9
V__GW_REVAP.gw	Groundwater "revap" coefficient	1.337	0.182	10
V__ALPHA_BF.gw	Baseflow alpha factor (days)	1.247	0.213	11
V__CH_N2.rte	Manning's "n" value for the main channel	0.976	0.330	12
R__SOL_ALB(..).sol	Moist soil albedo	0.895	0.371	13
R__CH_K1.sub	Effective hydraulic conductivity in tributary channel alluvium	0.749	0.454	14
V__GW_DELAY.gw	Groundwater delay (days)	-0.541	0.588	15
A__REVAPMN.gw	Threshold depth of water in the shallow aquifer for "revap" to occur (mm)	-0.438	0.661	16
V__CH_K2.rte	Effective hydraulic conductivity in main channel alluvium	0.393	0.694	17
R__SLSUBBSN.hru	Average slope length	-0.317	0.751	18

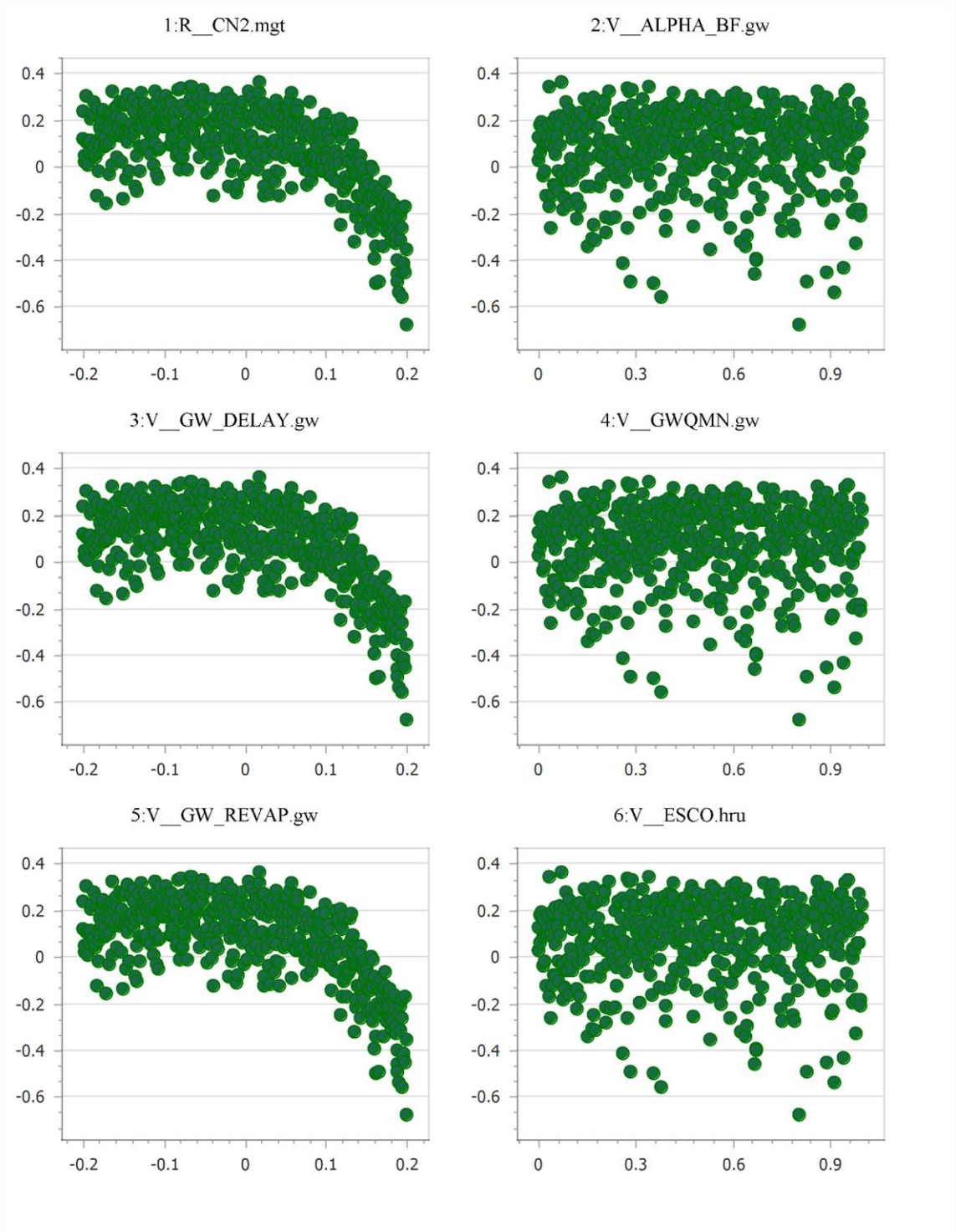

Figure 6.2. Dotty Plots of R__CN2.mgt, V__ALPHA_BF.gw,V__GW_DELAY.gw, V__GWQMN.gw, V__GW_REVAP.gw, V__ESCO.hru

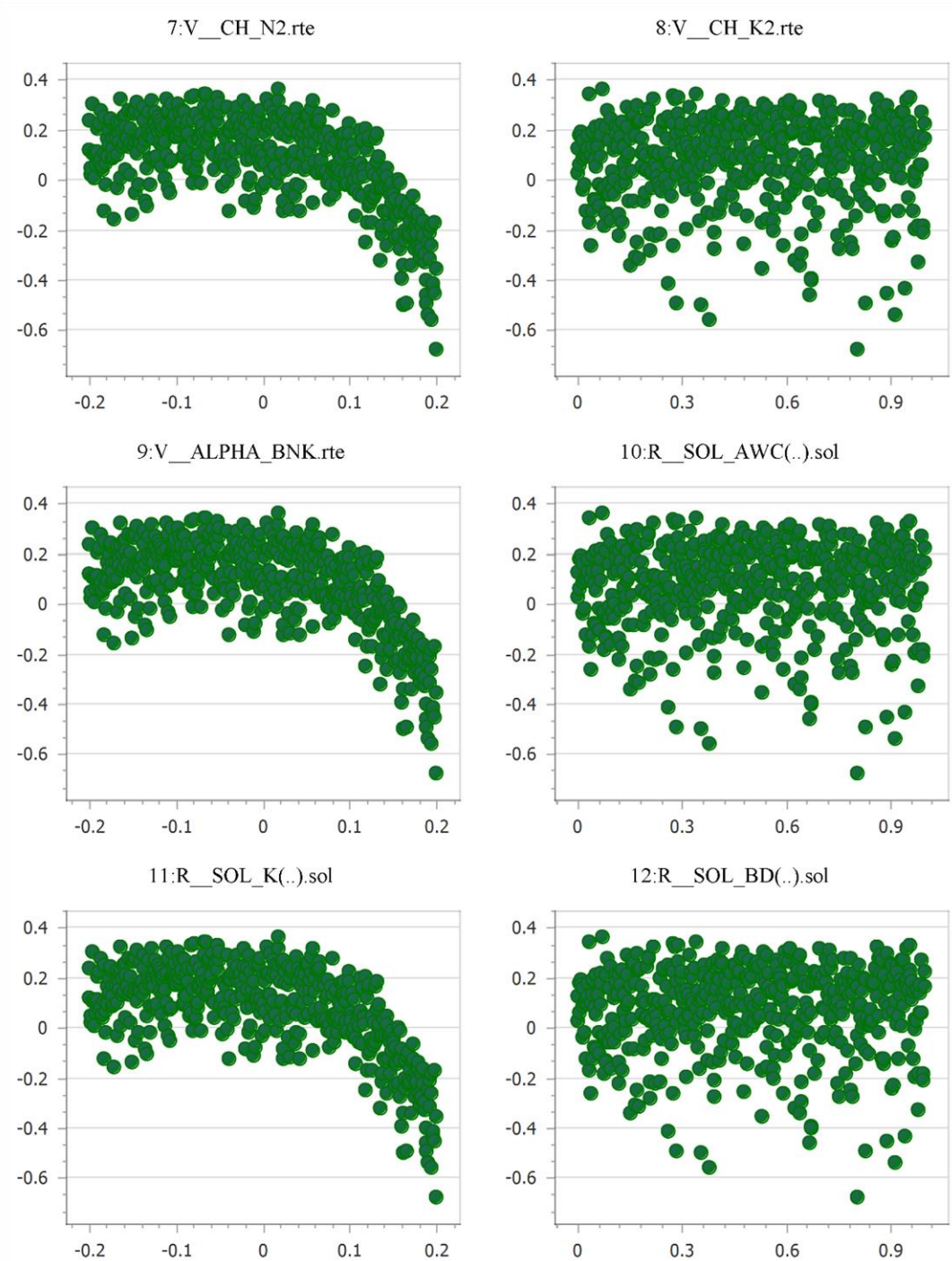

Figure 6.3. Dotty Plots of V__CH_N2.rte, V__CH_K2.rte, V__ALPHA_BNK.rte, R__SOL_AWC.sol, R__SOL_K.sol, R__SOL_BD.sol

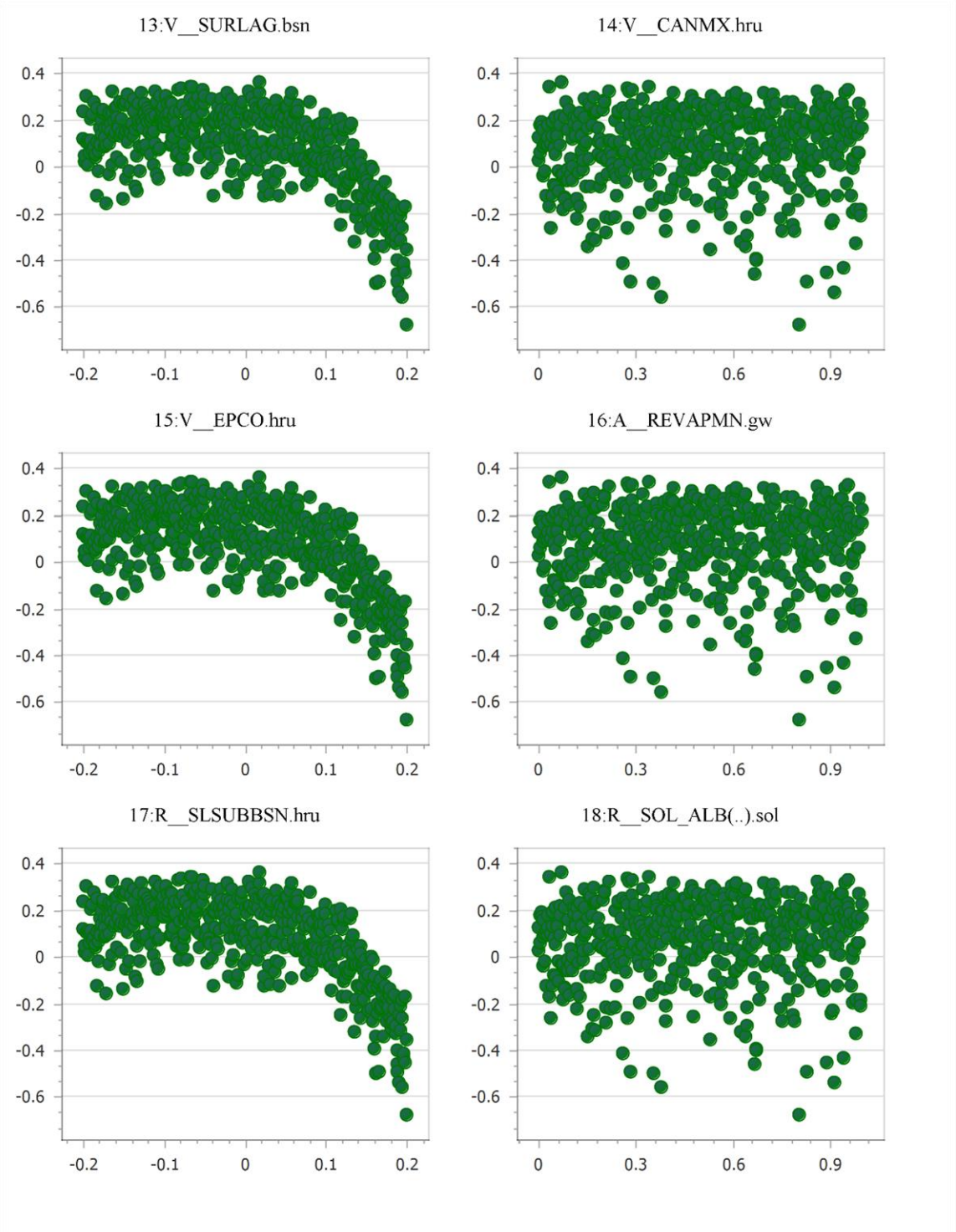

Figure 6.4. Dotty Plots of V__SURLAG.bsn, V__CANMX.hru, V__EPCO.hru, A__REVAPMN.gw, R__SLSUBBSN.hru, R__SOL_ALB.sol

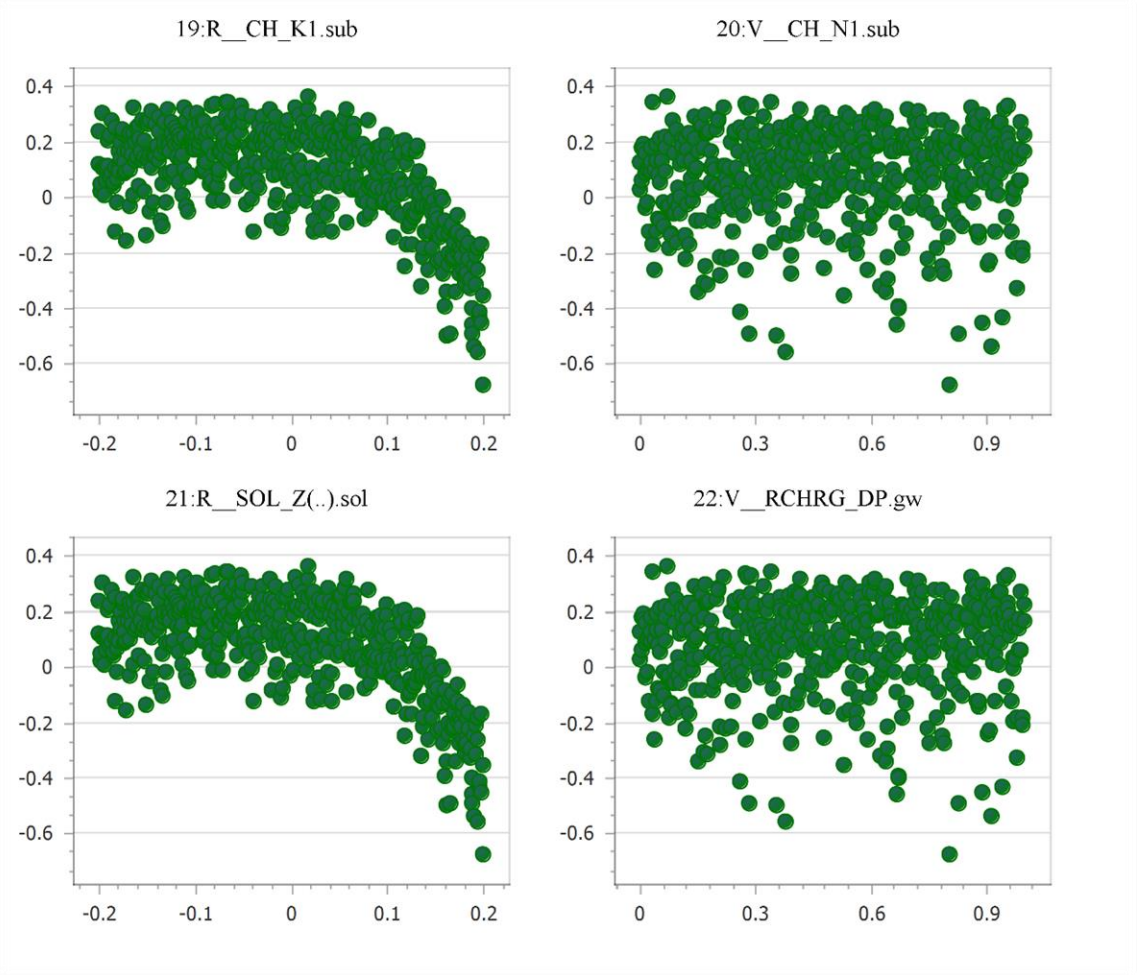

Figure 6.5. Dotty Plots of R__CH_K1.sub, V__CH_N1.sub, R__SOL_Z.sol, V__RCHRG_DP.gw

6.1.2. Calibration of the Models

After determining the most sensitive parameters, parameter ranges of the calibration parameters changed for each iteration with a reasonable range to obtain the optimum R^2 and NS values. After each iteration, SWAT-CUP creates a text file (new_pars.txt) within its output folder that contains suggested values for maximum and minimum values to be used for the next iteration. After each iteration, SWAT-CUP offers new sets of recommended minimum and maximum values. Several iterations were carried out to obtain the best results. For the calibration part, 1990-2004 monthly observed discharge data were used. Table 6.2 shows the final selected minimum and maximum values for the calibration and their calculated fitted values and method for later usage for these values. Using Table 6.2 table minimum and maximum values calibration was

completed. Figure 6.6 shows the comparison of observed and simulated model output discharge with calculated R^2= 0.84 and NS=0.80 for the calibration part. According to ASABE (2017), the results lie within a very good region.

Table 6.2. Final Min and Max Values for Calibration, Fitted Values and Methods

Parameter Code	**Min Value**	**Max Value**	**Fitted Value**	**Method**
R__CN2.mgt	0.010	0.024	0.018	Relative
V__EPCO.hru	0.843	0.890	0.883	Replace
V__ESCO.hru	0.562	0.570	0.564	Replace
R__SOL_Z(..).sol	0.631	0.657	0.652	Relative
R__SOL_AWC(..).sol	0.942	0.981	0.971	Relative
V__CANMX.hru	7.494	7.992	7.913	Replace
R__SOL_BD(..).sol	0.309	0.348	0.328	Relative
V__CH_N1.sub	0.175	0.187	0.181	Replace
R__SOL_K(..).sol	-0.447	-0.414	-0.446	Relative
V__GW_REVAP.gw	0.268	0.307	0.306	Replace
V__ALPHA_BF.gw	0.142	0.288	0.267	Replace
V__CH_N2.rte	0.223	0.236	0.228	Replace
R__SOL_ALB(..).sol	-0.314	-0.302	-0.309	Relative
R__CH_K1.sub	18.961	59.409	58.964	Relative
V__GW_DELAY.gw	301.572	376.462	323.664	Replace
A__REVAPMN.gw	253.229	325.431	323.914	Absolute
V__CH_K2.rte	-18.987	-13.059	-15.045	Replace
R__SLSUBBSN.hru	0.047	0.125	0.0928	Relative

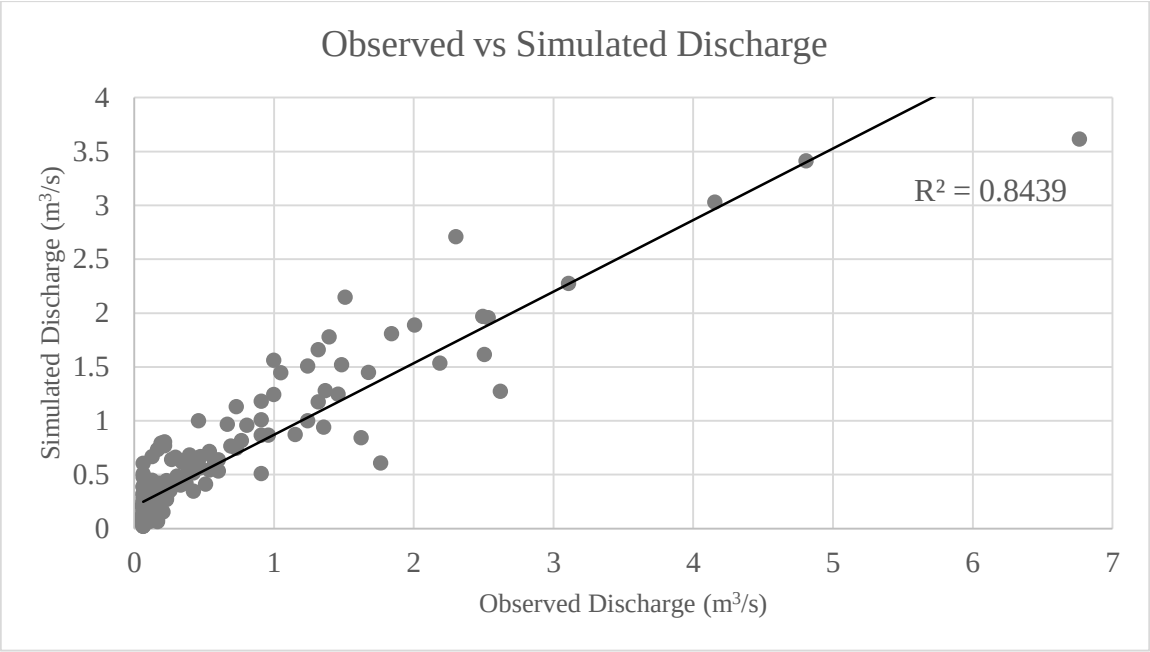

Figure 6.6. Comparison of the observed and simulated model output discharge for the calibration

6.1.3. Validation of the Models

2005-2014 data were used for the validation part. Adjusted parameters from the calibration part (Table 6.2) and observed discharge data from 2005-2014 were input in the SWAT-CUP. SWAT-CUP was then run for 500 simulations.

For the calibration part, Figure 6.7 compares observed and simulated model output discharge with calculated R^2= 0.84 and NS=0.82. The calibration and validation analysis results show a very good relation between observed and simulated discharge data. Figure 6.8 shows the comparison of observed and simulated discharge values for both calibration and validation periods.

Most of the errors between observed and simulated data are caused by low peak flows for the most peak flows and high base flow for the late calibration and early validation periods.

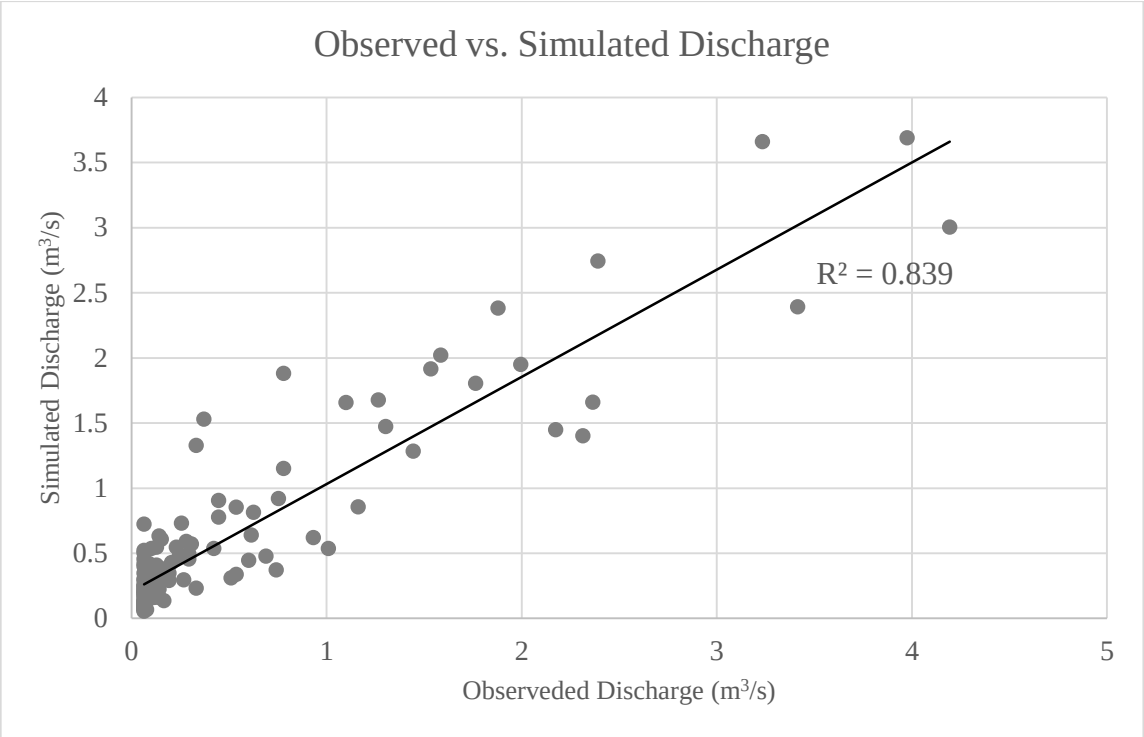

Figure 6.7. Comparison of the observed and simulated model output discharge for the validation

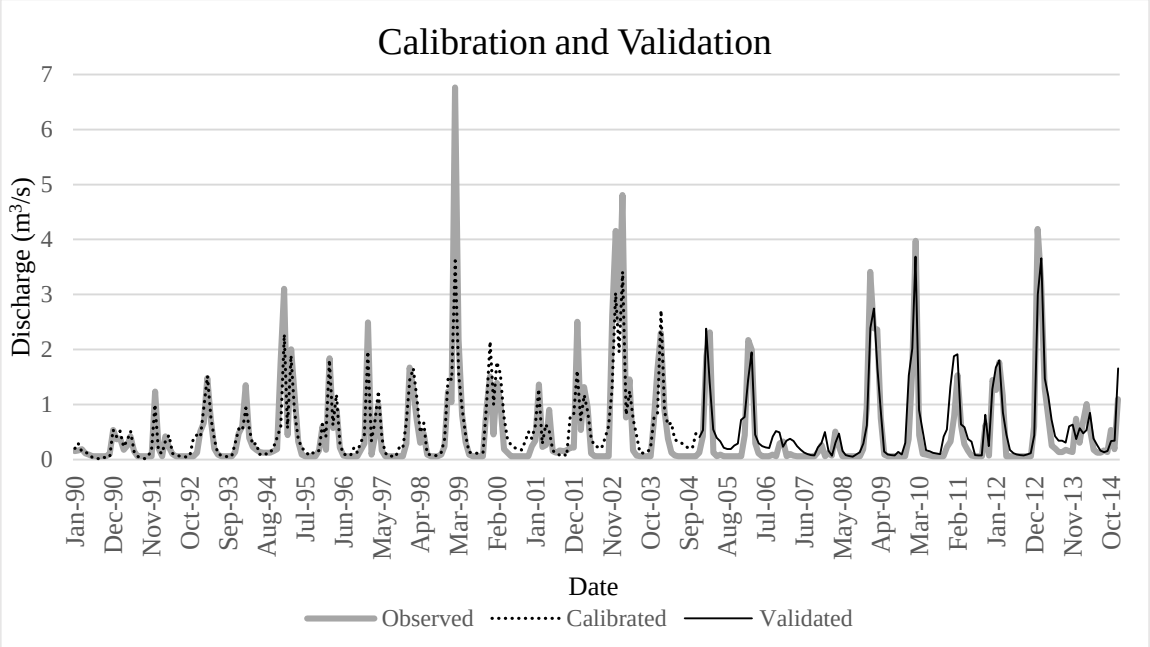

Figure 6.8. Observed vs. simulated discharge for the calibration (1990-2004) and validation (2005-2014) of the models

The difference between these values was higher for the first iterations. Abbaspour, Rouholahnejad, Vaghefi, Srinivasan, Yang, and Kløve (2015) suggested some parameter modifications for these differences. For low peak simulated flow, it is recommended to

decrease the parameter CN2.mgt and increase the parameters SOL_AWC.sol and ESCO.hru. For high simulated base flow, it is recommended to increase the parameter GWQMN.gw and GW_REVAP.gw and decrease the parameter REVAPMN.gw. Since GWQMN.gw was not found to be a sensitive parameter for our study, all the suggested parameters except for the GWQMN.gw were changed for each iteration according to those recommendations. After all those iterations, Figure 6.8 was the best representation obtained for our study.

Regarding everything, it can be said that the SWAT model created can represent our study area very well.

6.1.4. SWAT Models

After obtaining a satisfying correlation between calibration and validation, fitted parameters obtained in the calibration part must be input to ARCSWAT models according to their methods. Table 6.2 shows the fitted values obtained and their methods to be put into ARCSWAT.

For the relative method, the sensitive parameter is multiplied by the summation of the number one and the fitted value obtained using SWAT's Manual Calibration Tool. The sensitive parameter is replaced with the fitted value obtained using SWAT's Manual Calibration Tool for the replace method. The fitted value is added to the sensitive parameter calculated before the calibration process for the absolute method. Some of the sensitive parameters are not included in the Manual Calibration Tool. Subbasin Data Tool under the Edit SWAT Input tool was used for those parameters, and parameters were modified on a subbasin level. Both years 2004 and 2020 were calibrated, and Table 6.3 shows the SWAT Model results before and after the calibration period.

The calculations show that in the study area, with the increasing urbanization, the groundwater Recharge/Precipitation, Streamflow/Precipitation, and Baseflow/Total flow ratios decrease from 0.38 to 0.25, from 0.58 to 0.46, from 0.66 to 0.59, respectively, with the urbanization increment. Surface Runoff/Total Flow, and ET/Precipitation ratios increase from 0.34 to 0.41, and from 0.53 to 0.61 with the urbanization increment, respectively. Table 6.4 shows the percent increase or decrease of the calculated model

parameter ratios. The table shows, Recharge/Precipitation, Streamflow/Precipitation, and Baseflow/Total flow ratios decrease 52%, 26.09%, and 11.86%, respectively, and Surface Runoff/Total Flow and ET/Precipitation ratios increase 20.59% and 15.09% with urbanization increment comparing 2004 and 2020.

Table 6.3. SWAT Model results before and after calibration

Calculated SWAT Output Ratios	**2004**		**2020**	
	Before Calibration	**After Calibration**	**Before Calibration**	**After Calibration**
Streamflow/Precipitation	0.56	0.58	0.44	0.46
Baseflow/Total flow	0.65	0.66	0.56	0.59
Surface Runoff/Total flow	0.35	0.34	0.44	0.41
Recharge/Precipitation	0.35	0.38	0.24	0.25
ET/Precipitation	0.45	0.53	0.53	0.61

Table 6.4. Percent increase or decrease with the urbanization of compared years

Calculated SWAT Output Ratios	**Decrease (%) (from 2004 to 2020)**	**Increase (%) (from 2004 to 2020)**
Streamflow/Precipitation	26.09	-
Baseflow/Total flow	11.86	-
Surface Runoff/Total flow	-	20.59
Recharge/Precipitation	52	-
ET/Precipitation	-	15.09

Figure 6.9 shows all the other calculated terms of the water budget equation for 2004 and 2020.

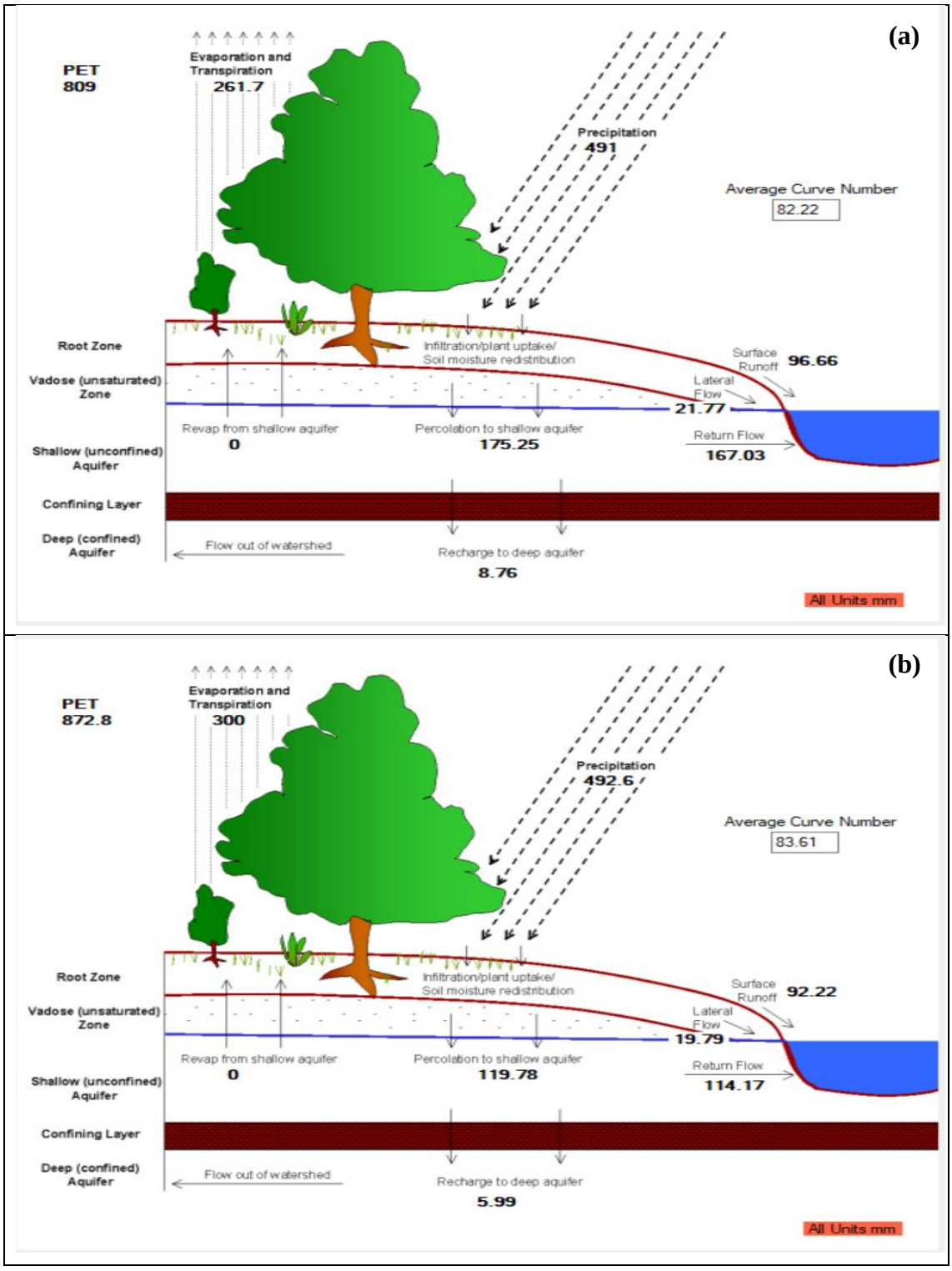

Figure 6.9. Calculated terms of the water budget equation (a) 2004, (b) 2020

6.2. Bearing Capacity Analysis

This chapter aimed to calculate the bearing capacity change of the soil throughout a year with groundwater level fluctuations. Geotechnical designs require groundwater levels to calculate the bearing capacity of the soil regarding the foundation type and parameters. In almost every geotechnical design, one single groundwater level taken from boring log data is used. Most constructions in our country take place in summers, so the construction site does not get affected by the rain. Boring log data are also taken in summers. Groundwater levels representing the construction site in summer are expected to be lower than in winter as the precipitation in summers is low and groundwater extraction is high. The difference between the groundwater level of an urbanized area in dry and wet seasons is expected to be greater than in rural areas.

A parametric study was carried out for our study area to understand the effects of groundwater level change on soil bearing capacity. A limited number of available boring log data was obtained for our study area. For selecting a parameter for the soil, those boring log data were taken as reference. For the soil parameters, one cohesion and one friction angle value were used as 10 for cohesion and 34 for friction angle, respectively. Strip type of footing was selected to investigate for this study. Four different widths of the foundation over the depth of foundation (B/D_f) were chosen for the parametric study as 1, 0.33, 0.2, 0.1. Each calculation changed the B/D_f parameter, so four different bearing capacity cases were created for each observation wells. Daily groundwater levels obtained from the observation wells were used to calculate the bearing capacity.

Groundwater levels of five different observation wells (SK-1, SK-3, SK-6, SK-7, SK-9) between 24-October-2020 and 24-October-2021 were used for this study to calculate the bearing capacity of the soil. Equations (4.11) and (4.12) were used to calculate the groundwater level with respect to ground level by using automatically saved equivalent hydrostatic pressure data obtained from the divers located in each well. Figure 6.10 shows groundwater level change with time for each well. Groundwater levels in all the observation wells were calculated to the ground level where the wells are located.

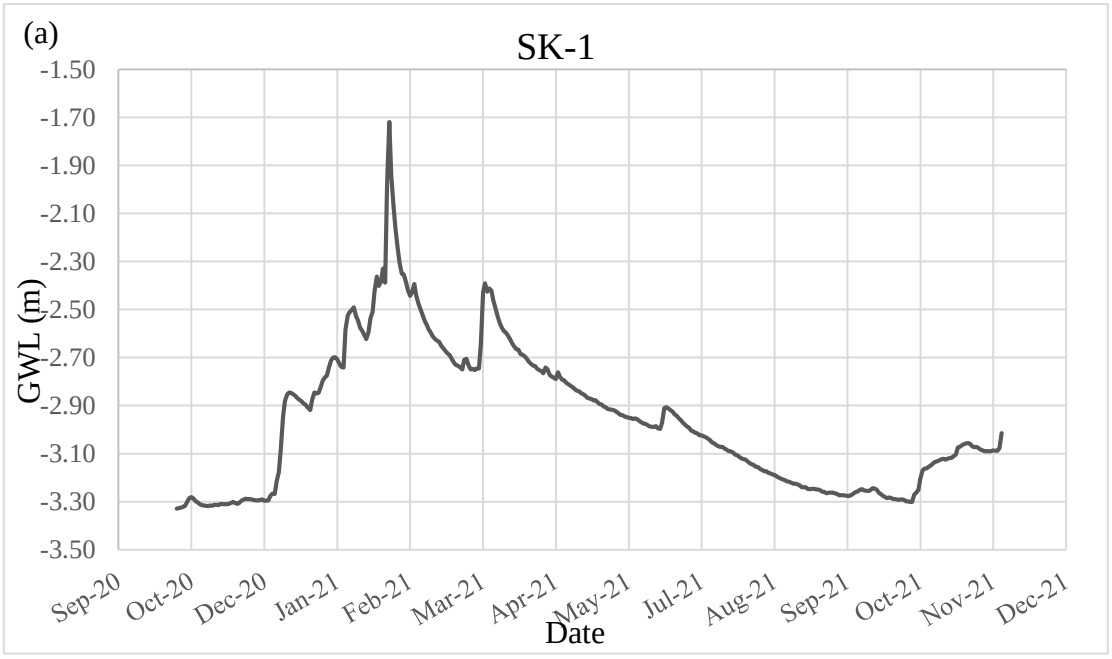
(a)
SK-1
-1.50
-1.70
-1.90
-2.10
-2.30
-2.50
-2.70
-2.90
-3.10
-3.30
-3.50
GWL (m)
Sep-20
Oct-20
Dec-20
Jan-21
Feb-21
Mar-21
Apr-21
May-21
Jul-21
Aug-21
Sep-21
Oct-21
Nov-21
Dec-21
Date

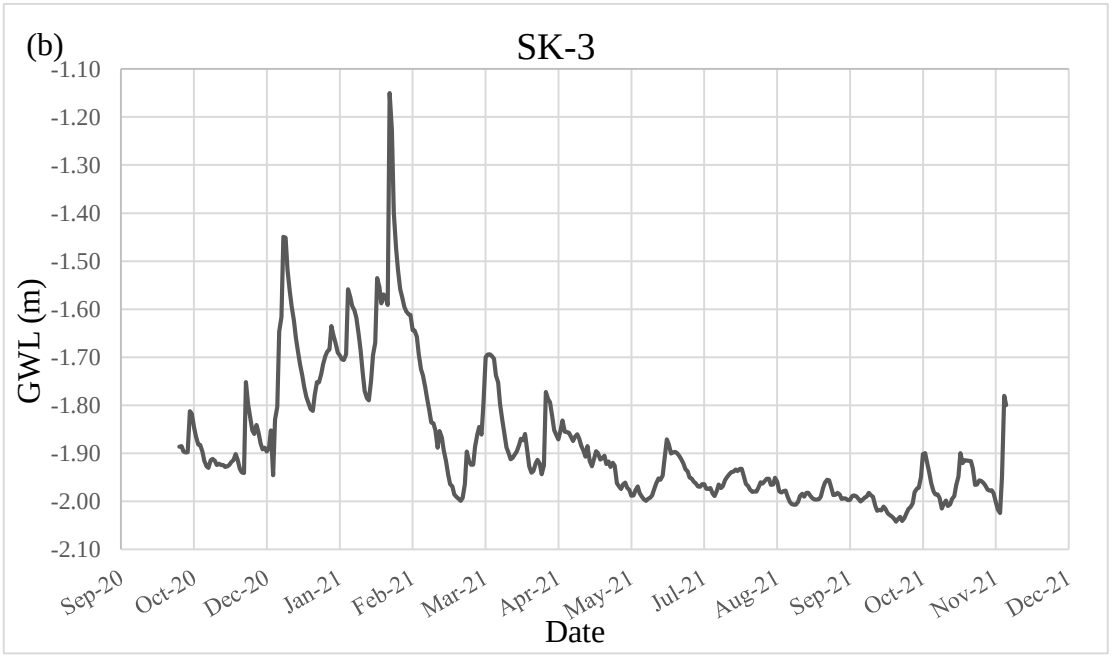
(b)
SK-3
-1.10
-1.20
-1.30
-1.40
-1.50
-1.60
-1.70
-1.80
-1.90
-2.00
-2.10
GWL (m)
Sep-20
Oct-20
Dec-20
Jan-21
Feb-21
Mar-21
Apr-21
May-21
Jul-21
Aug-21
Sep-21
Oct-21
Nov-21
Dec-21
Date

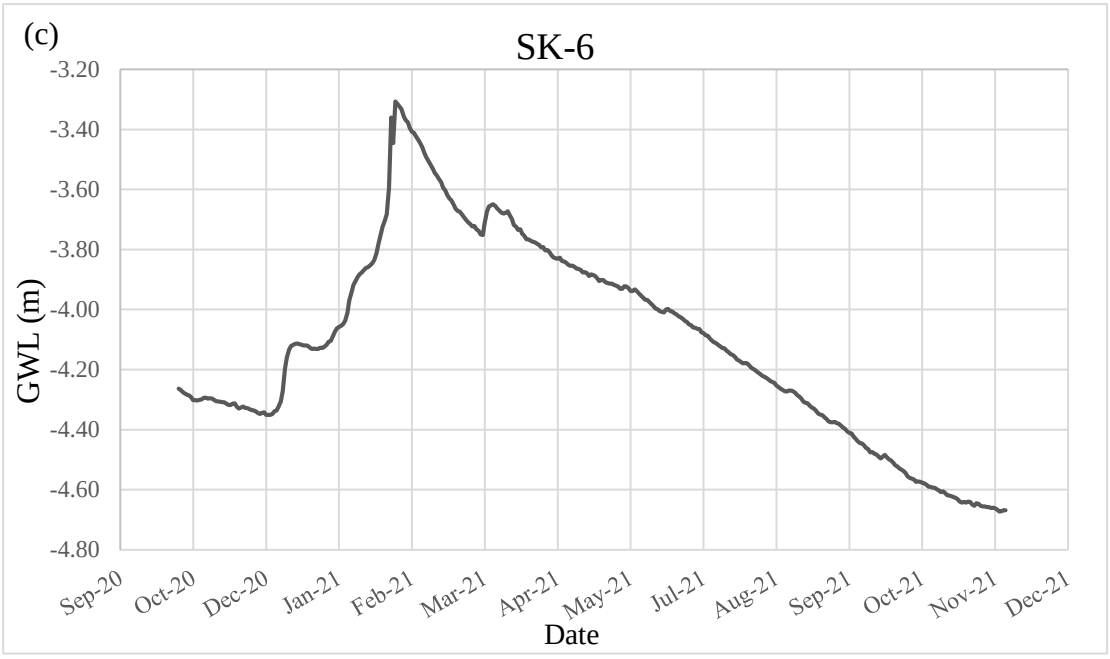
(c)
SK-6
-3.20
-3.40
-3.60
-3.80
-4.00
-4.20
-4.40
-4.60
-4.80
GWL (m)
Sep-20
Oct-20
Dec-20
Jan-21
Feb-21
Mar-21
Apr-21
May-21
Jul-21
Aug-21
Sep-21
Oct-21
Nov-21
Dec-21
Date

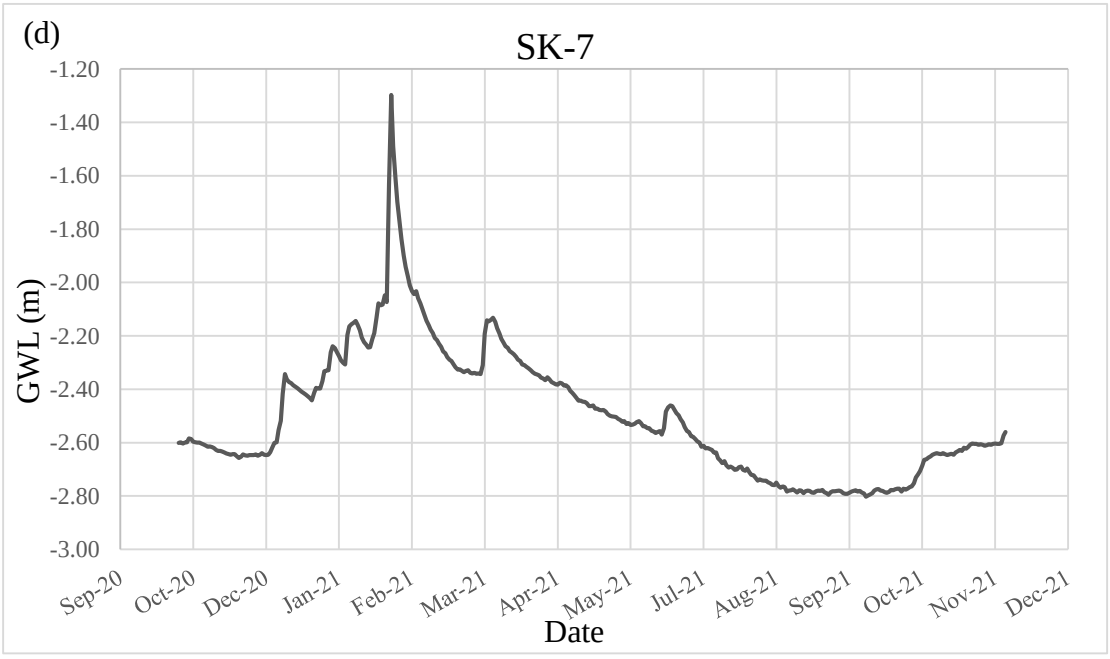
(d)
SK-7
-1.20
-1.40
-1.60
-1.80
-2.00
-2.20
-2.40
-2.60
-2.80
-3.00
GWL (m)
Sep-20
Oct-20
Dec-20
Jan-21
Feb-21
Mar-21
Apr-21
May-21
Jul-21
Aug-21
Sep-21
Oct-21
Nov-21
Dec-21
Date

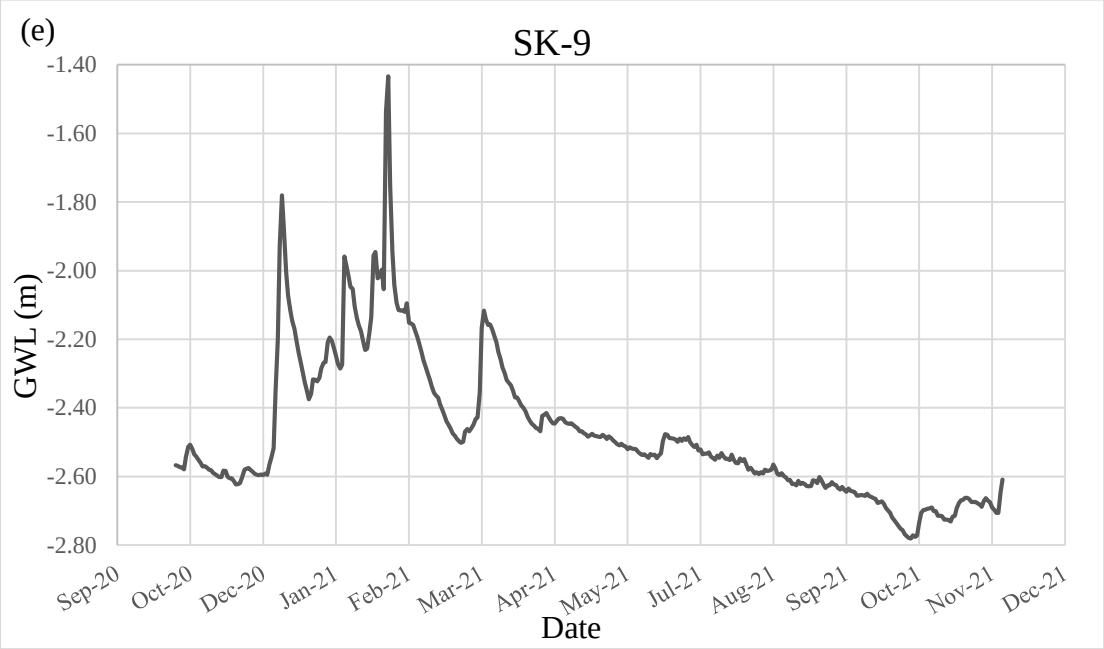

Figure 6.10. Groundwater levels obtained from the observation wells in the study area (a) SK-1, (b) SK-3, (c) SK-6, (d) SK-7, (e) SK-9

The spatial distribution of the groundwater levels calculated using Table 6.5 in ArcGIS is shown in Figure 6.11. Figure 6.11 also shows the groundwater flow direction calculated from higher groundwater level to lower. For the wet season and dry season data, February and October groundwater levels were selected, respectively. Their sea-level values were calculated by subtracting the groundwater level of wells from the elevations of the observation wells with respect to sea level. Groundwater levels referenced with the sea level were then transferred into ArcMap. Then, the Kriging Raster Interpolation tool under the 3D Analyst Tools was used to calculate the groundwater level distribution referenced to the sea level for the wet and dry seasons.

Table 6.5. Observation wells and their groundwater levels referenced to well location and sea level

Observation Well	X	Y	Elevation (m)	GWL (Wet Season well level) (m)	GWL (Dry Season well level) (m)	GWL (wet season sea level) (m)	GWL (dry season sea level) (m)
SK-1	515287.5	4256246	7	1.72	3.29	5.28	3.71
SK-3	514661.3	4257002	6	1.23	2.04	4.77	3.96
SK-6	516054.4	4256437	7	3.36	4.53	3.64	2.47
SK-7	515650.4	4257590	12	1.3	2.78	10.7	9.22
SK-9	515449.7	4255415	3	1.43	2.74	1.57	0.26

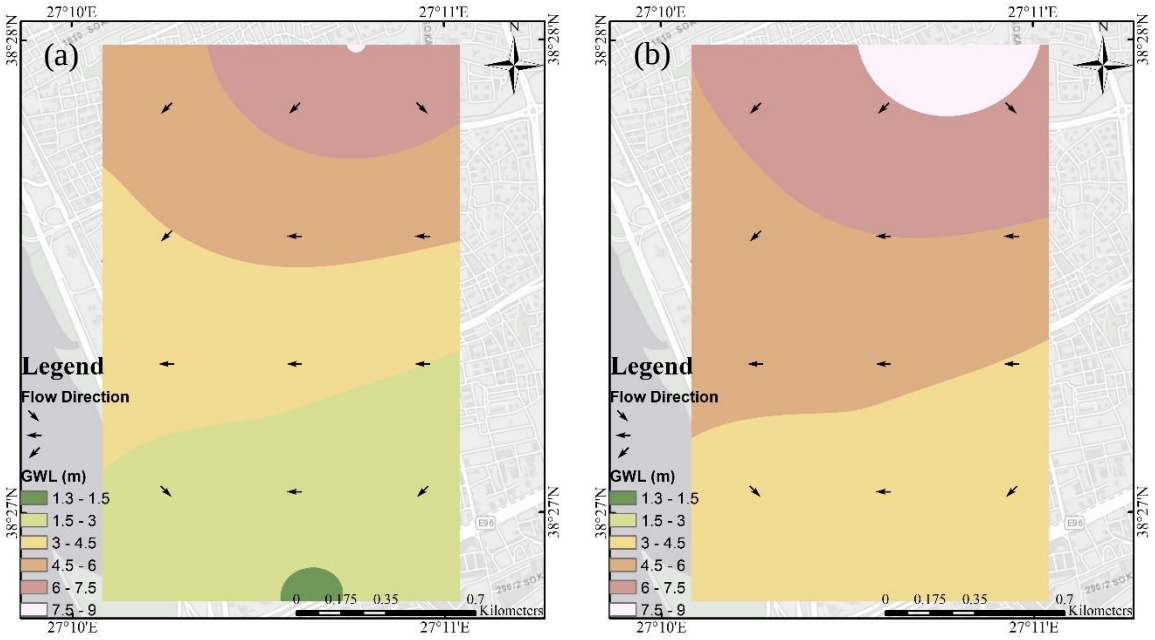

Figure 6.11. Groundwater level maps and flow directions of (a) wet season (b) dry season

Minimum and maximum groundwater levels measured in the wells are 1.72m and 3.33m in SK-1, 1.15m and 2.04m in SK-3, 3.31m and 4.67m in SK-6, 1.30m and 2.80m, and 1.43m and 2.78m in SK-9 wells, respectively. Groundwater level changes throughout the observation period 1.61m in SK-1, 0.89m in SK-3, 1.37m in SK-6, 1.5m in SK-7, and 1.35m in SK-9 wells. Maximum groundwater level change was observed in SK-1 (1.61m), and minimum groundwater level change was observed in SK-3 (0.89m) observation wells. The groundwater level rises to its maximum between January and February in each observation wells. Groundwater levels decrease to their minimum value in the summer and fall periods for all the wells.

Microsoft Excel software was used to calculate the bearing capacity of the soil. Different bearing capacity and surcharge loads equations were used for each case (Equations (4.6), (4.10)). The bearing capacity of the soil was calculated daily for each case for each well. Microsoft Excel's If Function was used to determine which case (Case I, Case II, or Case III) governs. The function checks the supplied foundation width and groundwater levels to determine which case occurs. The If Function was also used to calculate the surcharge load corresponding to the case. The function checks which case is valid and then calculates the surcharge load regarding that case. The If Function was

also used to determine the bearing capacity of the soil. The function checks the case and surcharge load and unit weight modification accordingly and calculates the bearing capacity of the soil. All the bearing capacity calculations were based on B/D_f non-dimensional parameterization.

Table 6.6 shows all the parameter changes and calculated minimum and maximum ultimate soil bearing capacity and percent change of increase concerning minimum soil bearing capacity using daily water level changes for SK-1 (Figure 6.10 (a)). Calculated bearing capacities and maximum bearing capacity decrease for four different B/D_f parameterizations are given in Table 6.6. The maximum bearing capacity decrease was observed for B/D_f= 0.33 parameterization as 13.44%. Figure 6.12 shows yearly q/q_{max} distribution over the observation well SK-1 for all the B/D_f parameterizations. The soil bearing capacity decrease was insignificant when B/D_f=1 compared to other parameterizations as it is 1.80%. The lowest bearing capacity was observed in February for all the parameterizations where the groundwater level reached its highest point. The bearing capacity decrease increased to B/Df=0.33, and it started to decrease to B/D_f=0.1.

Table 6.6. Calculated q_u decrease in percent for SK-1 for four parameterization

Parameterization	B/D_f	c	φ	q_u Decrease
	-	(kN/m^2)	(°)	(%)
1	1	10	34	1.80
2	0.33	10	34	13.44
3	0.2	10	34	11.43
4	0.1	10	34	7.04

Table 6.7 shows all the parameter changes and calculated minimum and maximum ultimate soil bearing capacity and percent change of increase concerning minimum soil bearing capacity using daily water level changes for SK-3 (Figure 6.10 (b)). Calculated bearing capacities and maximum bearing capacity decrease for four different B/D_f parameterizations are given in Table 6.7. The maximum bearing capacity decrease was observed for B/D_f= 0.33 parameterization as 8.92%. Figure 6.13 shows yearly q/q_{max} distribution over the observation well SK-3 for all the B/D_f parameterizations. The lowest bearing capacity was observed in February for all the parameterizations where the

groundwater level reached its highest point. The bearing capacity decrease increased up to B/D_f=0.33, and then it started to decrease up to B/D_f=0.1.

Table 6.7. Calculated q_u decrease in percent for SK-3 for four parameterization

Parameterization	B/D_f	c	φ	q_u Decrease
	-	(kN/m^2)	(°)	(%)
1	1	10	34	5.64
2	0.33	10	34	8.92
3	0.2	10	34	6.60
4	0.1	10	34	4.00

Table 6.8 shows all the parameter changes and calculated minimum and maximum ultimate soil bearing capacity and percent change of increase concerning minimum soil bearing capacity using daily water level changes for SK-6 (Figure 6.10 (c)). Calculated bearing capacities and maximum bearing capacity decrease for four different B/D_f parameterizations are given in Table 6.8. The maximum bearing capacity decrease was observed for B/D_f= 0.2 parameterization as 8.71%. Figure 6.14 shows yearly q/q_{max} distribution over the observation well SK-6 for all the B/D_f parameterizations. The lowest bearing capacity was observed in February for all the parameterizations where the groundwater level reached its highest point. No change in the bearing capacity of the soil for B/Df = 1was observed, which means the change of groundwater level does not affect the bearing capacity of the soil, which means Case III (more details in Chapter 4.1) was valid for all year. SK-6 has a lower groundwater table than other observation wells, resulting in no change of bearing capacity for one parameter throughout the year. The bearing capacity decrease increased up to B/D_f=0.20, and then it started to decrease up to B/D_f=0.1.

Table 6.8. Calculated q_u decrease in percent for SK-6 for four parameterization

Parameterization	B/D_f	c	φ	q_u Decrease
	-	(kN/m^2)	(°)	(%)
1	1	10	34	0.00
2	0.33	10	34	2.46
3	0.2	10	34	8.71
4	0.1	10	34	5.59

Table 6.9 shows all the parameter changes and calculated minimum and maximum ultimate soil bearing capacity and percent change of increase concerning minimum soil bearing capacity using daily water level changes for SK-7 (Figure 6.10 (d)). Calculated bearing capacities and maximum bearing capacity decrease for four different B/D_f parameterizations are given in Table 6.9. The maximum bearing capacity decrease was observed for B/D_f= 0.33 parameterization as 14.82%. Figure 6.15 shows yearly q/q_{max} distribution over the observation well SK-7 for all the B/D_f parameterizations. The lowest bearing capacity was observed in February for all the parameterizations where the groundwater level reached its highest point. The soil bearing capacity decrease was insignificant when B/D_f=1 compared to other parameterizations as it is 4.62%. The bearing capacity decrease increased up to B/D_f=0.33, and then it started to decrease up to B/D_f=0.1.

Table 6.9. Calculated q_u decrease in percent for SK-7 for four parameterization

Parameterization	B/D_f	c	φ	q_u Decrease
	-	(kN/m^2)	(°)	(%)
1	1	10	34	4.62
2	0.33	10	34	14.82
3	0.2	10	34	11.01
4	0.1	10	34	6.71

Table 6.10 shows all the parameter changes and calculated minimum and maximum ultimate soil bearing capacity and percent change of increase concerning minimum soil bearing capacity using daily water level changes for SK-9 (Figure 6.10 (e)). Calculated bearing capacities and maximum bearing capacity decrease for four different B/D_f parameterizations are given in

The maximum bearing capacity decrease was observed for B/D_f= 0.33 parameterization as 13.10%. Figure 6.16 shows yearly q/q_{max} distribution over the observation well SK-9 for all the B/D_f parameterizations. The lowest bearing capacity was observed in February for all the parameterizations where the groundwater level reached its highest point. The soil bearing capacity decrease was insignificant B/D_f=1 compared to other parameterizations as it is 3.69%, respectively. The bearing capacity decrease increased up to B/D_f=0.33, and then it started to decrease up to B/D_f=0.1.

Table 6.10. Calculated q_u decrease in percent for SK-9 for four parameterization

Parameterization	B/D_f	c	φ	q_u Decrease
	-	(kN/m^2)	(^{o})	(%)
1	1	10	34	3.69
2	0.33	10	34	13.10
3	0.2	10	34	9.77
4	0.1	10	34	5.97

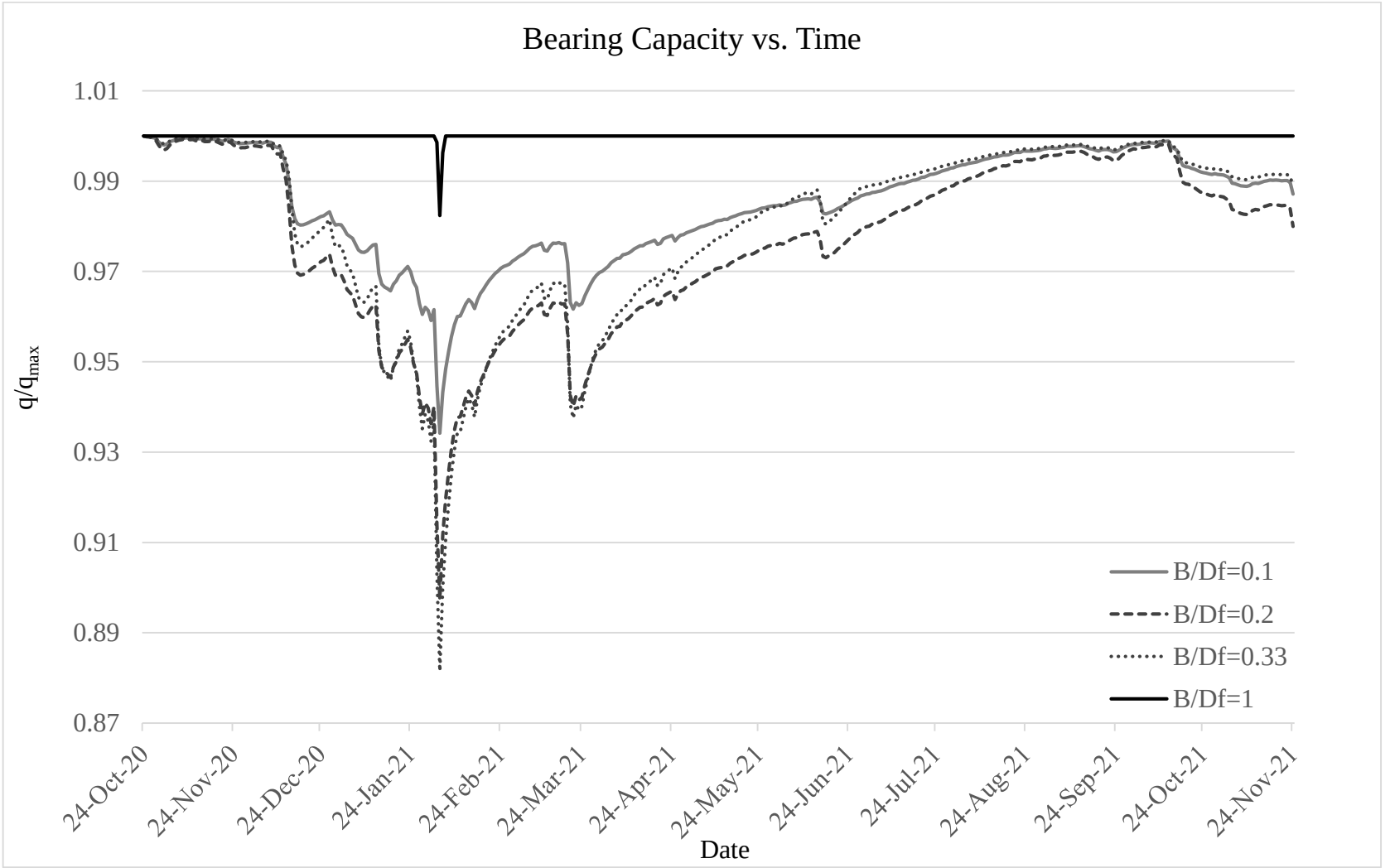

Figure 6.12. Bearing capacity change over a year for four different B/D_f parameterizations for observation well SK-1

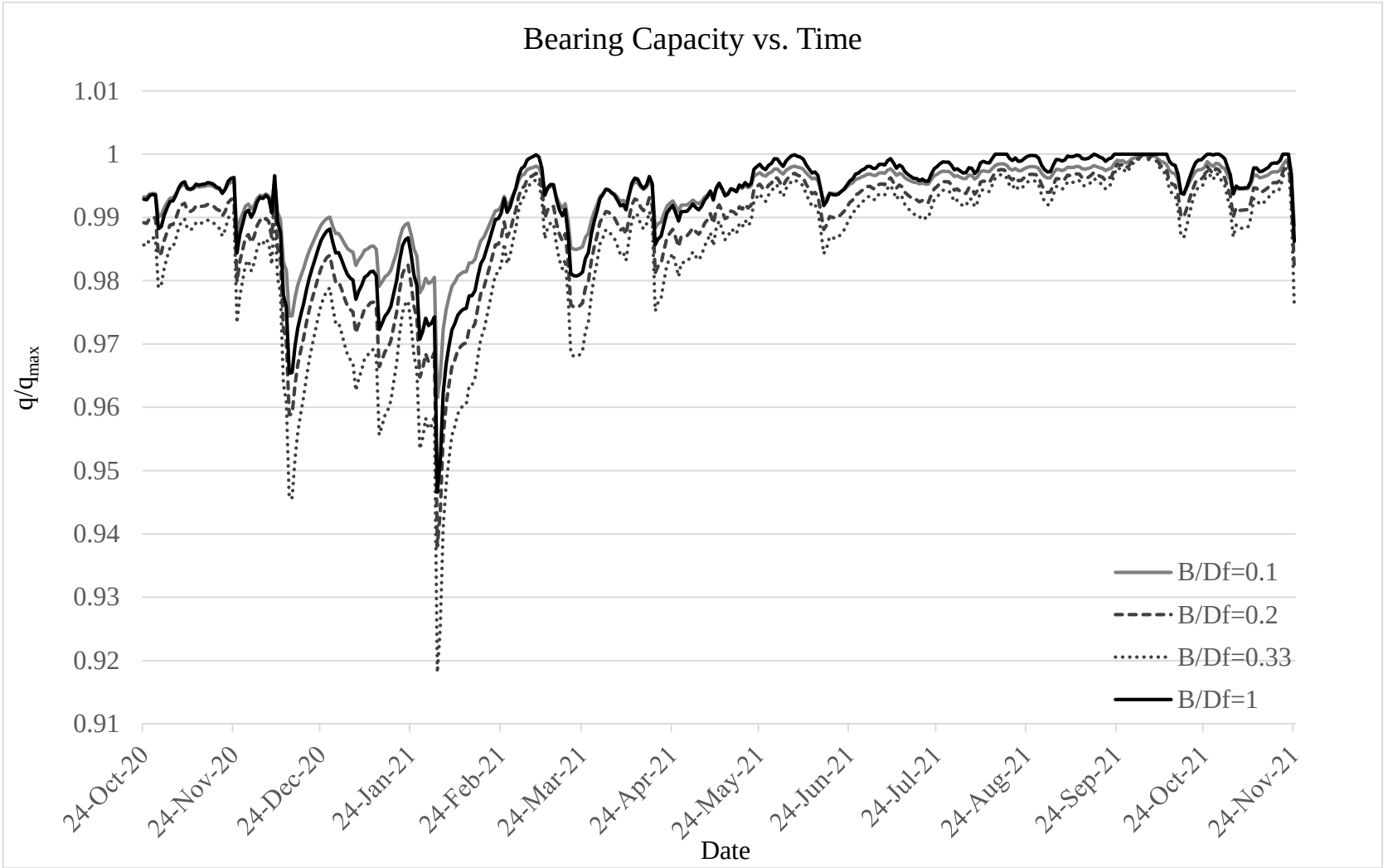

Figure 6.13. Bearing capacity change over a year for four different B/D_f parameterizations for observation well SK

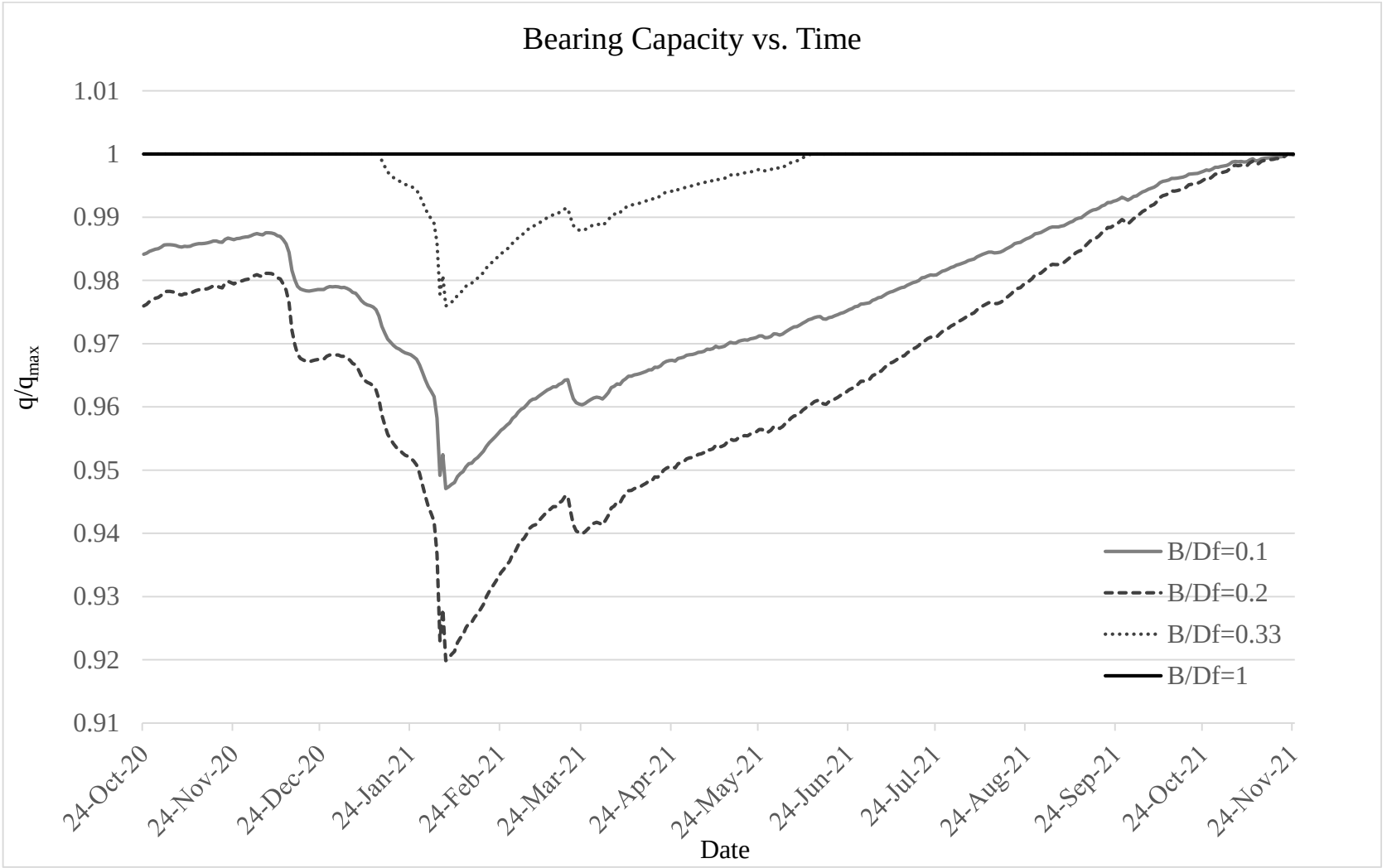

Figure 6.14. Bearing capacity change over a year for four different B/D_f parameterizations for observation well SK-6

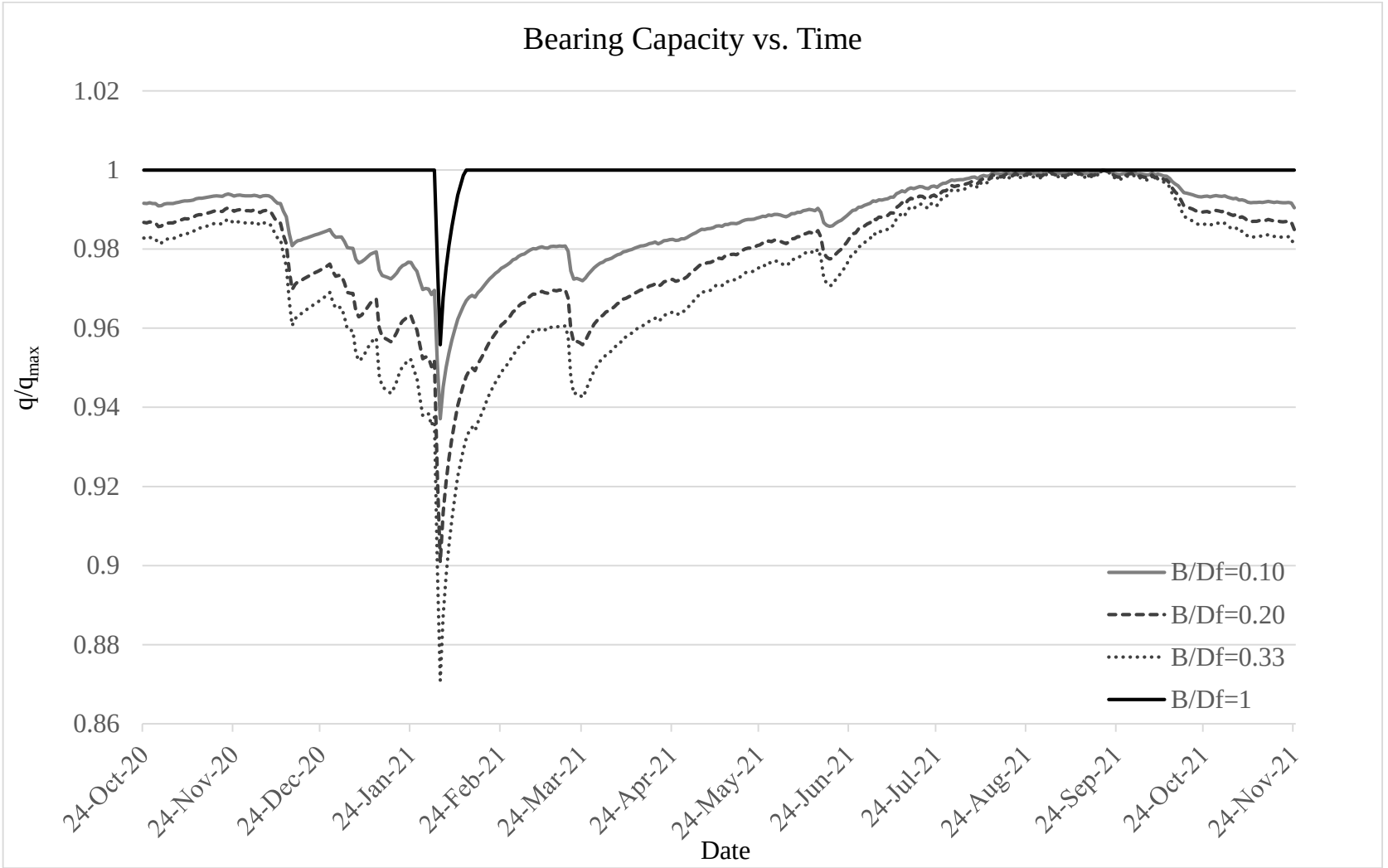

Figure 6.15. Bearing capacity change over a year for four different B/D_f parameterizations for observation well SK-7

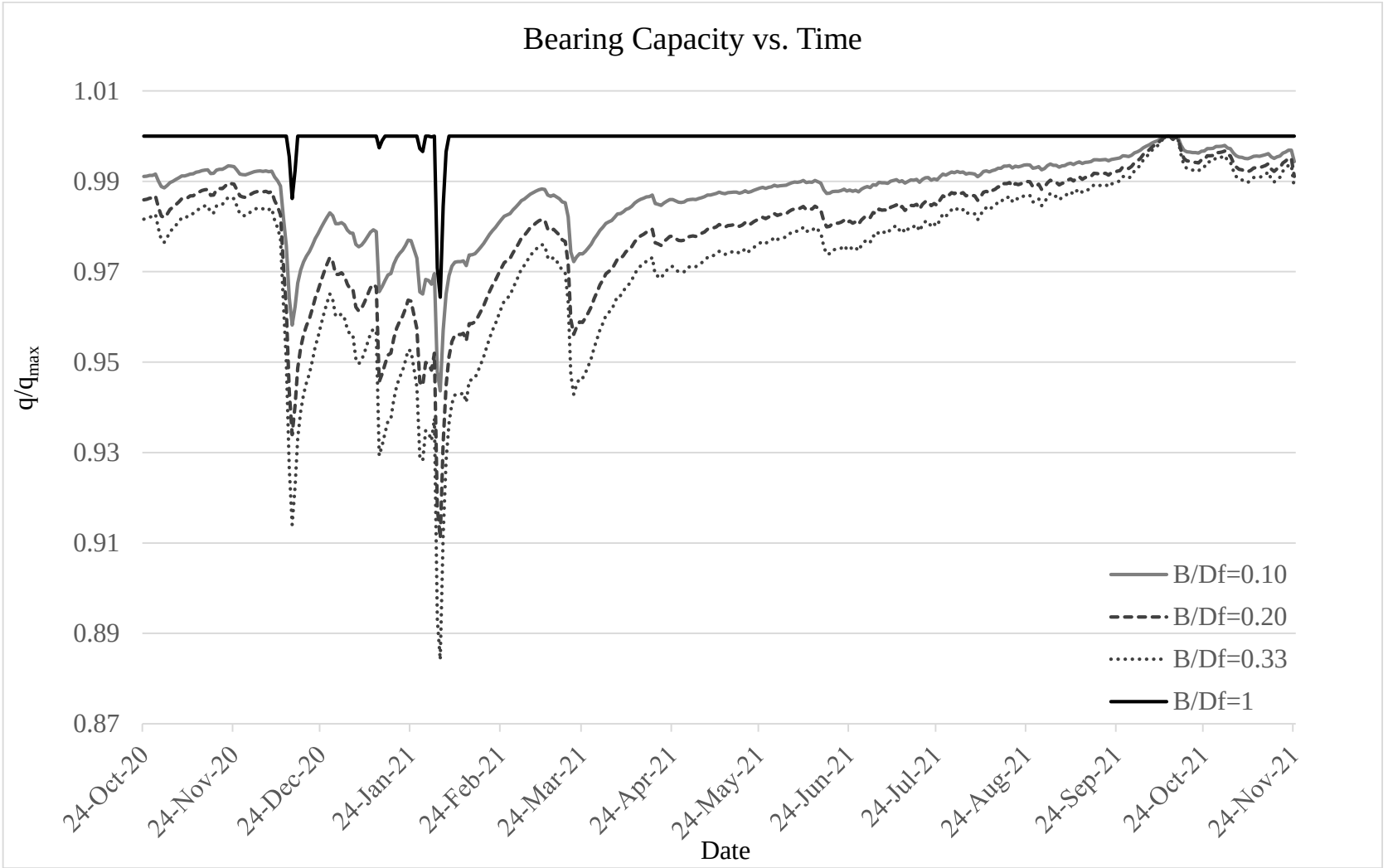

Figure 6.16. Bearing capacity change over a year for four different B/D_f parameterizations for observation well SK-9

6.3. Deformation Analysis

This chapter investigates the settlement change within a densely urbanized area since urbanized areas are more vulnerable to groundwater level fluctuations. Urbanized groundwater level changes within dry and wet seasons expect to be greater than of rural groundwater. The following calculations show how the selected groundwater levels affect the settlement of a single pile. The study area is known to be consist of silty, clayey, and sandy soil classes. Two different soil classes were selected for this study: clay and sand. Wet season groundwater level was selected as 1.8m, and dry season groundwater level was selected as 3.5m. Three different diameter of the pile over the length of the pile (D_p/L_p) was selected as parameterization as 1/10, 1/25, and 1/50. The friction angle was selected as 34^o for sand and cohesion as 10 kN/m^3 for clay. A total of 12 PILAXIS 3D models were created to understand the effect of groundwater change on pile settlement.

6.3.1. Numerical Results

Figure 6.17 shows the perspective and top views of the very fine meshing.

Figure 6.19 shows the settlement calculations of sandy soils for the groundwater level of 1.8 m, and Figure 6.20 shows the settlement calculations of sandy soils for the groundwater level of 3.5 m, for D_p/L_p=1/10, 1/25, and 1/50. Figure 6.21 shows the settlement calculations of clayey soils for the groundwater level of 1.8 m, and Figure 6.22 shows the settlement calculations of clayey soils for the groundwater level of 3.5 m and. In clay calculations, there isn't a significant decrease of the settlement as the groundwater level decreases. It makes sense as the piles are designed to counter settlement in clayey soils since the skin and tip friction values of the clay is high. On the other hand, maximum settlement decrease was observed as 12.74%, which might be an important ratio for the sandy soils when D_p/L_p=1/10. Figure 6.18 shows the load vs. vertical displacement (in –z-direction) for the parameterization D_p/L_p=1/10 for sandy soils.

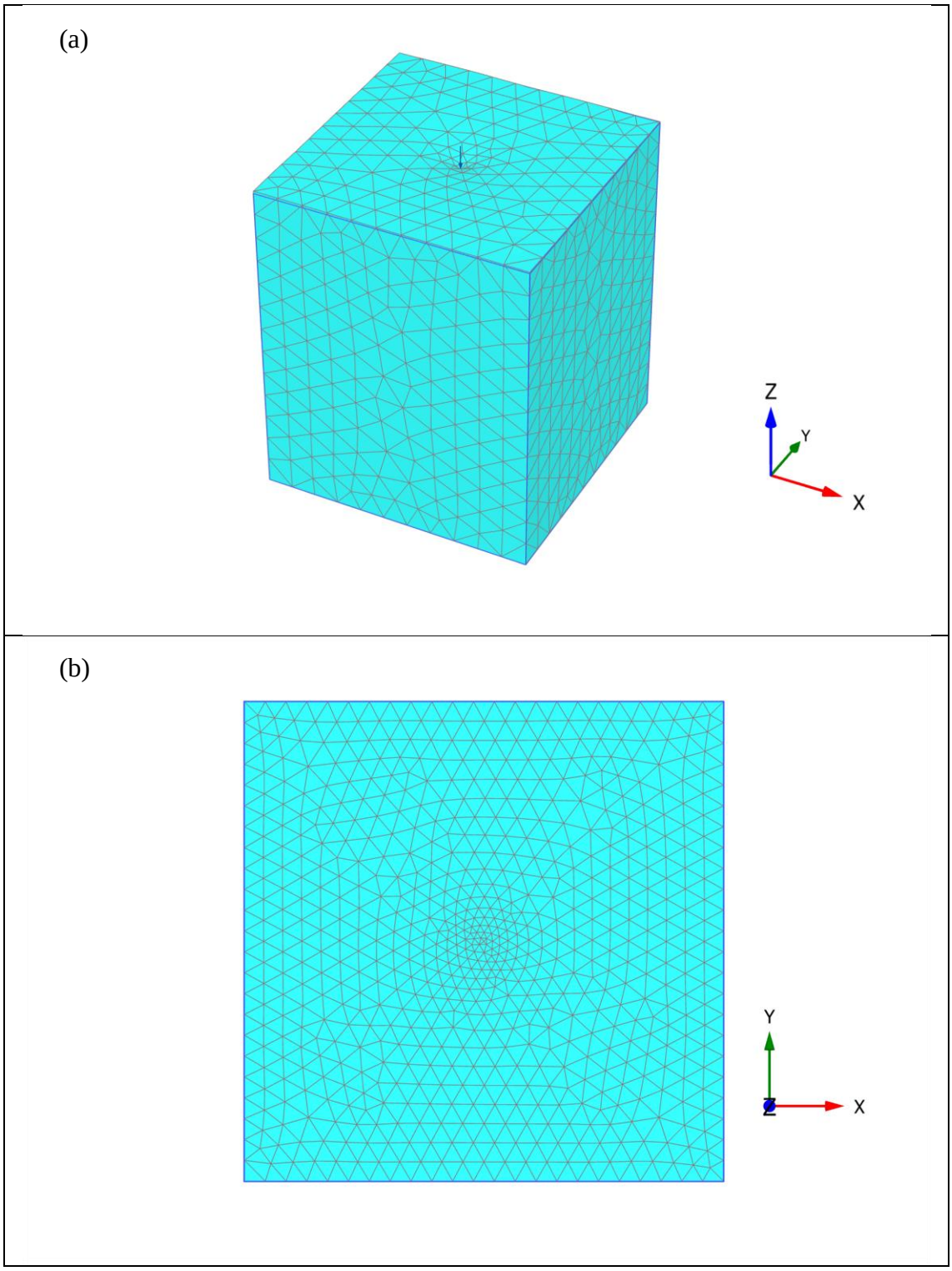

Figure 6.17. Very fine mesh created outside boundaries (a) perspective view, (b) top view for $D_f/L_f=1/5$

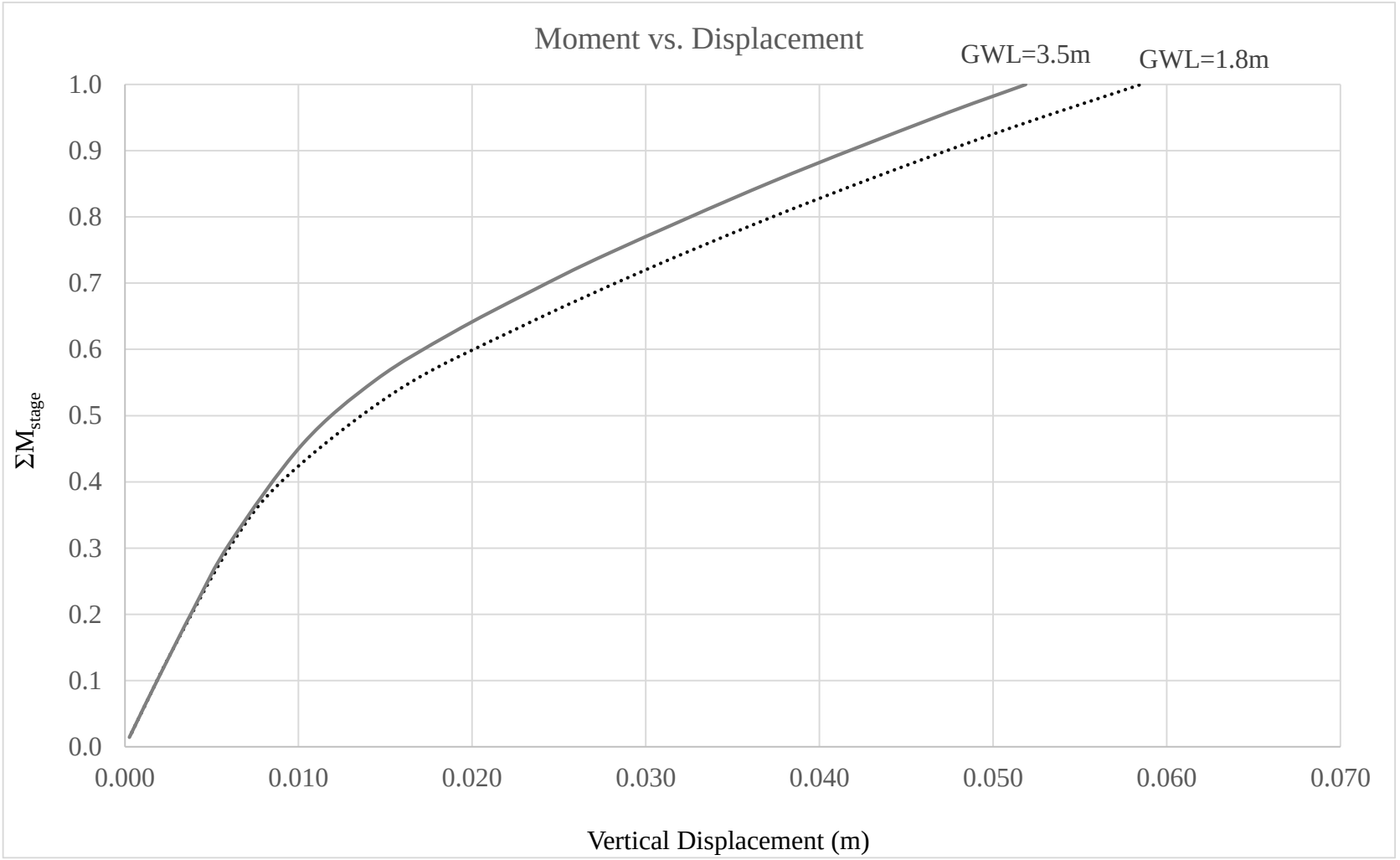

Figure 6.18. Load vs. Vertical Deflection for D_p/L_p=1/10 for sandy soils

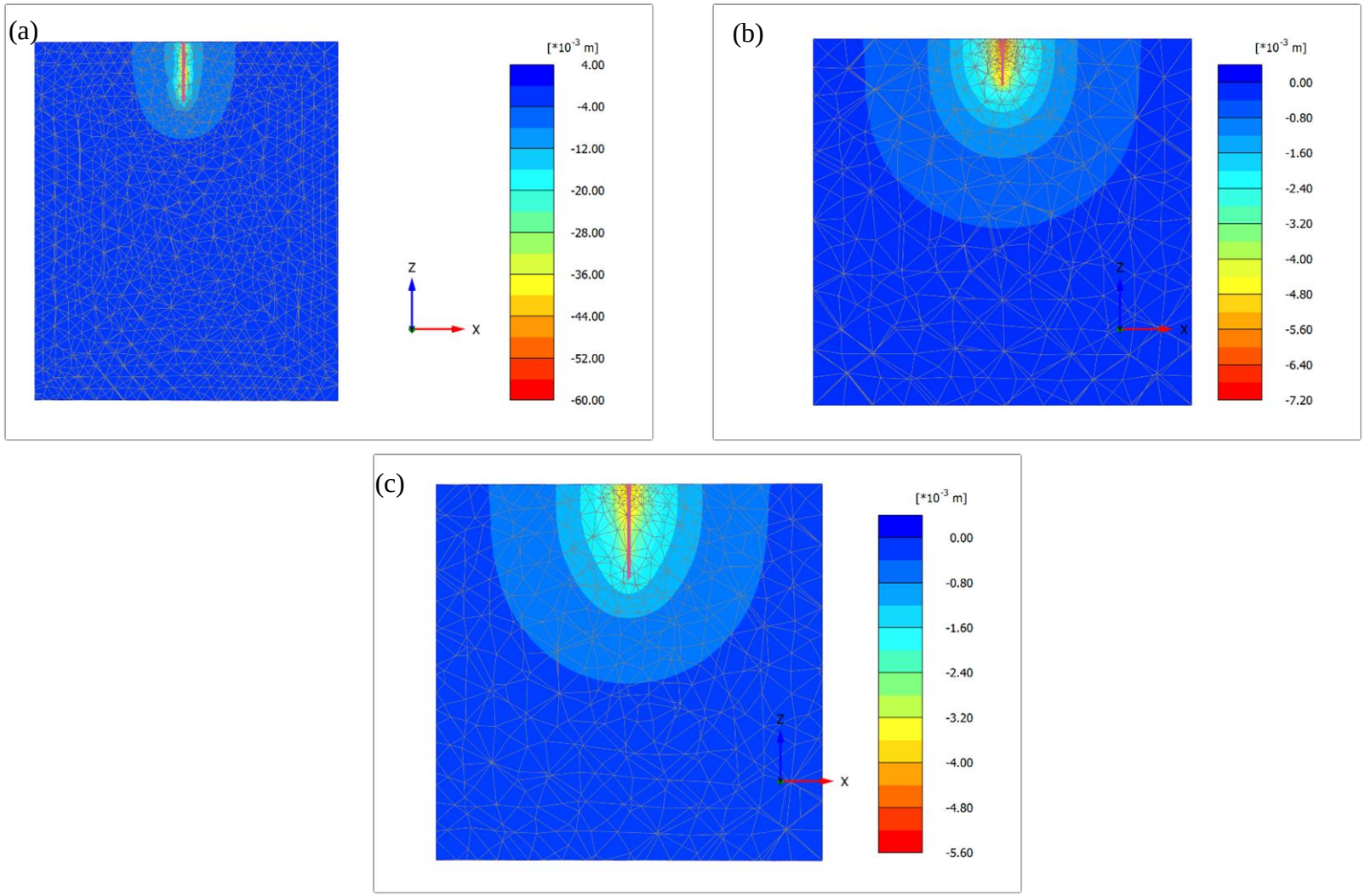

Figure 6.19. Settlement calculation representation of sandy soil when for GWL=1.8 m for (a) D_p/L_p=1/10, (b)1/25, (c) 1/50

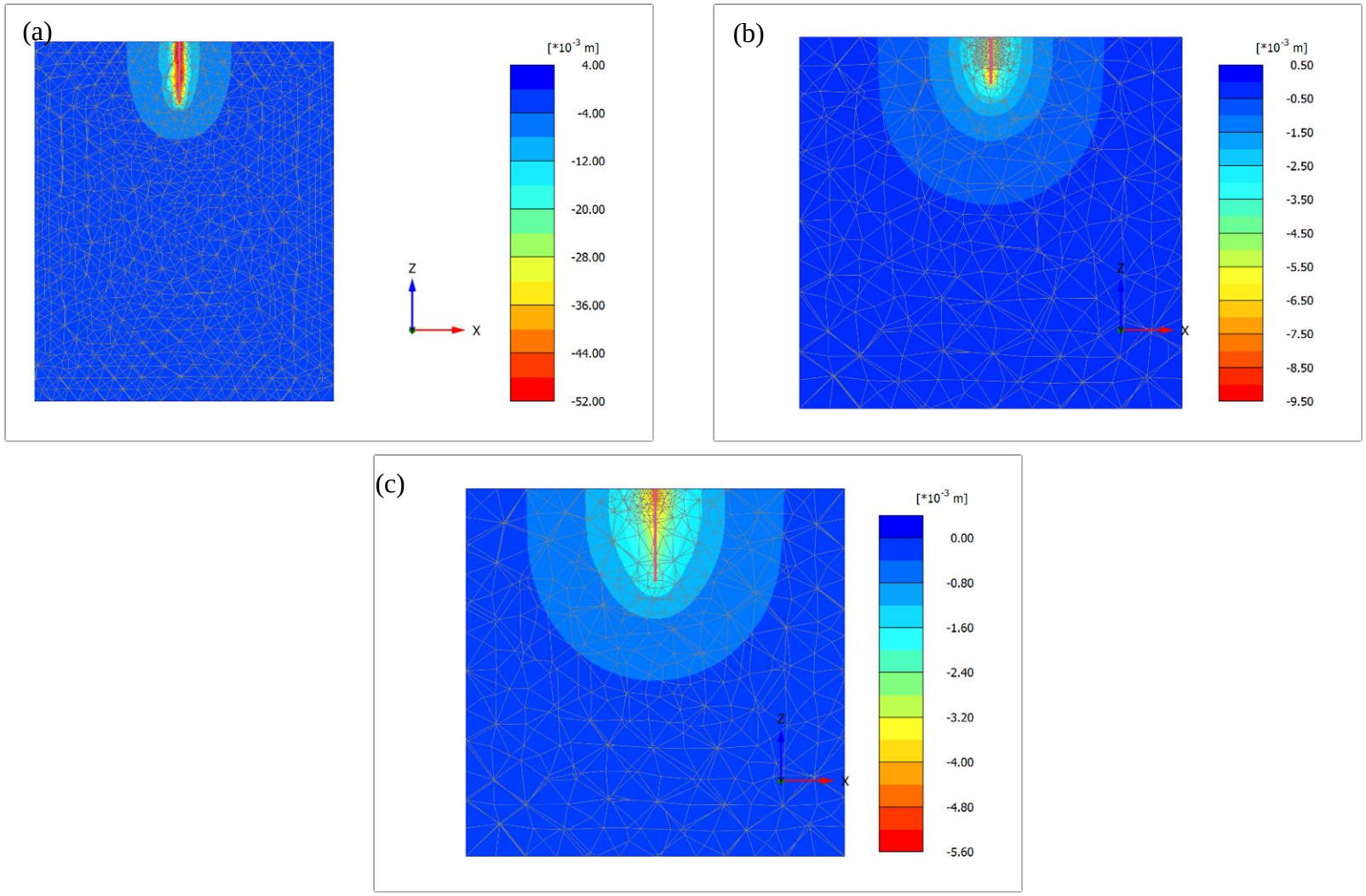

Figure 6.20. Settlement calculation representation of sandy soil when for GWL=3.5 m for (a) D_p/L_p=1/10, (b)1/25, (c) 1/50

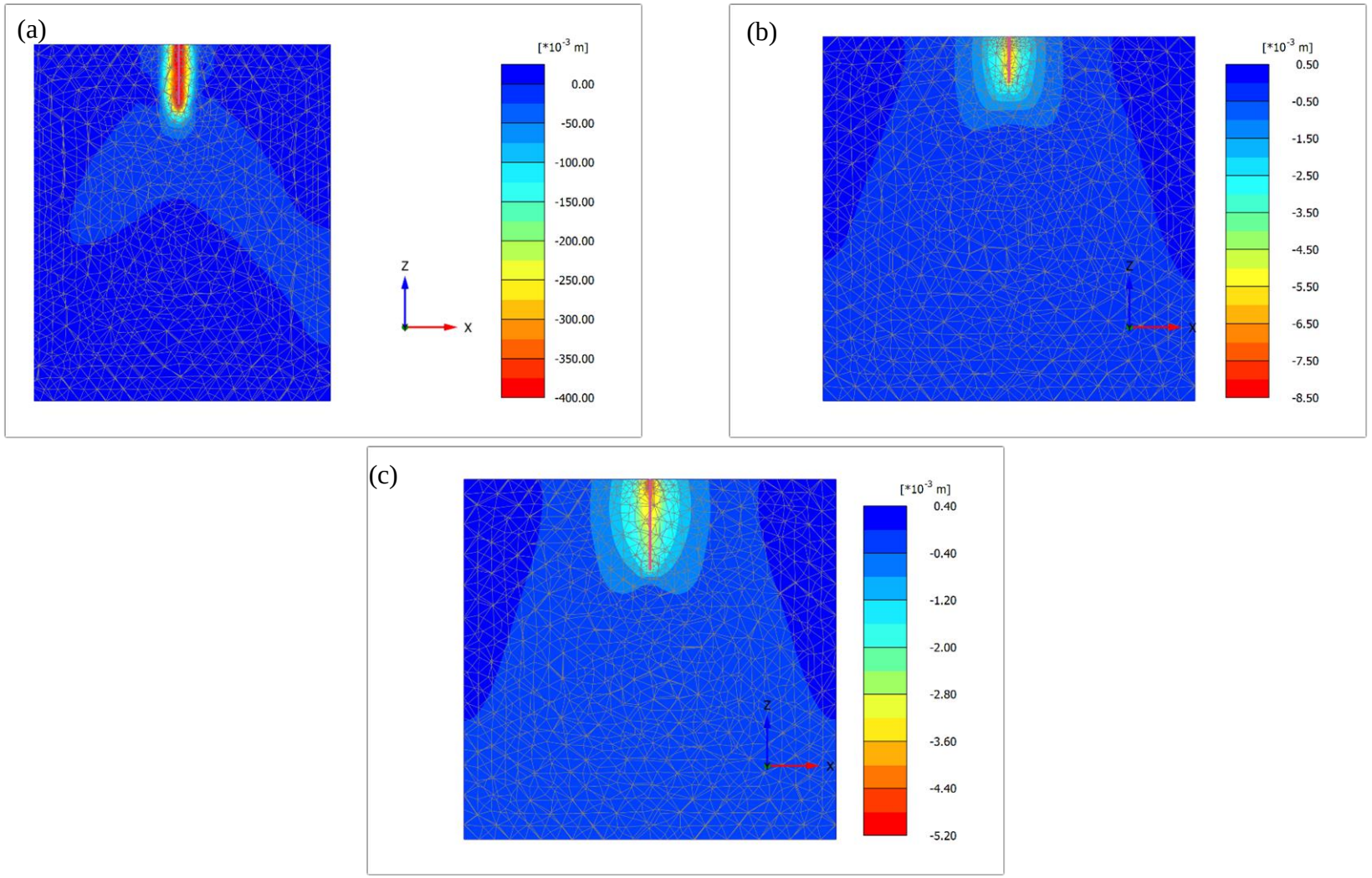

Figure 6.21. Settlement calculation representation of clayey soil when for GWL=1.8 m for (a) D_p/L_p=1/10, (b)1/25, (c) 1/50

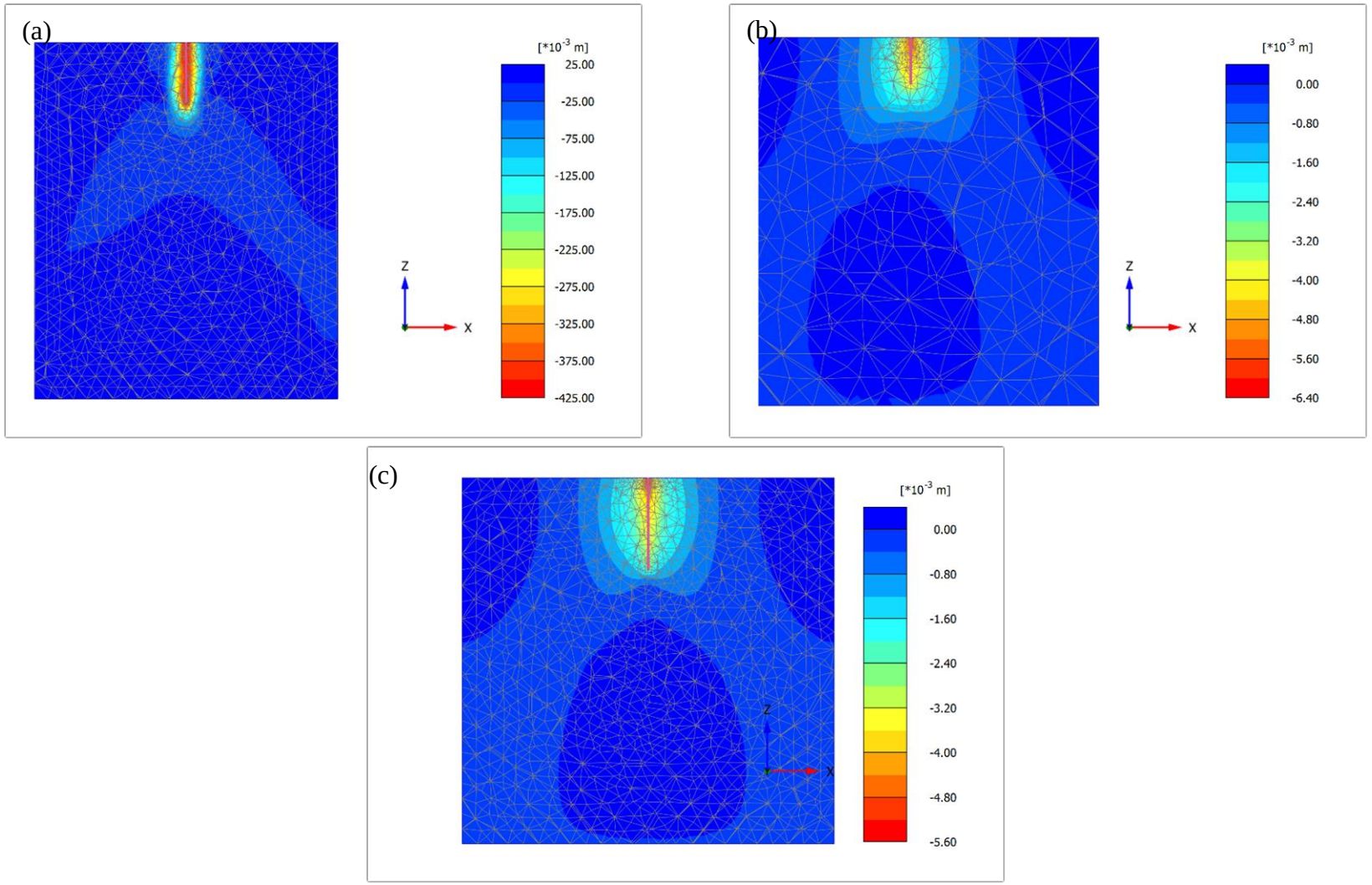

Figure 6.22. Settlement calculation representation of clayey soil when for GWL=3.5 m for (a) D_p/L_p=1/10, (b)1/25, (c) 1/50

CHAPTER 7

CONCLUSION

Hydrodynamic underground systems are directly influenced by urbanization, population increase, and climate change. In the study area, Bornova Plain, rapid urbanization within the last few decades happened, and as a result, hydraulic conductivity of the surface area decreased with surface coverings. The impact of urbanization and these surface covering were investigated in three parts for this thesis.

Firstly, the impact of urbanization on groundwater recharge rates was investigated with the help of the SWAT models. In order to understand the groundwater recharge rate change concerning urbanization, two time periods (2004 and 2020) were modeled with ArcSWAT. All the input data necessary for a SWAT model were prepared in ArcMap. LULC maps were created with supervised classification on Google Earth Historical Images obtained for the desired years. According to those LULC maps, urban land in the study area was increased by around 8% within 16 years. Calibrated SWAT Models show that the Recharge/Precipitation ratio decreased from 0.38 to 0.25 from 2004 to 2020, and the Surface Runoff/Total Flow increased from 0.34 to 0.41 from 2004 to 2020.

SWAT-CUP software was used to calibrate and validate the performed SWAT Models. A sensitivity analysis including 22 hydraulic parameters was conducted with an acceptable parameter range obtained from literature to obtain the most sensitive hydraulic parameters. Eighteen out of those twenty-two parameters were found to be sensitive and used for calibration and validation. One stream gauge monthly discharge data required from DSİ was used for calibration. The data between 1990 and 2005 were used for calibration, and the data between 2006-2014 were used for validation. For the calibration part, R^2=0.84 and NS=0.80, and for the validation part R^2=0.84, and NS=0.82 were found, which shows that the SWAT Models represent the study area very well.

Secondly, the impact of urbanization and groundwater levels changes on the soil's bearing capacity in the study area was investigated. Terzaghi's method was used to calculate the bearing capacity changes within the year with groundwater level changes.

Ten observation wells were drilled in the region to observe the groundwater level fluctuations within October 2020 and October 2021. Groundwater data loggers were placed in five, and manual measurements were taken from the other five. Maximum and minimum groundwater level differences were established to be 1.61m in SK-1, 0.89m in SK-3, 1.37m in SK-6, 1.5m in SK-7, and 1.35m in SK-9 wells. Four different B/D_f non-dimensional parameterizations were created, and daily bearing capacities were calculated for each of them for one year using Microsoft Excel. Maximum and minimum bearing capacities for each parameterization were calculated, and bearing capacity decrease (%) was calculated for each well. It was established that the bearing capacity of the soil (concerning groundwater level changes) decreased 13.44% in SK-1, 8.92% in SK-3, 8.71% in SK-6, 14.82% in SK-7, and 13.10% in SK-9 for different parameterizations.

Thirdly, the impact of urbanization and groundwater levels changes on the pile foundations in the study area was investigated. Conceptual models were created using PLAXIS 3D models. Twelve PLAXIS 3D models were conducted for six clay and six sand soil layers. Three different D_p/L_p parameterizations were used as 1/10, 1/25, and 1/50. And two different groundwater levels were used as 1.8 m and 3.5 m. Automatic meshing with very fine mesh option was used to get the best results. Piles are designed to resist the settlements, so as expected, the groundwater level changes within the study area did not affect the pile settlement except for the case D_p/L_p = 1/10. 12.74% of settlement changes with changing groundwater levels for D_p/L_p = 1/10. All other models give insignificant settlement changes, which are so small, assumed as numerical errors.

For the future works of this study, artificial intelligence methods are planned to be used to predict groundwater level changes for the future. These calculations and analysis are planned to be applied on future groundwater levels to compare design calculations nowadays to future parameters.

REFERENCES

Abbaspour, K. C. 2015. “SWAT-CUP: SWAT Calibration and Uncertainity Programs - A User Manual.”

Abbaspour, K. C., E. Rouholahnejad, S. Vaghefi, R. Srinivasan, H. Yang, and B. Kløve. 2015. “A Continental-Scale Hydrology and Water Quality Model for Europe: Calibration and Uncertainty of a High-Resolution Large-Scale SWAT Model.” *Journal of Hydrology* 524: 733–52. https://doi.org/10.1016/j.jhydrol.2015.03.027.

Allen, Joe, Herb Sauer, Lou Frank, and Patricia Reiff. 1989. “Effects of the March 1989 Solar Activity.” *Eos, Transactions American Geophysical Union* 70 (46): 1479–88. https://doi.org/10.1029/89EO00409.

ASABE. 2017. “Guidelines for Calibrating, Validating, and Evaluating Hydrologic and Water Quality (H/WQ) Models,” 1–15. https://swat.tamu.edu/media/115778/ep621.pdf.

Baba, Alper, and Hamidreza Yazdani. 2012. “Effect of Urbanization on Groundwater Resources of Izmir City,” 1–11.

Berilgen, M. 1996. “Ankrajlı Perdelerde Zemin Yapı Etkilerinin İncelenmesi.” *Yıldız Technical University, PhD. Thesis (In Turkish).*

Bowles, J. E. 1997. “Foundation Analysis and Design.” *McGraw-Hill*.

Clough, G. W., and Y. Tsui. 1974. “Performance of Tied-Back Walls in Clay.” *Journal of Geotechnical Engineering Division, ASCE* 100: 1259–73.

Das, B. M. 2007. “Principles of Foundation Engineering.” *Cengage Learning*. https://doi.org/10.1201/9780429094811-16.

Devine, R. S. 1995. “The Trouble with Dams.” *Atlantic Monthly* 276(2): 64–74.

Erdoğan, Burhan. 1990. “İzmir-Ankara Zonu Ile Karaburun Kuşağının Tektonik Ilişkisi.” *Maden Tetkik ve Arama Dergisi* 110 (110). https://doi.org/10.19076/mta.39198.

Gee, G. W., and D. Hillel. 1988. “Groundwater Recharge in Arid Regions: Review and Critique of Estimation Methods.” *Hydrol. Process* 2: 255–66.

HAPS. 2006. “Hydrological Assessment of the Northern Regions of Ghan: A Bibliographical Review of Selected Papers.” *CIDA, WRC, SNC-LAVALIN International*.

Hargreaves, George H., and Richard G. Allen. 2003. “History and Evaluation of Hargreaves Evapotranspiration Equation.” *Journal of Irrigation and Drainage Engineering* 129 (1): 53–63. https://doi.org/10.1061/(asce)0733-9437(2003)129:1(53).

Hooghoudt, S. B. 1940. “Bijdrage Tot de Kennis van Enige Natuurkundige Grootheden van de Grond.” *Versl. Landbouwkd. Onderz* 46: 515–707.

İncecik, M. 1986. “Yeni Avusturya Tünel İnşa Yöntemine Uygun Kaplama Hesapları (In Turkish).” *Tünellerin Projelendirilmesi ve İnşası Semineri*.

Jat, Mahesh K., Deepak Khare, and P. K. Garg. 2009. “Urbanization and Its Impact on Groundwater: A Remote Sensing and GIS-Based Assessment Approach.” *Environmentalist*. https://doi.org/10.1007/s10669-008-9176-2.

Lerner, D. N., A. S. Issar, and I Simmer. 1990. “Groundwater Recharge. A Guide to Understanding and Estimating Natural Recharge.” *International Contributions to Hydrogeology. Verlag Heinz Heise* 8.

Lloyd, J. W. 1986. “A Review of Aridity and Groundwater.” *Hydrol. Process* 1: 63–78.

Marsalek, Jiri, Blanca Jiménez-Cisneros, Mohammad Karamouz, Per Arne Malmquist, Joel Goldenfum, and Bernard Chocat. 2006. “Urban Water Cycle Processes and Interactions: Urban Water Series - UNESCO-IHP.” *Urban Water Cycle Processes and Interactions: Urban Water Series - UNESCO-IHP*, no. 78: 1–131.

Meyerhof, G. G. 1963. “Some Recent Research on the Bearing Capacity of Foundations.” *Canadian Geotechnical Journal* 1 (1): 16–26.

Minnig, Morgane, Christian Moeck, Dirk Radny, and Mario Schirmer. 2018. “Impact of Urbanization on Groundwater Recharge Rates in Dübendorf, Switzerland.” *Journal of Hydrology* 563: 1135–46.

Monteith, J. L. 1965. “EVAPORATION AND ENVIRONMENT.” *Symposia of the Society for Experimental Biology*, 19, pp. 205–34.

Neitsch, S.L, J.G Arnold, J.R Kiniry, and J.R Williams. 2011. “Soil & Water Assessment Tool Theoretical Documentation Version 2009.” *Texas Water Resources Institute*, 1–647. https://doi.org/10.1016/j.scitotenv.2015.11.063.

Nicks, A. D. 1974. “No Title.” *In Proc. Symp. Statistical Hydrology*, 154–71.

Okay, A. I., and M. Siyako. 1993. “The New Position of the İzmir-Ankara Neo-Tethyan Suture between İzmir and Balıkesir. In Tectonics and Hydrocarbon Potential of Anatolia and Surrounding Regions,.” *Proceedings of the Ozan Sungurlu Symposium*, 333–55.

Okay, A.I, Muharrem Satir, H Maluski, M Siyako, P Monie, R Metzger, and S. Akyüz. 1996. “Paleo- and Neo-Tethyan Events in Northwest Turkey : Geological and Geochronological Constraints.” *The Tectonic Evolution of Asia*, no. JANUARY: 420–41.

Okay, Aral I., and Demir Altiner. 2007. “A Condensed Mesozoic Succession North of İzmir: A Fragment of the Anatolide-Tauride Platform in the Bornova Flysch Zone.” *Turkish Journal of Earth Sciences* 16 (3): 257–79.

PLAXIS. 2021. “CONNECT Edition V21.01 - Material Models Manual,” 1–274.

Priestley, C. H. B., and R. J. Taylor. 1972. “On the Assessment of Surface Heat Flux and Evaporation Using Large-Scale Parameters.” *Monthly Weather Review* 100 (2): 81–92. https://doi.org/10.1175/1520-0493(1972)100<0081:otaosh>2.3.co;2.

Scanlon, B. R., R. W. Healy, and P. G. Cook. 2002. “Choosing Appropriate Techniques for Quantifying Groundwater Recharge.” *Hydrogeology Journal* 10(1): 18–39.

SCS, Soil Conservation Service. 1972. “Estimation of Direct Runoff from Storm Rainfall by Victor Mockus.” *National Engineering Handbook*.

Silva, C. De. 2015. “Simulation of Potential Groundwater Recharge from the Jaffna Peninsula of Sri Lanka Using HYDRUS-1D Model.” *OUSL Journal*.

Tam, Vu Thanh, and Tran Thi Viet Nga. 2018. “Assessment of Urbanization Impact on Groundwater Resources in Hanoi, Vietnam.” *Journal of Environmental Management* 227: 107–16.

Terzaghi, K. 1943. “Theoretical Soil Mechanics.” *Wiley, New York*.

Todd, David Keith, and Larry W. Mays. 1959. “Groundwater Hydrology: Conceptual and Computational Models.” *Groundwater Hydrology*. https://doi.org/10.1002/0470871660.

Uma, K. O., and B. C. Egboka. 1988. “Groundwater Recharge from Three Cheap and Independent Methods in the Small Watersheds of the Rain Forest Belt of Nigeria. In Estimation of Natural Groundwater Recharge.” *Springer, Dordrecht*, 435–47.

Uzel, Bora, Hasan Sozbilir, and Çağlar Özkaymak. 2012. “Neotectonic Evolution of an Actively Growing Superimposed Basin in Western Anatolia: The Inner Bay of İzmir, Turkey.” *Turkish Journal of Earth Sciences* 21 (4): 439–71. https://doi.org/10.3906/yer-0910-11.

Venetis, C. 1969. “A Study of the Recession of Unconfined Aquifers.” *Bull. Int. Assoc. Sci. Hydrol.* 14(4): 119–25.

Wakode, Hemant Balwant, Klaus Baier, Ramakar Jha, and Rafig Azzam. 2018. “Impact of Urbanization on Groundwater Recharge and Urban Water Balance for the City of Hyderabad, India.” *InternationalSoilandWaterConservationResearch* 6 (1): 51–62.

Wood, W. W., and W. E. Sanford. 1995. “Chemical and Isotopic Methods for Quantifying Ground-water Recharge in a Regional, Semiarid Environment.” *Groundwater* 33(3): 458–68.

Xanthakos, P. P. 1991. “Ground Anchors and Anchored Structures.” *John Wiley & Sons, Inc., New York, NY*.

Yevjevich, Vujica. 1992. “Water and Civilization.” *Water International* 17 (4): 163–71. https://doi.org/10.1080/02508069208686135.